FONSEKA, GAMPOLA WADUGE NALIN, Ph.D. Mathematical and Computational Analysis of Reaction Diffusion Models Arising in Ecology. (2020)
Directed by Dr. Ratnasingham Shivaji. 106 pp.

The focus of this thesis is to study long term solutions for classes of steady state reaction diffusion equations. In particular, we study reaction diffusion models arising in mathematical ecology. We study how the patch size affects the existence, nonexistence, multiplicity, and uniqueness of the steady states. Our focus is also to study how various forms of density dependent emigrations at the boundary, and the effective matrix hostility, affect steady states. These considerations lead to the study of various forms of nonlinear boundary conditions. Further, they lead to the study of reaction diffusion models where a parameter (related to the patch size) gets involved in the differential equation as well as the boundary conditions.

We establish analytical results in any dimension, namely, establish existence, nonexistence, multiplicity, and uniqueness results. Our existence and multiplicity results are achieved by a method of sub-supersolutions and uniqueness results via comparison principles and a-priori estimates.

Via computational methods, we also obtain exact bifurcation diagrams describing the structure of the steady states. Namely, we obtain these bifurcation diagrams via a modified quadrature method and Mathematica computations in the one-dimensional case, and via the use of finite element methods and nonlinear solvers in Matlab in the two-dimensional case.

This dissertation aims to significantly enrich the mathematical and computational analysis literature on reaction diffusion models arising in ecology.

MATHEMATICAL AND COMPUTATIONAL ANALYSIS OF REACTION DIFFUSION MODELS ARISING IN ECOLOGY

by

Gampola Waduge Nalin Fonseka

A Dissertation Submitted to
the Faculty of The Graduate School at
The University of North Carolina at Greensboro
in Partial Fulfillment
of the Requirements for the Degree
Doctor of Philosophy

Greensboro
2020

Approved by

____
Committee Chair

To all my teachers.

APPROVAL PAGE

This dissertation written by Gampola Waduge Nalin Fonseka has been approved by the following committee of the Faculty of The Graduate School at The University of North Carolina at Greensboro.

Committee Chair ______________________
Ratnasingham Shivaji

Committee Members ______________________
Maya Chhetri

____
Jerome Goddard II

____
Thomas Lewis

____
Stephen B. Robinson

____
Yi Zhang

____
Date of Acceptance by Committee

____
Date of Final Oral Examination

ACKNOWLEDGMENTS

First and foremost, I wish to acknowledge my advisor, Professor Ratnasingham Shivaji, not only for guiding me through my Ph.D. thesis, but also for teaching me how to be a researcher, a teacher, and a mathematician. His support, encouragement, and kindness have made me a better researcher, a teacher, and a mathematician.

Second, I wish to acknowledge Professor Jerome Goddard for co-directing (with Shivaji) the sections of the thesis related to the NSF funded project: DMS1516519, and for serving in my committee.

Third, I wish to acknowledge all members of my committee, Professors Maya Chhetri, Jerome Goddard II, Tom Lewis, Yi Zhang, and Stephen Robinson for their time, energy, and dedication not only to my dissertation but to my success and development across the past five years.

Fourth, I would like to acknowledge all my teachers at UNCG, Ms. Haley Childers, Mrs. Carri Richter, and Ms. Katelyn Young. Each of you is indispensable.

Finally, I wish to acknowledge my friends and family. Without twenty-five years of support from my parents, Sarath & Sriyani Fonseka, and without the love and support of my wife, Limali, over the past 5 years, I never would have completed this dissertation.

TABLE OF CONTENTS

LIST OF TABLES

LIST OF FIGURES

CHAPTER I

INTRODUCTION

Let $\Omega_0 \subset \mathbb{R}^N$ (for $N = 2, 3$) be a bounded domain (see Figure 1) with a smooth boundary $\partial\Omega_0$ or $\Omega_0 = (0, l)$ for some $l > 0$.

Figure 1. The Domain Ω_0.

We assume that the diffusion rate in the habitat Ω_0 is D. In the matrix (exterior to Ω_0) $\Omega_N := \mathbb{R}^N \setminus \overline{\Omega}_0$, we assume that the diffusion rate is D_0 and the death rate is S_0. We further assume that the population exhibits density dependent emigration (DDE) on the boundary $\partial\Omega_0$. We denote the probability of the population staying in Ω_0 when it reaches the boundary by $\alpha(u)$ (here u is the population density of the species living in the habitat).

Then the resulting time dependent model is (see [CFG$^+$19], [CGS19], [GMPS19], [GMRS18], and [LAW79]):

$$\begin{cases} u_t = D\Delta u + rf(u);\ x \in \Omega_0, t > 0, \\ D\alpha(u)\frac{\partial u}{\partial \eta} + \frac{\sqrt{S_0 D_0}}{k}[1-\alpha(u)]u = 0;\ x \in \partial\Omega_0, t > 0, \\ u(0,x) = u_0(x);\ x \in \Omega_0, \end{cases}$$

with the corresponding steady state equation:

$$\begin{cases} -\Delta u = \frac{r}{D} f(u);\ x \in \Omega_0, \\ D\alpha(u)\frac{\partial u}{\partial \eta} + \frac{\sqrt{S_0 D_0}}{k}[1-\alpha(u)]u = 0;\ x \in \partial\Omega_0, \end{cases}$$

or equivalently

$$\begin{cases} -\Delta u = \frac{rl^2}{D} f(u);\ x \in \Omega, \\ \frac{\partial u}{\partial \eta} + \frac{\sqrt{S_0 D_0} l}{kD}\left[\frac{1-\alpha(u)}{\alpha(u)}\right]u = 0;\ x \in \partial\Omega, \end{cases} \tag{1.1}$$

where $\Delta u := \mathrm{div}(\nabla u)$ is the Laplacian operator of u, $r > 0$ is the patch intrinsic growth rate, the reaction term $f : [0,\infty) \to \mathbb{R}$ is a continuous function representing the product of u and the per-capita growth rate, $\frac{\partial u}{\partial \eta}$ is the outward normal derivative of u, Ω is a domain with unit measure such that $\Omega_0 := \{lx \mid x \in \Omega\}$, and $\kappa > 0$ is a parameter related to the movement behavior of the species (see [CGS19] and [GMRS18]). Let $\lambda := \frac{rl^2}{D}$ and $\gamma := \frac{\sqrt{S_0 D_0}}{k\sqrt{rD}}$. Then (1.1) reduces to

$$\begin{cases} -\Delta u = \lambda f(u);\ x \in \Omega, \\ \frac{\partial u}{\partial \eta} + \gamma\sqrt{\lambda} g(u) u = 0;\ x \in \partial\Omega, \end{cases} \tag{1.2}$$

where $\lambda > 0$ is a domain scaling parameter, $\gamma > 0$ is the effective matrix hostility, and

$$g(s) := \frac{1-\alpha(s)}{\alpha(s)}. \tag{1.3}$$

Throughout this thesis, by a solution we mean a function $u \in C^2(\Omega) \cap C^1(\overline{\Omega})$ that solves (1.2). We note that in the recent history there has been considerable interest in elliptic boundary value problems where a parameter is involved in the differential equation as well as the boundary conditions (see [CGS19], [CFG+19], [FSSS19], [FMS20], [FGM+], [GMPS19], and [GMRS18]). In this thesis, we enrich this study for problems with linear and nonlinear boundary conditions.

Recently, in [GMRS18], the authors established an exact bifurcation diagram (see Figure 3) for positive solutions to the boundary value problem:

$$\begin{cases} -\Delta u = \lambda u(1-u); \ x \in \Omega, \\ \frac{\partial u}{\partial \eta} + \gamma\sqrt{\lambda} u = 0; \ x \in \partial\Omega, \end{cases} \tag{1.4}$$

where, as noted earlier, $\gamma > 0$ is the effective matrix hostility and $\lambda > 0$ is a domain scaling parameter. Such a steady state reaction diffusion equation arises in modeling problems in ecology (see [CC06], [CGS19], [FSSS19], [GMRS18], and [LAW79]). Note that when $\alpha(s) = \frac{1}{2}$ and $f(s) = s(1-s)$ in (1.2) we get the model in (1.4) with linear boundary conditions. Corresponding emigration $(1-\alpha(s))$ is given in Figure 2. Here, f represents a scaled logistic growth, with the scaled per-capita growth rate $\tilde{f}(s) = \frac{f(s)}{s} = 1 - s$ being a linearly decreasing function.

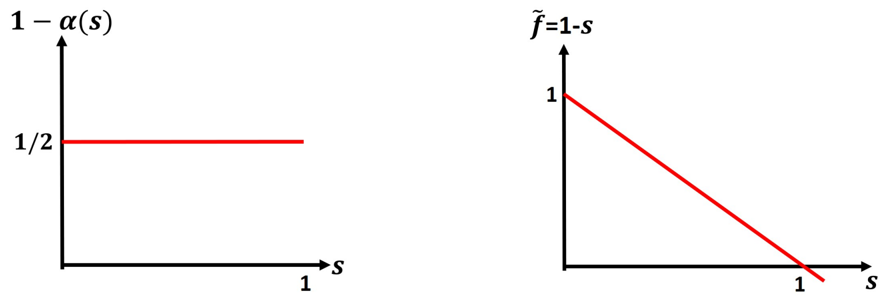

Figure 2. Density Independent Emigration $1-\alpha(s)$ and the Scaled Per-capita Growth Rate $\tilde{f}$.

Here, the authors established the following exact description of the bifurcation diagram of positive steady states (see Figure 3):

Theorem 1.1. *Let $\gamma > 0$ be given. Then,*

(a) if $\lambda > E_1(\gamma, 1)$, then the trivial solution of (1.4) is unstable and there exists a unique positive solution u_λ to (1.4) which is globally asymptotically stable. Furthermore, $\|u_\lambda\|_\infty \to 0^+$ as $\lambda \to E_1(\gamma, 1)^+$ and $\|u_\lambda\|_\infty \to 1$ as $\lambda \to \infty$,

(b) if $\lambda \leq E_1(\gamma, 1)$, then the trivial solution of (1.4) is globally asymptotically stable and there is no positive solution to (1.4).

Here, $E_1(\gamma, D) > 0$ is the principal eigenvalue of the eigenvalue problem:

$$\begin{cases} -\Delta\phi = E\phi; \ x \in \Omega, \\ \frac{\partial\phi}{\partial\eta} + \gamma\sqrt{E}D\phi = 0; \ x \in \partial\Omega. \end{cases} \tag{1.5}$$

Note that the existence of $E_1(\gamma, 1) > 0$ was first established in [GMRS18]. For convenience of the reader we give the details here again.

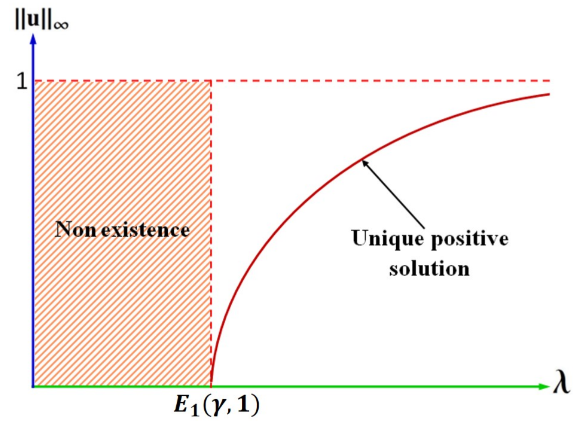

Figure 3. Exact Bifurcation Diagram for (1.4).

In [RR19], the authors studied the eigenvalue problem:

$$\begin{cases} -\Delta\phi = B\phi;\ x \in \Omega, \\ \frac{\partial\phi}{\partial\eta} = \kappa\phi;\ x \in \partial\Omega, \end{cases}$$

for any $\kappa \in \mathbb{R}$. They proved that for each κ, the principal eigenvalue $B(\kappa)$ exists, and the eigencurve $B(\kappa)$ is Lipschitz continuous, strictly decreasing, and concave. Further, $B(0) = 0$ and $\lim\limits_{\kappa\to-\infty} B(\kappa) \to A_1$, where A_1 is the principal eigenvalue of

$$\begin{cases} -\Delta\phi = A\phi;\ x \in \Omega, \\ \phi = 0;\ x \in \partial\Omega. \end{cases} \tag{1.6}$$

In the case of (1.5), treating $\kappa = -\gamma\sqrt{E}$ (or $E = \frac{\kappa^2}{\gamma^2}$), we see that the principal eigenvalue $E_1(\gamma, 1)$ of (1.5) is given by $E_1(\gamma, 1) = C$ where $(-\gamma\sqrt{C}, C)$ with $C > 0$ is the point of intersection of the curves $B(\kappa)$ and $\frac{\kappa^2}{\gamma^2}$ as shown in Figure 4.

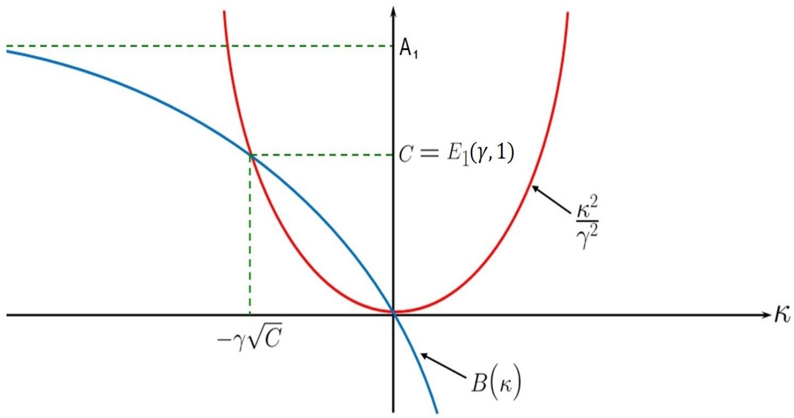

Figure 4. Eigencurve $B(\kappa)$ and Principal Eigenvalue of (1.5).

Next, in [GMPS19], the authors established existence, multiplicity, and uniqueness results for positive solutions to the following steady state reaction diffusion equation with a scaled logistic reaction term and U-shaped density dependent emigration on the boundary:

$$\begin{cases} -\Delta u = \lambda u(1-u); \; x \in \Omega, \\ \frac{\partial u}{\partial \eta} + \gamma\sqrt{\lambda}(A-u)^2 u = 0; \; x \in \partial\Omega, \end{cases} \tag{1.7}$$

where $A \in (0,1)$ is a constant. Note that taking $\alpha(s) = \frac{1}{[1+(A-s)^2]}$ and $f(s) = s(1-s)$ in (1.2) gives the model in (1.7) with nonlinear boundary conditions. The corresponding emigration $(1-\alpha(s))$ is given in Figure 6 (we note here the minimum emigration is zero). Namely, the authors in [GMPS19] established (see Figure 7):

Theorem 1.2. *Let* $\gamma > 0$ *and* $\Gamma := \{v \in C^2(\Omega) \cap C^1(\overline{\Omega}) \mid v(x) \in [A, 1]\ \forall x \in \overline{\Omega}\}$. *For each* $\lambda > 0$ (1.7) *has a positive solution* $u_{1,\lambda} \in \Gamma$ *and this solution is unique. Further, for* $\lambda \in (0, E_1(\gamma, A^2))$, (1.7) *has another positive solution* $u_{2,\lambda}$ *with* $u_{2,\lambda} \notin \Gamma$, *where* $E_1(\gamma, A^2) > 0$ *is the principal eigenvalue of the eigenvalue problem:*

$$\begin{cases} -\Delta\phi = E\phi; \quad \Omega, \\ \frac{\partial\phi}{\partial\eta} + \gamma A^2\sqrt{E}\phi = 0; \quad \partial\Omega. \end{cases}$$

Theorem 1.3. *Let* $\gamma \gg 1$. *There exists* $\delta_\gamma > E_1(\gamma, A^2)$ *so that for* $\lambda = \delta_\gamma$, (1.7) *has at least two positive solutions* $u_{i,\lambda}$ *with* $u_{i,\lambda} \notin \Gamma$ *for* $i = 2, 3$.

Density dependent emigration on the boundary has been observed among several species including the blue footed booby (see Figure 5).

Figure 5. Blue-footed Booby Which Exhibits Density Dependent Emigration. Source: www.shutterstock.com

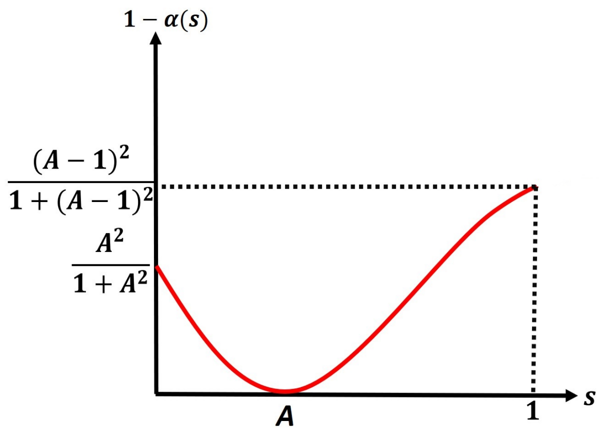

Figure 6. U-shaped Density Dependent Emigration with a Zero Minimum Emigration.

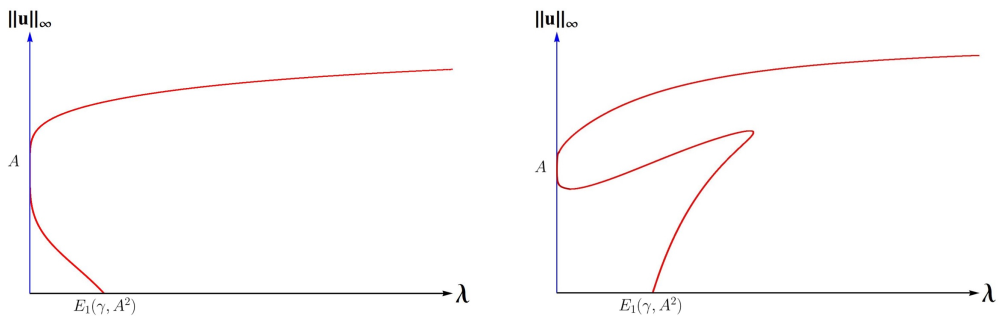

Figure 7. Bifurcation Diagrams for (1.7).

Our focus in this thesis is to enrich this study for ecological models with linear boundary conditions ($\alpha(u)$ constant) as well as with nonlinear boundary conditions (emigration at the boundary dependent on density). First, we will focus on extending the results in [GMRS18] for more general reaction terms and more general involvement of the parameter λ on the boundary conditions. Further, we will discuss an application of our results to a model where the reaction term is scaled logistic growth with grazing. Our second focus will be to extend the study in [GMPS19] to a biologically more relevant and challenging case when the minimum emigration in a U-shaped density dependent emigration is positive. In our third focus, we study a scaled weak Allee growth model (the scaled per-capita growth rate is positive and increasing for $s \approx 0$ as represented in Figure 8) with a U-shaped density dependent emigration on the boundary. Our fourth focus will be to study a scaled weak Allee growth model arising in ecology in the one-dimensional setting. Here, we consider various forms of density dependent emigration; namely, we consider density independent emigration (DIE), positive density dependent emigration (+DDE), negative density dependent emigration (-DDE), U-shaped density dependent emigration (UDDE), and hump-shaped density dependent emigration (hDDE) (see Figure 9). See [CC07], [CCY20], [CCY18], [CGS19], [FOP06], [HGSC20], [LMVL09], and [SB11] for studies on density dependent emigration on the boundary. In focuses 1 - 4, we will also obtain exact bifurcation diagrams of the steady states when $N = 1$. Finally, in our fifth focus, we will numerically study and obtain exact bifurcation diagrams of the steady states for certain models for the case when $N = 2$.

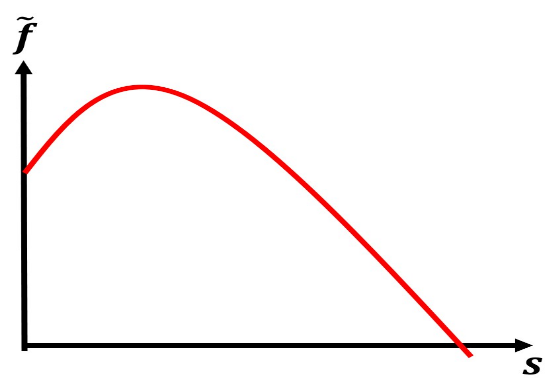

Figure 8. Scaled Per-capita Growth Rate of a Weak Allee Growth.

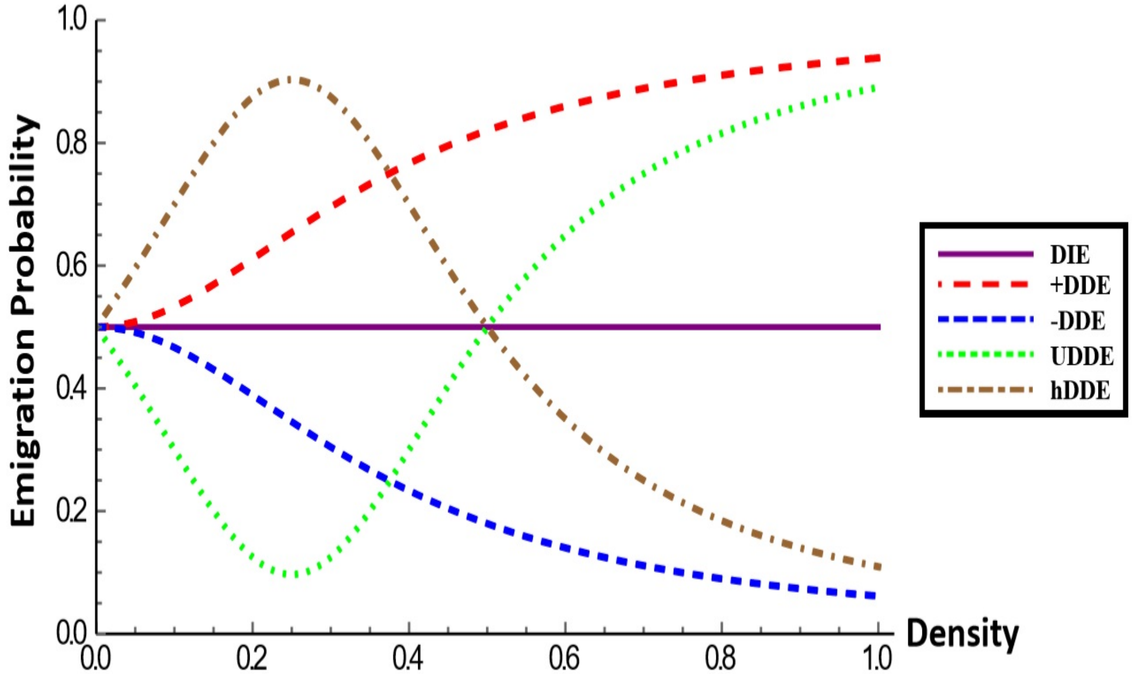

Figure 9. Emigration Forms.

1.1 Focus 1

Motivated by the study in [GMRS18], we first consider boundary value problems of the form:

$$\begin{cases} -\Delta u = \lambda f(u);\ x \in \Omega, \\ \frac{\partial u}{\partial \eta} + \mu(\lambda) u = 0;\ x \in \partial\Omega, \end{cases} \tag{1.8}$$

where $f \in C^2([0, r_0))$ with $0 < r_0 \leq \infty$. $\mu \in C([0,\infty))$ is strictly increasing such that $\mu(0) \geq 0$. We establish nonexistence, existence, multiplicity, and uniqueness of positive solutions of (1.8) for a class of reaction terms f satisfying $f(0) = 0$ and $f'(0) = 1$.

We first introduce hypotheses that we use to establish our results.

(H_1) if $r_0 < \infty$, then $f \in C^2([0, r_0])$ with $f(r_0) = 0$ and $f(s) \leq 0$ for $s \in (r_0, \infty)$, while if $r_0 = \infty$, then $\lim\limits_{s\to\infty} f(s) > 0$ and $\lim\limits_{s\to\infty} \frac{f(s)}{s} = 0$ (see Figure 11),

(H_2) there exists $\kappa_0 \in -\mu((0,\infty))$ such that $(\kappa - \kappa_0)(B(\kappa) - \mu^{-1}(-\kappa)) > 0$ for $\kappa \in -\mu((0,\infty)) \setminus \{\kappa_0\}$,

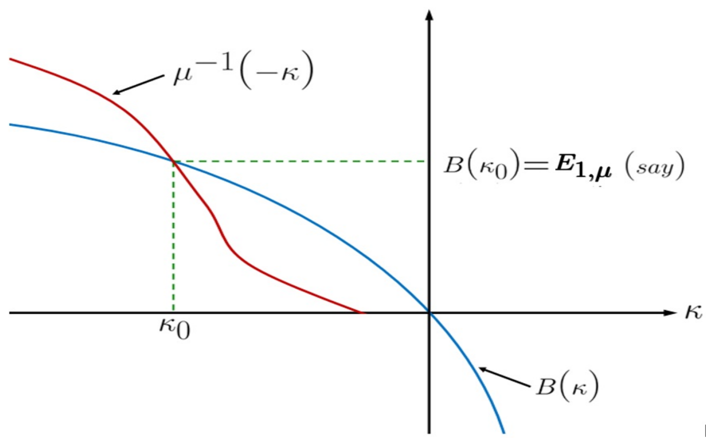

Figure 10. A Function μ Satisfying (H_2).

Remark. Note that $E_{1,\mu} = B(\kappa_0)$ is the principal eigenvalue of

$$\begin{cases} -\Delta\phi = E\phi;\ x \in \Omega, \\ \frac{\partial\phi}{\partial\eta} + \mu(E)\phi = 0;\ x \in \partial\Omega, \end{cases}$$

(H_3) there exist $a > 0$ and $b > 0$ such that $a < b < \frac{r_0}{C_N}$ and $\frac{a}{f^*(a)} / \frac{b}{f(b)} > \frac{2NC_N \|v_{\mu_b}\|_\infty}{R^2}$, where $f^*(s) := \max_{r \in [0,s]} f(r)$, $C_N := \frac{(N+1)^{N+1}}{2N^N}$ (> 1), $\mu_b := \mu\left(\frac{2bNC_N}{R^2 f(b)}\right)$, R is the radius of the largest inscribed ball on Ω, and v_{μ_b} is the unique solution of $-\Delta v = 1;\ \Omega,\ \frac{\partial v}{\partial \eta} + \mu_b v = 0;\ \partial\Omega$,

(H_4) there exist $r_1 \in (0, b)$ and $r_2 \in (bC_N, r_0)$ such that f is nondecreasing on (r_1, r_2),

(H_5) $E_{1,\mu} < \frac{2bNC_N}{R^2 f(b)}$.

We discuss existence, multiplicity, and uniqueness of positive solutions u_λ ($u_\lambda > 0$; $\overline{\Omega}$).

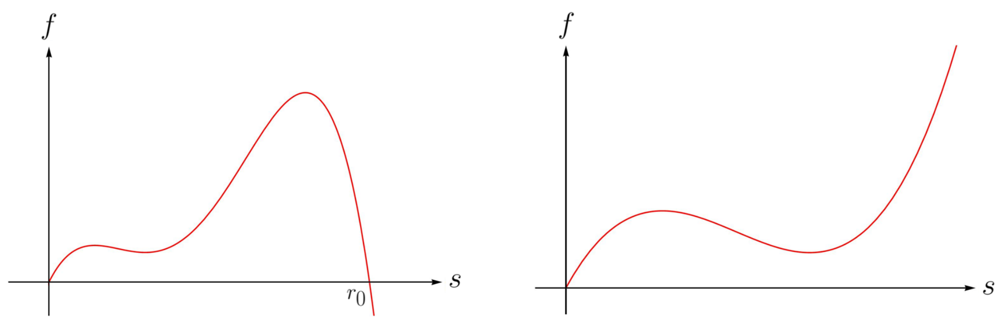

(a) $r_0 < \infty$ (b) $r_0 = \infty$

Figure 11. Graphs of f.

We establish:

Theorem 1.4. *Let $(H_1)-(H_2)$ hold and $f''<0$ on $[0,r_0)$. Then (1.8) has no positive solution u_λ for $\lambda<E_{1,\mu}$ and a unique positive solution u_λ for $\lambda>E_{1,\mu}$ such that $\|u_\lambda\|_\infty\to 0$ as $\lambda\to E_{1,\mu}^+$ and $\|u_\lambda\|_\infty\to r_0$ as $\lambda\to\infty$ (See Figure 12 for bifurcation diagrams).*

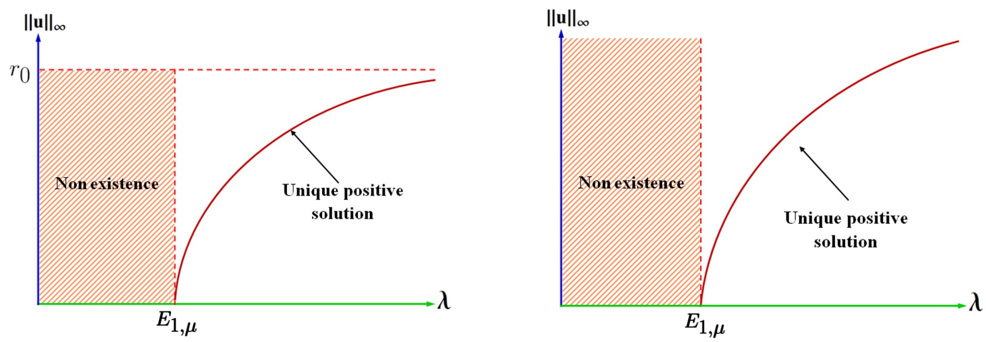

(a) $r_0<\infty$ (b) $r_0=\infty$

Figure 12. Bifurcation Diagrams of (1.8) When $f''<0$.

Remark. An application of this theorem can be found in [GMRS18] where the authors studied the case when $f(s)=s(1-s)$ and $\mu(\lambda)=\gamma\sqrt{\lambda}$.

Next we establish the occurrence of an S-shaped bifurcation curve (at least one solution for all $\lambda>E_{1,\mu}$ and three solutions for a certain range of λ) for classes of f which are not concave for all $s\in[0,r_0)$. Note when $f''(s)<0$ on $[0,r_0)$, $\frac{s}{f(s)}$ is increasing on $(0,r_0)$ and there can exist at most one positive solution. We consider f such that there exist $a>0$ and $b>0$ such that $a<b<r_0$ and $\frac{a}{f(a)}/\frac{b}{f(b)}\gg 1$ (see Figure 13) and establish:

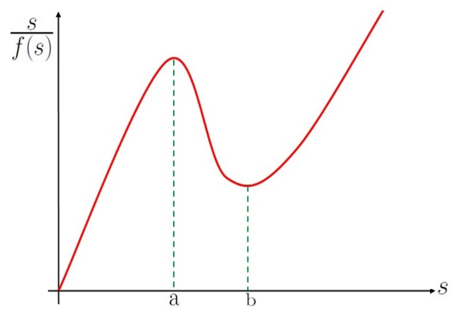

Figure 13. A Function $\frac{s}{f(s)}$ Satisfying $\frac{a}{f(a)}/\frac{b}{f(b)} \gg 1$.

Theorem 1.5. *Let* $(H_1)-(H_5)$ *hold. Then* (1.8) *has at least one positive solution for all* $\lambda > E_{1,\mu}$ *and three positive solutions for* $\lambda \in \left(\frac{2bNC_N}{R^2 f(b)}, \min\left\{\frac{a}{f^*(a)\|v_{\mu_b}\|_\infty}, \frac{2r_2 N}{f(b)R^2}\right\}\right)$ (*See Figure* 14 *for bifurcation diagrams*).

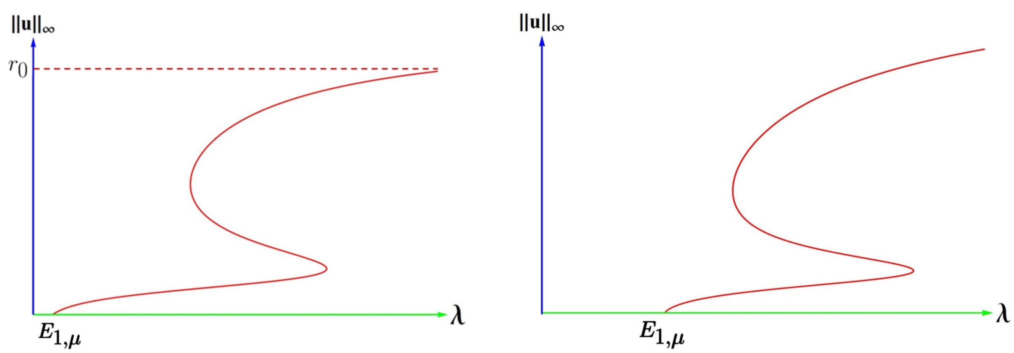

(a) $r_0 < \infty$ (b) $r_0 = \infty$

Figure 14. Occurrence of an S-shaped Bifurcation Curve for 1.8.

Now we provide an application of Theorem 1.4 and Theorem 1.5. Consider the steady state scaled logistic growth model with grazing in a spatially homogeneous ecosystem (see Figure 15):

$$\begin{cases} -\Delta u = \lambda f(u) = \lambda\left(u - \frac{u^2}{K} - \frac{Mu^2}{1+u^2}\right);\ \Omega, \\ \frac{\partial u}{\partial \eta} + \sqrt{\lambda}u = 0; \quad \partial\Omega, \end{cases} \tag{1.9}$$

where $K > 0$, $0 < M < 2$, and Ω is a bounded domain in $\mathbb{R}^N$; $N \geq 1$ with smooth boundary $\partial\Omega$ or $\Omega = (0,1)$. We first note that when $K \gg 1$, $f(s) = s - \frac{s^2}{K} - \frac{Ms^2}{1+s^2}$ has a unique zero r_0 (see [LSS11]). Here, we note that $\mu(s) = \sqrt{s}$.

Figure 15. Grazing. Source: https://www.shutterstock.com

We prove following two theorems for this model:

Theorem 1.6. *Let* $KM < 4$. *Then* (1.9) *has no positive solution* u_λ *for* $\lambda < E_{1,\mu}$ *and a unique positive solution* u_λ *for* $\lambda > E_{1,\mu}$ *such that* $\|u_\lambda\|_\infty \to 0$ *as* $\lambda \to E_{1,\mu}^+$ *and* $\|u_\lambda\|_\infty \to r_0$ *as* $\lambda \to \infty$.

Theorem 1.7. *Let $\Omega := B_R$ (ball centered at 0 with radius R) $\subset \mathbb{R}^N$; $N = 1, 2, 3$. If $M \approx 2$ and $K \gg 1$, then (1.9) has at least one positive solution for all $\lambda > E_{1,\mu}$ and three positive solutions for a certain range of λ.*

Finally, we consider the one-dimensional model:

$$\begin{cases} -u'' = \lambda\left(u - \frac{u^2}{K} - \frac{Mu^2}{1+u^2}\right);\ x \in (0,1), \\ -u'(0) + \sqrt{\lambda}u(0) = 0, \\ u'(1) + \sqrt{\lambda}u(1) = 0. \end{cases} \tag{1.10}$$

Here, for various values of K and M, we provide exact bifurcation diagrams for (1.10) via Theorem 2.3, namely, equations (2.3) and (2.4) in Chapter II and Mathematica computations. In particular, for certain K and M values, we show that the bifurcation diagrams of (1.10) are in fact exactly s-shaped. See Figure 17 for the exact bifurcation diagram for the case when $K = 30$ and $M = \frac{9}{5}$. For more bifurcation diagrams, see Chapter III.

Remark. Via Theorem 1.19, we note that all positive solutions of (1.10) are symmetric about $x = \frac{1}{2}$ (see and Figure 16).

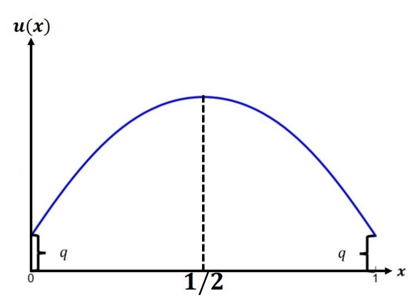

Figure 16. A Solution of (1.10).

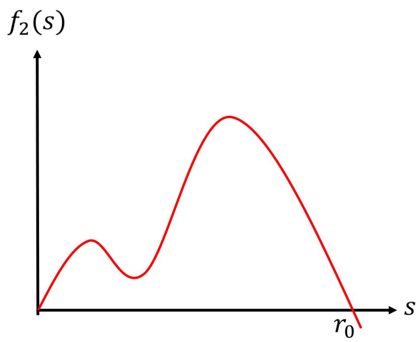

(a) $f(s) = f_2(s) = s - \frac{s^2}{30} - \frac{9s^2}{5+5s^2}$

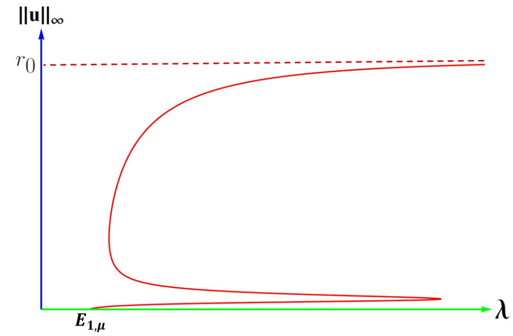

(b) Exact Bifurcation Diagram for (1.10) When $f = f_2$

Figure 17. Graph of $f = f_2$ and the Corresponding Exact Bifurcation Diagram for (1.10) When $\mu(s) = \sqrt{s}$.

1.2 Focus 2

Motivated by the study in [GMPS19], and to extend the study to a biologically more relevant emigration (positive minimum emigration) on the boundary, here we study the scaled logistic growth model:

$$\begin{cases} -\Delta u = \lambda u(1-u); \; x \in \Omega, \\ \frac{\partial u}{\partial \eta} + \gamma\sqrt{\lambda}[(A-u)^2 + \epsilon]u = 0; \; x \in \partial\Omega, \end{cases} \tag{1.11}$$

with U-shaped density dependent emigration on the boundary (see Figure 18), where $\epsilon > 0$ and $A \in (0,1)$ are parameters. Note that when $\alpha(s) = \frac{1}{1+(A-s)^2+\epsilon}$; $s \in [0,1]$ and $f(s) = s(1-s)$, (1.2) becomes (1.11).

Note that the minimum emigration is $\frac{\epsilon}{1+\epsilon}$. In [GMPS19] the authors studied the case when $\epsilon = 0$. However, ecologists have noted that, in general, the minimum emigration on the boundary is rarely zero ($\epsilon > 0$). Here, we focus on the case when

$\epsilon > 0$, and establish nonexistence, existence, uniqueness, and multiplicity results for (1.11).

Let $E_1(\gamma, D)$ be as described in (1.5). We establish the following results:

Theorem 1.8. *Let $\gamma > 0$ and $\epsilon > 0$. There is no positive solution of* (1.11) *for $\lambda \in (0, E_1(\gamma, \epsilon)]$.*

Theorem 1.9. *Let $\gamma > 0$ and $\epsilon > 0$. Then* (1.11) *has a positive solution for $\lambda > E_1(\gamma, A^2 + \epsilon)$.*

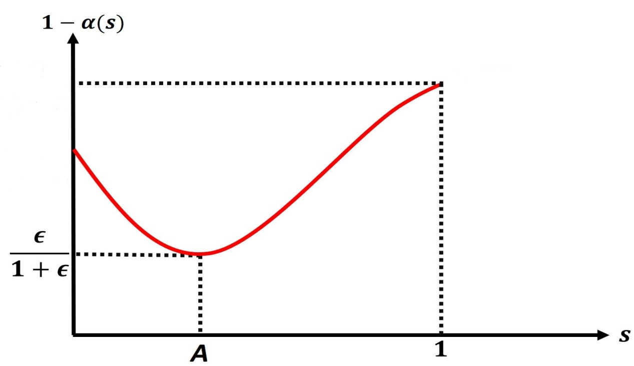

Figure 18. U-shaped Density Dependent Emigration with a Positive Minimum Emigration.

Next, we recall that for $\gamma > 0$ fixed, the boundary value problem:

$$\begin{cases} -\Delta w = \lambda w(1-w);\ x \in \Omega, \\ \frac{\partial w}{\partial \eta} + 2\gamma\sqrt{\lambda}(A-w)^2 w = 0;\ x \in \partial\Omega, \end{cases} \tag{1.12}$$

has a positive solution w_λ for $\lambda > 0$ such that $A < w_\lambda(x) \leq 1$ for $x \in \overline{\Omega}$, and this solution is unique (see [GMPS19]). We also note that w_λ is continuous with respect to λ and $E_1(\gamma, A^2) < E_1(\gamma, A^2+\epsilon) < E_1(\gamma, 2A^2)$ for $\epsilon \in (0, A^2)$ (see [GMRS18]). Let $w_\lambda^* := \min_{x\in\partial\Omega} w_\lambda(x)$ and $\delta_\gamma := \min_{\lambda\in[E_1(\gamma,A^2),E_1(\gamma,2A^2)]} (w_\lambda^* - A)^2$.

We establish the following result and remark which ensures a patch-level Allee effect.

Theorem 1.10. *Let $\gamma > 0$, $\epsilon_\gamma^* := \min\{\delta_\gamma, A^2\}$, and $\Gamma := \{u \in C^2(\Omega)\cap C^1(\overline{\Omega}) \mid u(x) \in [A,1]$ for $x \in \overline{\Omega}\}$. For each $\epsilon \in (0, \epsilon_\gamma^*)$, there exists $\lambda_* > 0$ such that, if $\lambda \in (\lambda_*, E_1(\gamma, A^2+\epsilon))$, then (1.11) has at least two positive solutions u_* and u^* such that $u_* \in \Gamma$ and $u^* \notin \Gamma$. In particular, in Γ, (1.11) has a unique solution and this solution is u_* (see Figure 19 for possible bifurcation diagrams).*

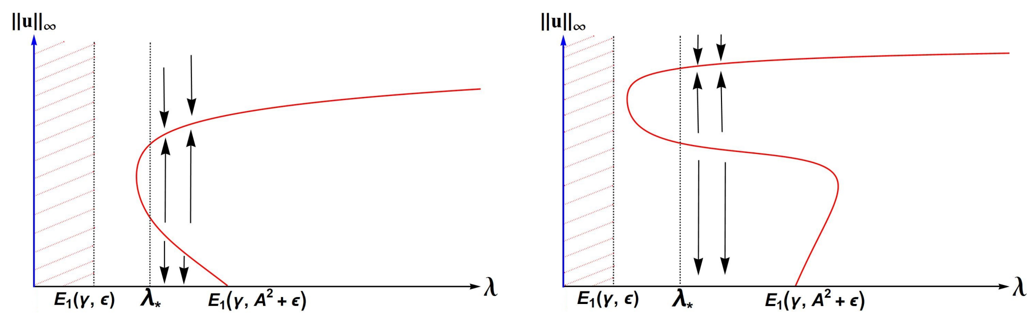

Figure 19. Bifurcation Diagrams for (1.11).

Remark. Note that the time dependent problem related to (1.11) is of the form:

$$\begin{cases} u_t = \frac{1}{\lambda}\Delta u + u(1-u);\ x \in \Omega,\ t > 0, \\ \frac{\partial u}{\partial \eta} + \gamma\sqrt{\lambda}[(A-u)^2+\epsilon]u = 0;\ x \in \partial\Omega,\ t > 0, \\ u(0,x) = u_0(x);\ x \in \Omega. \end{cases} \tag{1.13}$$

A solution u of (1.11) is called stable if for every $\epsilon > 0$ there exists $\delta > 0$ such that $\|v(t,.) - u\|_\infty < \epsilon$ for $t > 0$ whenever $\|u_0 - u\|_\infty < \delta$, where $v(t,x)$ is a solution of (1.13).

In addition, if there exists $\tilde{\delta} > 0$ such that when $\|u_0 - u\|_\infty < \tilde{\delta}$, $\|v(t,.) - u\|_\infty \longrightarrow 0$ as $t \longrightarrow \infty$, then u is called asymptotically stable. The solution u is called unstable if it is not stable. We note that the solution $u_* \in \Gamma$ in Theorem 1.10 is asymptotically stable (see Theorem 6.7 of Chapter 5 in [Pao92]). We also note that the trivial solution of (1.11) is asymptotically stable for $\lambda < E_1(\gamma, A^2 + \epsilon)$ and unstable for $\lambda > E_1(\gamma, A^2 + \epsilon)$ following the proof of Theorem 1.8 in [GS17]. In particular, when $\lambda \in (\lambda_*, E_1(\gamma, A^2 + \epsilon))$, if $\|u_0\|_\infty \approx 0$, then $\|v(t,.)\|_\infty \longrightarrow 0$ as $t \longrightarrow \infty$, while if $\|u_0 - u_*\|_\infty \approx 0$, then $\|v(t,.) - u_*\|_\infty \longrightarrow 0$ as $t \longrightarrow \infty$. Hence, there is a patch-level Allee effect for $\lambda \in (\lambda_*, E_1(\gamma, A^2 + \epsilon))$. See also [CC07] where the authors show existence of a patch-level Allee effect in a logistic growth model but with negative density dependent emigration. Note that with Dirichlet boundary conditions, a patch-level Allee effect does not occur for a logistic growth model. For more details on the discussion of a patch-level Allee effect, see [SS06].

Next we consider the case, when $\Omega = (0, 1)$. In this case, (1.11) reduces to the two-point boundary value problem:

$$\begin{cases} -u'' = \lambda u(1-u); \; x \in (0,1), \\ -u'(0) + \gamma\sqrt{\lambda}[(A - u(0))^2 + \epsilon]u(0) = 0, \\ u'(1) + \gamma\sqrt{\lambda}[(A - u(1))^2 + \epsilon]u(1) = 0. \end{cases} \tag{1.14}$$

We establish conditions that ensure the symmetry of positive solutions of (1.14) (see Figure 20). Namely, we prove:

Theorem 1.11. *If $\epsilon > \frac{A^2}{3}$ then all positive solutions of* (1.14) *are symmetric about $x = \frac{1}{2}$.*

Theorem 1.12. *If $\gamma \gg 1$ or $\gamma \approx 0$ then all positive solutions of* (1.14) *are symmetric.*

Finally, via Theorem 2.3, namely, equations (2.3) and (2.4) in Chapter II, for various values of A, ϵ, and γ, we obtain exact bifurcation diagrams for (1.14) via Mathematica computations. We also provide the evolution of bifurcation diagrams of (1.14) with respect to the effective matrix hostility parameter γ (see Figure 21), and we demonstrate the occurrence of non-symmetric solutions. Further, when $\epsilon \approx 0$, we note that the shapes of the bifurcation diagrams predicted in Theorem 1.10 are in fact exact (see Figure 21). Here, we provide a sample of bifurcation diagrams for (1.14) (see Figures 21 and 22). For more bifurcation diagrams, see Chapter IV.

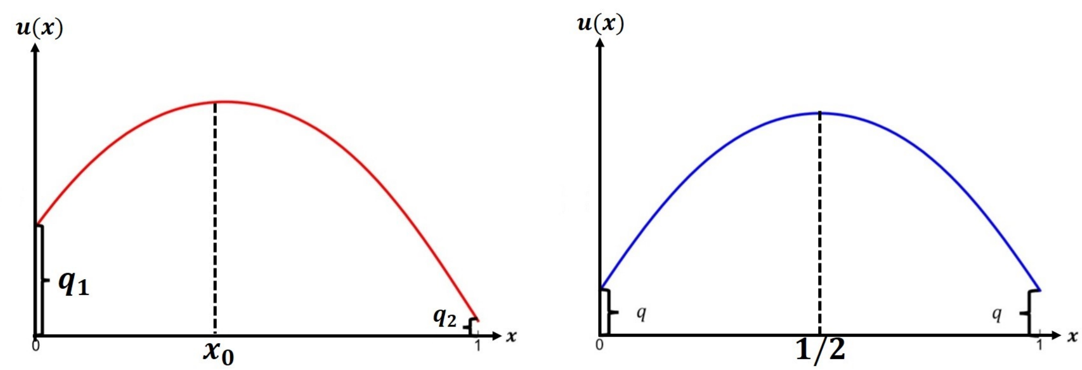

Figure 20. An Asymmetric Positive Solution of (1.14) (left) and a Symmetric Positive Solution of (1.14) (right).

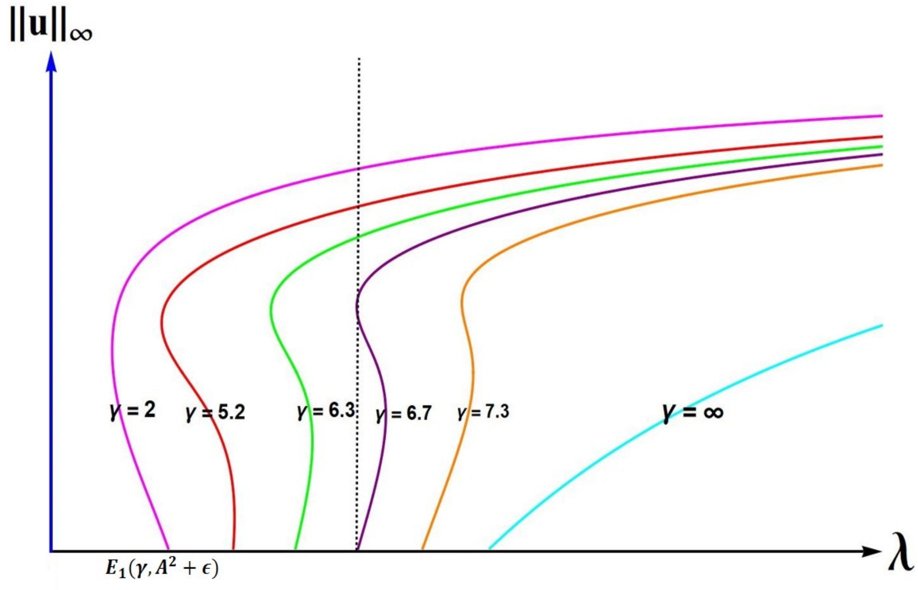

Figure 21. Evolution of Bifurcation Diagrams for (1.14) as γ Varies When $\epsilon = 0.1$ and $A = 0.5$.

1.3 Focus 3

Here, we study the weak Allee growth model:

$$\begin{cases} -\Delta u = \lambda f(u);\ x \in \Omega, \\ \frac{\partial u}{\partial \eta} + \gamma\sqrt{\lambda}[(A-u)^2 + \epsilon]u = 0;\ x \in \partial\Omega, \end{cases} \tag{1.15}$$

with U-shaped density dependent emigration on the boundary, where $\epsilon > 0$ is a parameter and $f(s) := \frac{1}{a}s(s+a)(1-s)$ represents a scaled weak Allee effect type growth of the population with $a \in (0,1)$ a parameter measuring the strength of the weak Allee effect (in the sense that per-capita growth rate is increasing for $s \in [0, \frac{1-a}{2})$). See [CC07], [CBG08], [Gro98], [JBR07], [Ama98], and [SS06] for studies on weak Allee models.

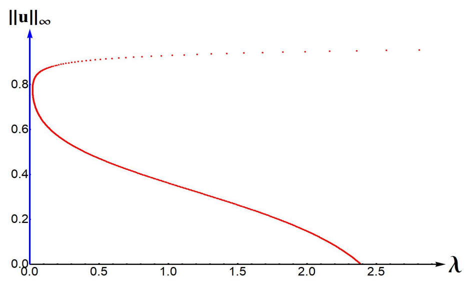

(a) $\gamma = 1$

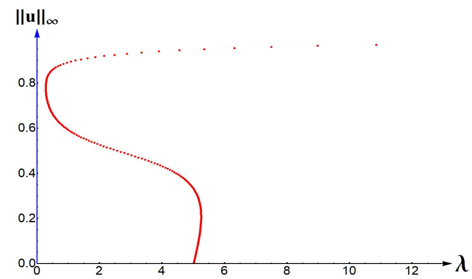

(b) $\gamma = 3$

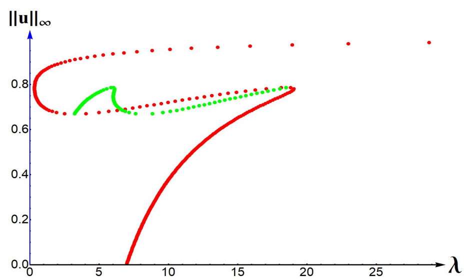

(c) $\gamma = 6$

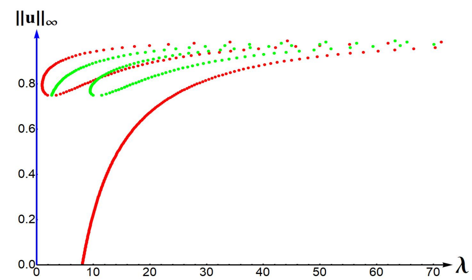

(d) $\gamma = 10$

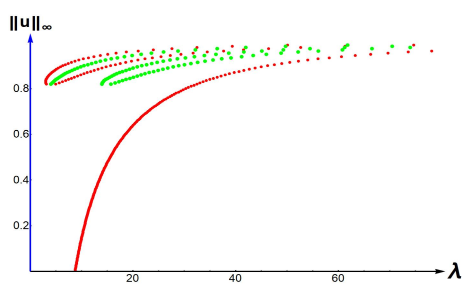

(e) $\gamma = 16$

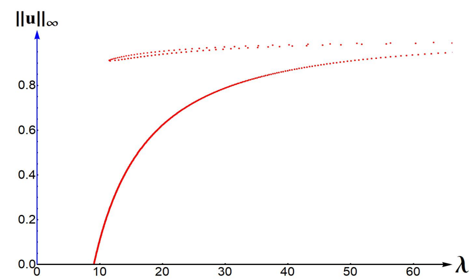

(f) $\gamma = 23$

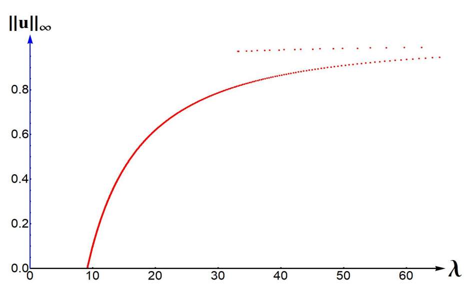

(g) $\gamma = 25$

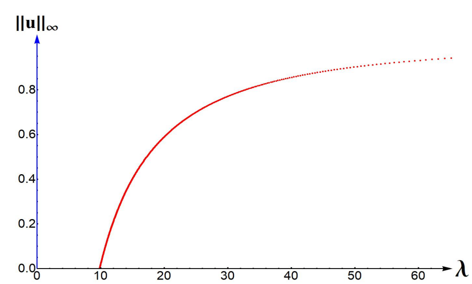

(h) $\gamma = \infty$

Figure 22. Bifurcation Diagrams for (1.14) for Several Values of γ, When $\epsilon = 0.01$ and $A = 0.8$. Symmetric Solutions are in Red and Non-symmetric Solutions are in Green.

Let $\overline{E}_1 := E_1(\gamma, A^2 + \epsilon)$. Our first task is to determine whether our solution set has *Property* $\mathcal{A}$, by which we mean:

<u>*Property* $\mathcal{A}$</u>

There exists $\overline{\lambda}(A, \gamma, \epsilon) < \overline{E}_1$ *such that* (1.15)

(1) *has at least one positive solution* u_λ *for* $\lambda \geq \overline{\lambda}$ *such that* $\|u_\lambda\|_\infty \longrightarrow 1$ *as* $\lambda \longrightarrow \infty$,

(2) *has at least two positive solutions for* $\lambda \in [\overline{\lambda}, \overline{E}_1)$, *and*

(3) *has no positive solutions for* $\lambda \approx 0$ *(see Figure* 23*).*

Clearly when *Property* $\mathcal{A}$ is satisfied the solution set exhibits a patch-level Allee effect for $\lambda \in [\overline{\lambda}, \overline{E}_1)$. We prove:

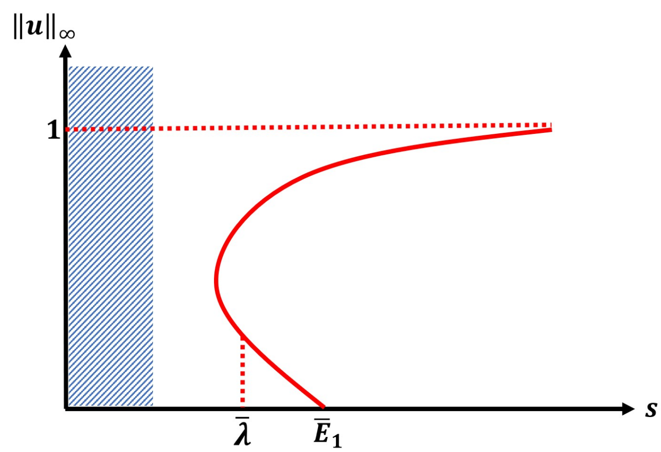

Figure 23. Bifurcation Diagram for the Solution Set of (1.15) Showing a Patch-level Allee Effect for $\lambda \in [\overline{\lambda}, \overline{E}_1)$.

Theorem 1.13. *Let $A \in (0,1)$, $\epsilon > 0$, and $\gamma > 0$. Then the solution set of* (1.15) *has Property $\mathcal{A}$.*

Next we establish a multiplicity result for a range of λ to the right of $\overline{E}_1$. Let A_1 be as in (1.6). We prove:

Theorem 1.14. *Let $\tilde{\lambda} > A_1$. Then there exists $\gamma^*(\tilde{\lambda})$ and, for $\gamma > \gamma^*$, $\epsilon^*(\tilde{\lambda}, \gamma) > 0$ such that* (1.15) *has at least three positive solutions for $\lambda \in [\overline{E}_1, \tilde{\lambda}]$ when $\epsilon < \epsilon^*$ (see Figure* 24).

Finally, we study the one-dimensional model:

$$\begin{cases} -u'' = \lambda \frac{1}{a} u(u+a)(1-u); \; x \in (0,1), \\ -u'(0) + \gamma\sqrt{\lambda}[(A - u(0))^2 + \epsilon]u(0) = 0, \\ u'(1) + \gamma\sqrt{\lambda}[(A - u(1))^2 + \epsilon]u(1) = 0, \end{cases} \tag{1.16}$$

using the quadrature method described in Theorem 2.3. We use equations (2.3) and (2.4) in Chapter II to obtain exact bifurcation diagrams for (1.16) via Mathematica computations. We also provide the evolution of bifurcation diagrams with respect to the effective matrix hostility parameter γ.

Remark.

(1) We note that the Theorems 1.11 - 1.12 remain valid for (1.16), as well.

(2) When $\epsilon = 0.084$, the hypothesis of Theorem 1.11 is satisfied and hence all positive solutions are symmetric. In this case, we note that the exact bifurcation diagram predicted via Theorem 1.13 occurs for each γ (see Figure 25).

(3) When $\epsilon = 0.01$, the hypothesis of Theorem 1.11 is not satisfied. In this case, we note that both symmetric and non-symmetric solutions occur for certain

γ values and the bifurcation diagrams corresponding to all solutions are more than that was predicted via Theorem 1.14 (see Figure 26).

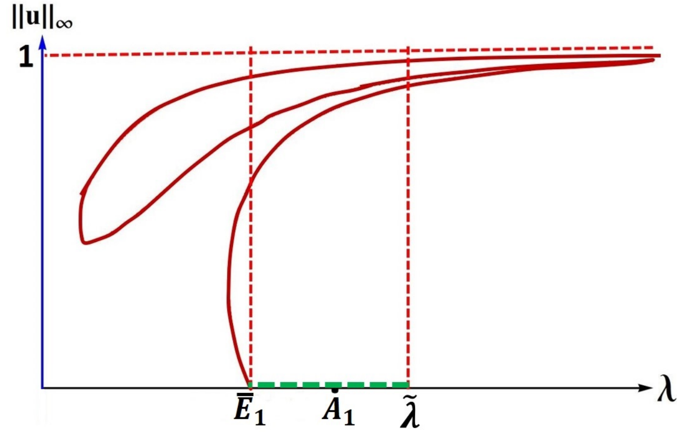

Figure 24. Bifurcation Diagram for the Solution Set of (1.15) for $\gamma \gg 1$ and $\epsilon \approx 0$.

Here, we provide a sample of bifurcation diagrams for (1.16) (see Figures 25 and 26). For more bifurcation diagrams, see Chapter V.

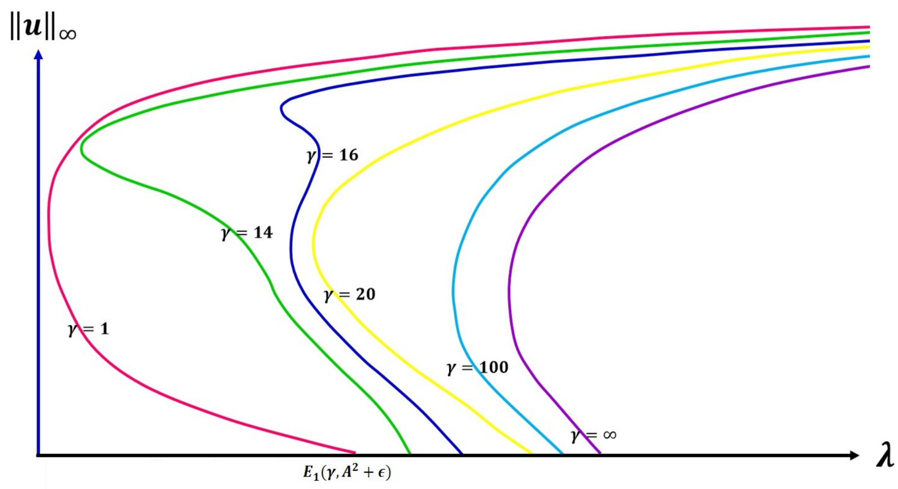

Figure 25. Evolution of the Bifurcation Diagrams for (1.16) as γ Varies, When $\epsilon = 0.084$ and $A = 0.5$.

1.4 Focus 4

We study the one dimensional weak Allee growth model:

$$\begin{cases} u_t = \frac{1}{\lambda}u_{xx} + f(u);\ t > 0,\ x \in \Omega_0, \\ \frac{\partial u}{\partial \eta} + \sqrt{\lambda}\gamma g(u)u = 0;\ t > 0,\ x \in \partial\Omega_0, \\ u(0, x) = u_0(x);\ x \in \Omega_0, \end{cases} \tag{1.17}$$

with corresponding steady state equation:

$$\begin{cases} -u'' = \lambda f(u);\ x \in (0, 1), \\ -u'(0) + \sqrt{\lambda}\gamma g(u(0))u(0) = 0, \\ u'(1) + \sqrt{\lambda}\gamma g(u(1))u(1) = 0, \end{cases} \tag{1.18}$$

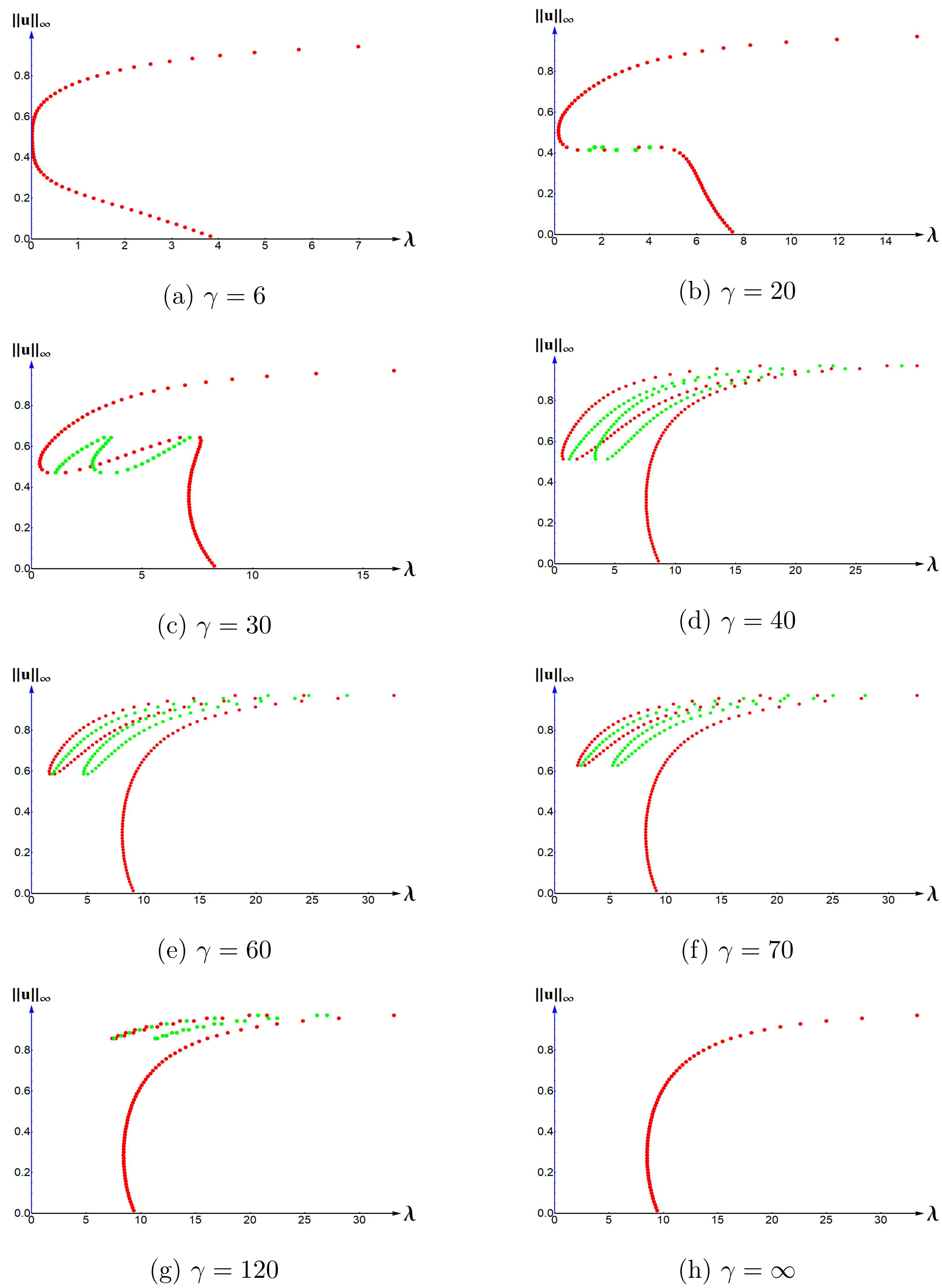

(a) $\gamma = 6$ (b) $\gamma = 20$

(c) $\gamma = 30$ (d) $\gamma = 40$

(e) $\gamma = 60$ (f) $\gamma = 70$

(g) $\gamma = 120$ (h) $\gamma = \infty$

Figure 26. Bifurcation Diagrams for (1.16) for Several Values of γ, When $\epsilon = 0.01$ and $A = 0.5$. Symmetric Solutions are in Red and Non-symmetric Solutions are in Green.

where $\Omega_0 = (0,1)$, g is as defined in (1.3), and f is as defined in (1.15). Here, we treat five different forms of emigration. Namely, we study density independent emigration (DIE), positive density dependent emigration (+DDE), negative density dependent emigration (-DDE), U-shaped density dependent emigration (UDDE), and hump-shaped density dependent emigration (hDDE).

We next choose prototypical functions for the five most common DDE forms reported in the recent literature review in [HGSC20].

In order to remain consistent in choosing these forms, we employ a single $\alpha(u)$ template and it's mirror image, namely

$$\begin{aligned} \alpha_1(u) &:= \frac{M_1}{2M_1 + m(u)}, \\ \alpha_2(u) &:= 1 - \alpha_1(u) = \frac{M_1 + m(u)}{2M_1 + m(u)}, \end{aligned} \tag{1.19}$$

where $M_1 > 0$ and $m(u) \geq 0$ with $m(0) = 0$ are appropriately chosen to model a given DDE form. Note that the emigration rate at zero will be the same across all forms, i.e. $1 - \alpha_i(0) = 0.5$, $i = 1, 2$. Table 1 lists the exact $m(u)$'s that were chosen to model the five DDE forms (also, see Figure 27).

We state and prove several mathematical results that will aid in the study of the model (1.17). First, we consider the stability of the trivial steady state, $u(x) \equiv 0$, of (1.17). Let $E_1(\gamma, 1)$ be the principal eigenvalue of the boundary value problem:

$$\begin{cases} -\phi'' = E\phi; \ x \in (0,1), \\ -\phi'(0) + \gamma\sqrt{E}g(0)\phi(0) = 0, \\ \phi'(1) + \gamma\sqrt{E}g(0)\phi(1) = 0. \end{cases} \tag{1.20}$$

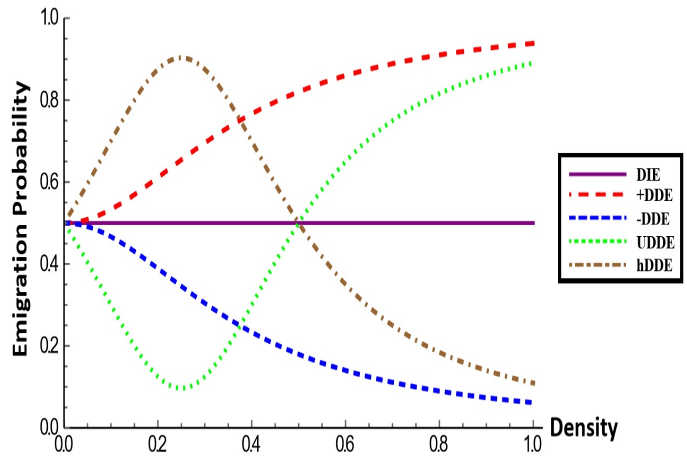

Figure 27. Graph of Density vs Emigration Probability for DIE, +DDE, -DDE, UDDE, and hDDE.

Table 1. Listing of the Five DDE Forms. The Parameter Combination $M_1M_2 > 0$ Controls the Shape of the DDE Form by Affecting the Concavity/convexity of the Form, Whereas, $M_3 \in (0, 1)$ is the Location of the Minimal and Maximal Emigration Probabilities for UDDE and hDDE, Respectively.

DDE Form	$\boldsymbol{m(u)}$	$\boldsymbol{\alpha(u)}$	$\boldsymbol{g(u)}$	**Restrictions**
DIE	$m(u) \equiv 0$	0.5	1	none
+DDE	$m(u) = \frac{u^2}{M_2}$	$\frac{M_1M_2}{2M_1M_2+u^2}$	$\frac{M_1M_2+u^2}{M_1M_2}$	none
-DDE	$m(u) = \frac{u^2}{M_2}$	$\frac{M_1M_2+u^2}{2M_1M_2+u^2}$	$\frac{M_1M_2}{M_1M_2+u^2}$	none
UDDE	$m(u) = \frac{u^2-2M_3u}{M_2}$	$\frac{M_1M_2}{2M_1M_2+u^2-2M_3u}$	$\frac{M_1M_2+u^2-2M_3u}{M_1M_2}$	$M_1M_2 > M_3^2$
hDDE	$m(u) = \frac{u^2-2M_3u}{M_2}$	$\frac{M_1M_2+u^2-2M_3u}{2M_1M_2+u^2-2M_3u}$	$\frac{M_1M_2}{M_1M_2+u^2-2M_3u}$	$M_1M_2 > M_3^2$

We now state the following theorem which connects $E_1(\gamma, 1)$ to the stability of $u(x) \equiv 0$. Namely, we prove:

Theorem 1.15. *The trivial solution of* (1.18) *is asymptotically stable if* $\lambda < E_1(\gamma, 1)$, *and it is unstable if* $\lambda > E_1(\gamma, 1)$.

We recall the following results from [GMPS19] and [GS17]:

Lemma 1.16. *[GS17] Let* σ_1 *be the principal eigenvalue of the linearized equation associated with* (1.18), *namely*

$$\begin{cases} -\phi'' - \lambda f_u(u)\phi = \sigma\phi; \ x \in (0,1), \\ -\phi'(0) + \gamma\sqrt{\lambda}[g_u(u(0))u(0) + g(u(0))]\phi(0) = \sigma\phi(0), \\ \phi'(1) + \gamma\sqrt{\lambda}[g_u(u(1))u(1) + g(u(1))]\phi(1) = \sigma\phi(1), \end{cases} \tag{1.21}$$

where u *is any solution of* (1.18). *Then the following hold.*

a) If $\sigma_1 > 0$, *then* u *is stable. Furthermore, if* u *is isolated then it is asymptotically stable.*

b) If $\sigma_1 < 0$, *then* u *is unstable.*

Lemma 1.17. *[GMPS19] Let* u *be a solution of* (1.18) *and* σ_1^* *be the principal eigenvalue of the following boundary value problem*

$$\begin{cases} -\phi'' - \lambda f_u(u)\phi = \sigma\phi; \ x \in (0,1), \\ -\phi'(0) + \gamma\sqrt{\lambda}[g_u(u(0))u(0) + g(u(0))]\phi(0) = 0, \\ \phi'(1) + \gamma\sqrt{\lambda}[g_u(u(1))u(1) + g(u(1))]\phi(1) = 0. \end{cases} \tag{1.22}$$

Then, $sign(\sigma_1^*) = sign(\sigma_1)$ *for* $\sigma_1^*, \sigma_1 \neq 0$.

In the light of Lemma 1.17, it suffices to study the relationship between σ_1^* and λ in order to prove Theorem 1.15.

The next result gives a sufficient condition for the model (1.17) to exhibit a patch-level Allee effect which only requires knowledge of the existence of a positive steady state of (1.17) and not its stability properties.

Theorem 1.18. *Let $\gamma > 0$ and $a \in (0,1)$ be given. If (1.17) has at least one positive steady state for $\lambda < E_1(\gamma, 1)$, then the model (1.17) will exhibit a patch-level Allee effect if the patch size is $\ell = \sqrt{\frac{\lambda D}{r}}$.*

We now establish sufficient conditions for all positive steady states of the model (1.17) to be symmetric (see Figure 28). Namely, we establish:

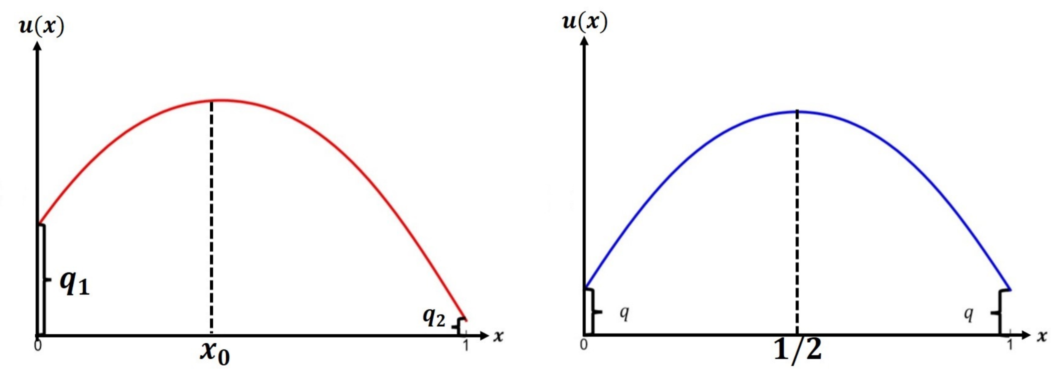

Figure 28. Density Profile of an Asymmetric Positive Steady State of (1.17) (left) and Symmetric Positive Steady State of (1.17) (right).

Theorem 1.19. *If $h(s) := g(s)s$ is increasing for all $s > 0$ then every positive solution of (1.18) is symmetric about $x = \frac{1}{2}$.*

Theorem 1.20. *Let $m(s) \geq 0$ for $s \geq 0$.*

(a) If $\alpha(u) = \alpha_1(u) = \frac{M_1}{2M_1 + m(u)}$, then

(i) if $m(s) \equiv 0$ *(DIE) then all positive solutions of* (1.18) *are symmetric.*

(ii) if $m'(s) \geq 0$ *(+DDE) then all positive solutions of* (1.18) *are symmetric.*

(iii) if $m(s) = \frac{s^2 - 2M_3 s}{M_2}$ *(UDDE) and* $M_1 M_2 > \frac{4M_3^2}{3}$ *then all positive solutions of* (1.18) *are symmetric.*

(b) If $\alpha(u) = \alpha_2(u) = \frac{M_1 + m(u)}{2M_1 + m(u)}$*, then*

(i) if $m(s) = \frac{s^2}{M_2}$ *(-DDE) and* $M_1 M_2 > 1$ *then all positive solutions of* (1.18) *are symmetric.*

(ii) if $m(s) = \frac{s^2 - 2M_3 s}{M_2}$ *(hDDE) and* $M_1 M_2 > 1$ *then all positive solutions of* (1.18) *are symmetric.*

Finally, we use the quadrature method described in Theorem 2.3 in Chapter II to obtain exact bifurcation diagrams for (1.18) via Mathematica computations. We provide an evolution of the structure of positive steady states of (1.17) as γ is varied. We also provide an analysis of the Allee effect region (AER) by which we mean the range of λ for which a Patch-Level Allee Effect will occur $(\lambda_m, E_1(\gamma, 1))$, where λ_m is the minimum patch size needed for the population to survive (see Figure 29). Namely, we study the variation of the AER length, $E_1(\gamma, 1) - \lambda_m$, with respect to the effective matrix hostility parameter for the five emigration types. Then, we numerically show that a +DDE can counteract a patch-level Allee effect. Here, we provide several numerical results obtained. Namely, we provide the variation of AER length with respect to γ for five emigration types, the region where a patch-level Allee effect is present on the $\gamma - M_1 M_2$ plane, and some bifurcation diagrams (see Figures 30, 31, and 32). More details will be provided in Chapter VI.

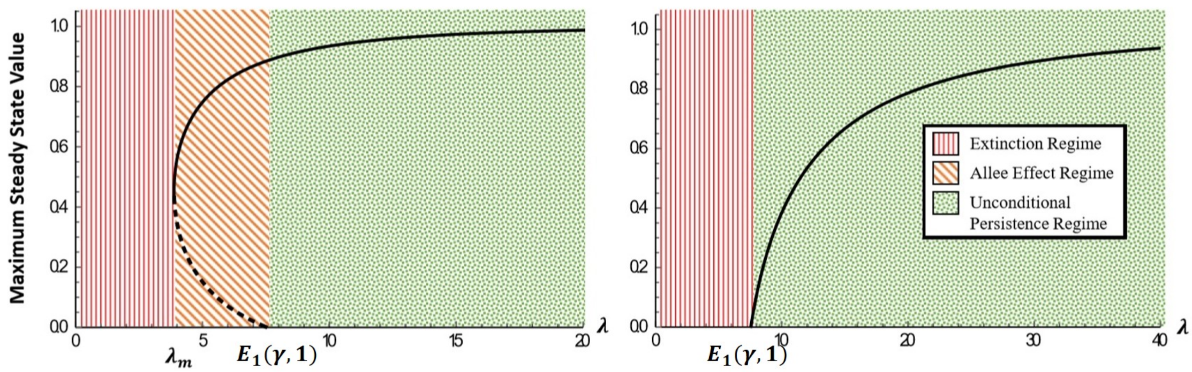

Figure 29. Bifurcation-stability Curves of Population Persistence with λ Proportional to Patch Size Squared. In These Diagrams, the Population Shows a Patch-level Allee effect (left) and No Patch-level Allee Effect (right). Solid Curves Correspond to Stable Steady States and Dashed Curves Correspond to Unstable Steady States. Note that the Trivial Steady State is Stable to the Left of $E_1(\gamma, 1)$ and Unstable to the Right of $E_1(\gamma, 1)$.

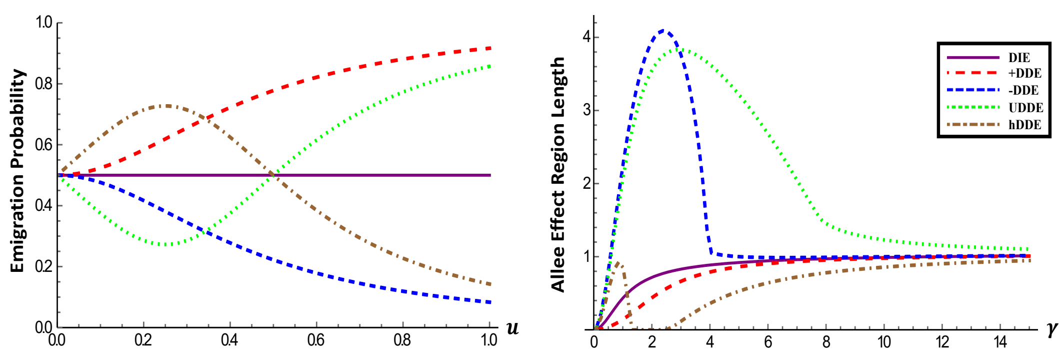

Figure 30. Graph of u vs Emigration Probability (left) and γ vs AER Length (right) for $M_1M_2 = 0.1, M_3 = 0.25$, and $a = 0.5$.

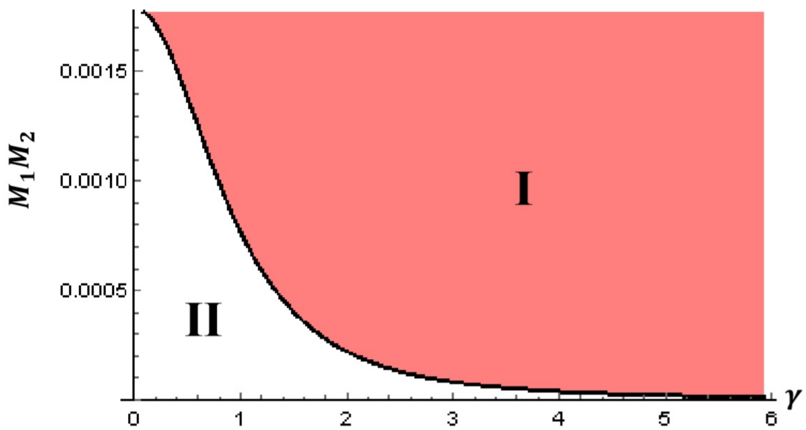

Figure 31. The Model Predicts a Patch-level Allee Effect for Parameters in Region I and No Patch-level Allee Effect in Region II. Note that $a = 0.9$ Indicating a Mild Weak Allee Effect in Per-capita Growth Rate, whereas, Small Values of $M_1 M_2$ Cause a Very Rapid Ascent for the Emigration Probability from 0.5 to Close to 1.

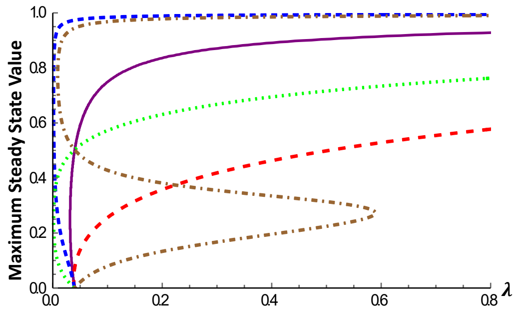

(a) $\gamma = 0.1$

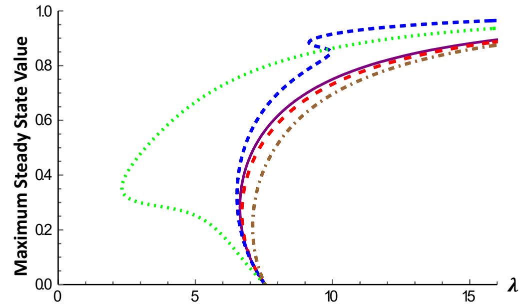

(b) $\gamma = 5$

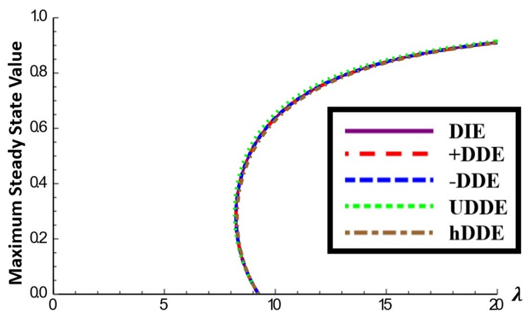

(c) $\gamma = 20$

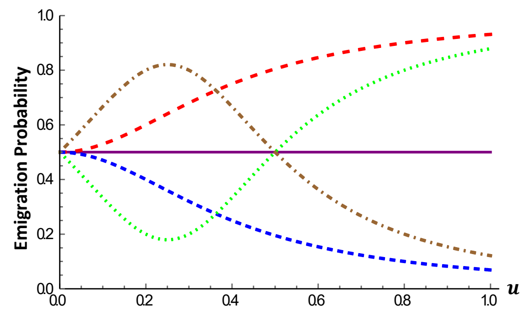

(d) Graph of u vs emigration probability

Figure 32. Bifurcation Curves of Positive Solutions of (1.18) for All Five DDE Forms When $a = 0.5$, $M_1M_2 = 0.08$, and $M_3 = 0.25$ for Various γ-values. This Choice of M_1, M_2, and M_3 Yield DDE Forms That are Quite Different in Shape From the DIE Form, and an M_3-value of 0.25 Causes the Minimum Emigration Probability and Maximum Emigration Probability of UDDE and hDDE, Respectively, to Both Occur at $u = 0.25$.

1.5 Focus 5

Here, our focus is to numerically study, the following models when $N = 2$:

$$\begin{cases} -\Delta u = \lambda u(1-u);\ x \in \Omega, \\ \frac{\partial u}{\partial \eta} + \gamma\sqrt{\lambda}u = 0;\ x \in \partial\Omega, \end{cases} \tag{1.23}$$

$$\begin{cases} -\Delta u = \lambda u(1-u);\ x \in \Omega, \\ \frac{\partial u}{\partial \eta} + \gamma\sqrt{\lambda}[(A-u)^2 + \epsilon]u = 0;\ x \in \partial\Omega, \end{cases} \tag{1.24}$$

where ϵ, A are as defined in (1.11) and $\Omega := (0,1) \times (0,1)$. Note that we treat both the cases $\epsilon = 0$ and $\epsilon > 0$ for (1.24). We numerically obtain the bifurcation diagrams for (1.23) and (1.24) and study the evolution of bifurcation curves with respect to the effective matrix hostility parameter γ. In the higher dimensional case, there are no explicit methods to completely characterize solutions, as in the one dimensional case When using a quadrature method. These results are obtained via finite element methods and Matlab computations. We also note that the bifurcation diagrams predicted in [FGM$^+$] and [GMPS19] are exact in this case. Figures 33 and 34 provide a sample of bifurcation diagrams obtained. For more bifurcation diagrams, see Chapter VII.

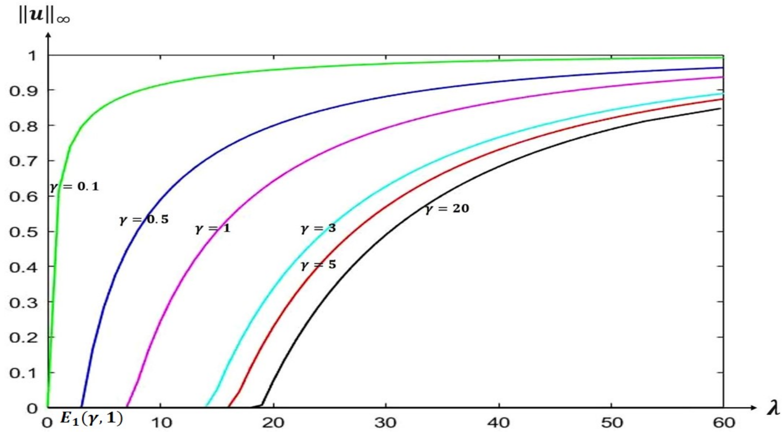

Figure 33. Evolution of Bifurcation Diagrams of (1.23) with Respect to γ.

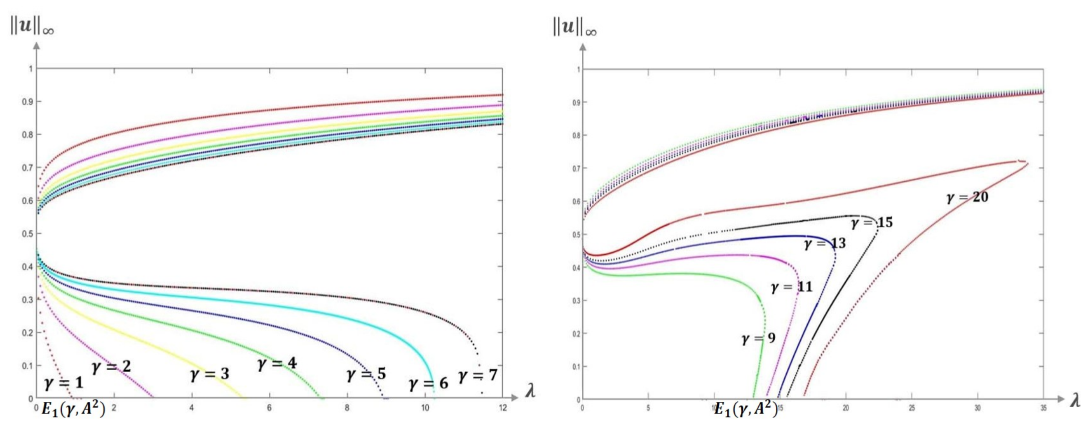

Figure 34. Evolution of Bifurcation Diagrams of (1.24) with Respect to γ When $A = 0.5$ and $\epsilon = 0$.

CHAPTER II

PRELIMINARIES

2.1 Method of Sub-Super Solutions

Consider the boundary value problem:

$$\begin{cases} -\Delta u = \lambda f(u); \; x \in \Omega, \\ \frac{\partial u}{\partial \eta} + \mu(\lambda) g(u) u = 0; \; x \in \partial\Omega, \end{cases} \tag{2.1}$$

where f, g are continuous functions, and $\mu \in C([0, \infty))$ is an increasing function such that $\mu(0) \geq 0$. We first introduce definitions of a (strict) subsolution and a (strict) supersolution of (2.1), and state a sub-supersolution theorem and a three solution theorem that are used to prove existence and multiplicity results for positive solutions. By a subsolution of (2.1) we mean $\psi \in C^2(\Omega) \cap C^1(\overline{\Omega})$ that satisfies

$$\begin{cases} -\Delta \psi \leq \lambda f(\psi); \; x \in \Omega, \\ \frac{\partial \psi}{\partial \eta} + \mu(\lambda) g(\psi) \psi \leq 0; \; x \in \partial\Omega. \end{cases}$$

By a supersolution of (2.1) we mean $Z \in C^2(\Omega) \cap C^1(\overline{\Omega})$ that satisfies

$$\begin{cases} -\Delta Z \geq \lambda f(Z); \; x \in \Omega, \\ \frac{\partial Z}{\partial \eta} + \mu(\lambda) g(Z) Z \geq 0; \; x \in \partial\Omega. \end{cases}$$

By a strict subsolution of (2.1) we mean a subsolution which is not a solution. By a strict supersolution of (2.1) we mean a supersolution which is not a solution. Then the following results hold (see [Ama76], [Ink82], and [Shi87]):

Lemma 2.1. *Let ψ and Z be a subsolution and a supersolution of* (2.1) *respectively such that $\psi \leq Z$. Then* (2.1) *has a solution u such that $u \in [\psi, z]$.*

Lemma 2.2. *Let $\underline{u}_1$ and $\overline{u}_2$ be a subsolution and a supersolution of* (2.1) *respectively such that $\underline{u}_1 \leq \overline{u}_2;\ x \in \Omega$. Let $\underline{u}_2$ and $\overline{u}_1$ be a strict subsolution and a strict supersolution of* (2.1) *respectively such that $\overline{u}_1, \underline{u}_2 \in [\underline{u}_1, \overline{u}_2]$ and $\underline{u}_2 \not\leq \overline{u}_1; x \in \Omega$. Then* (2.1) *has at least three solutions u_1, u_2 and u_3 where $u_i \in [\underline{u}_i, \overline{u}_i];\ i = 1, 2$ and $u_3 \in [\underline{u}_1, \overline{u}_2] \backslash ([\underline{u}_1, \overline{u}_1] \cup [\underline{u}_2, \overline{u}_2])$.*

2.2 Quadrature Method and the Proof of Theorem 2.3

Adapting the quadrature method discussed in [Lae71], we first briefly explain a method to analyze the structure of the positive solutions to:

$$\begin{cases} -u'' = \lambda f(u);\ x \in (0,1), \\ -u'(0) + \sqrt{\lambda}\gamma g(u(0))u(0) = 0, \\ u'(1) + \sqrt{\lambda}\gamma g(u(1))u(1) = 0. \end{cases} \tag{2.2}$$

Namely, the following result will allow us to study the structure of positive solutions of (2.2) as the parameters λ and γ vary.

Theorem 2.3. *A positive solution, $u(x)$, of* (2.2) *with $u(x_0) = ||u||_\infty = \rho$, $q_1 = u(0)$, and $q_2 = u(1)$ exists if and only if $\lambda > 0$, $\rho \in (0,1)$, and $q_1, q_2 \in [0, \rho)$ satisfy:*

$$\lambda = \frac{1}{2}\Big(\int_{q_1}^{\rho} \frac{ds}{\sqrt{F(\rho)-F(s)}} + \int_{q_2}^{\rho} \frac{ds}{\sqrt{F(\rho)-F(s)}} \Big)^2, \tag{2.3}$$

and

$$\begin{aligned} 2[F(\rho) - F(q_1)] &= \gamma^2 q_1^2 [g(q_1)]^2, \\ 2[F(\rho) - F(q_2)] &= \gamma^2 q_2^2 [g(q_2)]^2, \end{aligned} \tag{2.4}$$

where $F(s) = \int_0^s f(t)dt$*. Further,* x_0 *is given by*

$$x_0 = \frac{\int_{q_1}^{\rho} \frac{ds}{\sqrt{F(\rho)-F(s)}}}{\int_{q_1}^{\rho} \frac{ds}{\sqrt{F(\rho)-F(s)}} + \int_{q_2}^{\rho} \frac{ds}{\sqrt{F(\rho)-F(s)}}}.$$

Remark. For $\rho \in (0, 1)$, since $f(\rho) > 0$, it can be shown that the improper integral in (2.3) is convergent.

See Figure 35 for an illustration of a prototypical positive solution of (2.2). We now provide a proof of Theorem 2.3.

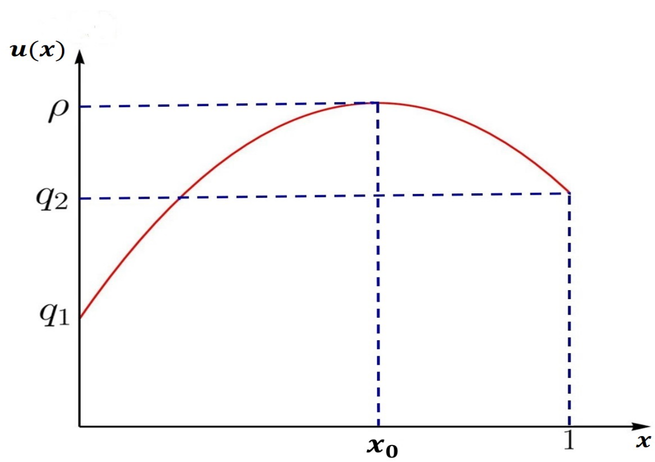

Figure 35. Shape of a Positive Solution of (2.2) When $q_1 \neq q_2$.

Proof of Theorem 2.3: Assume that $u(x)$ is a positive solution to (2.2) with $\rho := ||u||_\infty$, $q_1 := u(0)$, and $q_2 := u(1)$. Since (2.2) is an autonomous differential equation, if there exists an $x_0 \in (0,1)$ such that $u'(x_0) = 0$ then $v(x) := u(x_0 + x)$ and $w(x) := u(x_0 - x)$ will both satisfy the initial value problem:

$$\begin{cases} -z'' = \lambda f(z), \\ z(0) = u(x_0), \\ z'(0) = 0, \end{cases} \tag{2.5}$$

for all $x \in [0, d)$ with $d = \min\{x_0, 1 - x_0\}$. Picard's existence and uniqueness theorem asserts that $u(x_0 + x) \equiv u(x_0 - x)$. Hence, $u(x)$ must be symmetric about x_0, $u'(x) \geq 0;\ [0, x_0]$, and $u'(x) \leq 0;\ [x_0, 1]$. Multiplying both sides of (2.2) by u' we obtain

$$-u''u' = \lambda f(u)u'. \tag{2.6}$$

Integrating both sides gives

$$-\frac{[u'(x)]^2}{2} = \lambda F(u(x)) + C;\ x \in [0, 1]. \tag{2.7}$$

Substituting $x = x_0$, $x = 0$, and $x = 1$ into (2.7) gives

$$C = -\lambda F(\rho), \tag{2.8}$$

$$C = -\lambda F(q_1) - \lambda \frac{\gamma^2 g^2(q_1) q_1^2}{2}, \tag{2.9}$$

$$C = -\lambda F(q_2) - \lambda \frac{\gamma^2 g^2(q_2) q_2^2}{2}. \tag{2.10}$$

Combining (2.8) with (2.9) and (2.10) we have

$$F(\rho) = F(q_1) + \frac{\gamma^2 g^2(q_1) q_1^2}{2}, \tag{2.11}$$

$$F(\rho) = F(q_2) + \frac{\gamma^2 g^2(q_2) q_2^2}{2}. \tag{2.12}$$

Now substitution of (2.8) into (2.7) yields

$$\frac{[u'(x)]^2}{2} = \lambda \left[F(\rho) - F(u(x))\right]; \; x \in [0,1]. \tag{2.13}$$

Solving for $u'(x)$ in (2.13) and using the fact that $u'(x) > 0; \; [0, x_0)$ and $u'(x) < 0; \; (x_0, 1]$ we have

$$u'(x) = \sqrt{2\lambda}\sqrt{F(\rho) - F(u(x))}; \; x \in [0, x_0], \tag{2.14}$$

$$u'(x) = -\sqrt{2\lambda}\sqrt{F(\rho) - F(u(x))}; \; x \in [x_0, 1]. \tag{2.15}$$

Integration of (2.14) from 0 to x and (2.15) from x_0 to x yields

$$\int_0^x \frac{u'(s)ds}{\sqrt{F(\rho) - F(u(s))}} = \sqrt{2\lambda}x; \; x \in [0, x_0], \tag{2.16}$$

$$\int_{x_0}^x \frac{u'(s)ds}{\sqrt{F(\rho) - F(u(s))}} = -\sqrt{2\lambda}(x - x_0); \; x \in [x_0, 1]. \tag{2.17}$$

Through a change of variables and using the fact that $u(0) = q_1$ and $u(x_0) = \rho$ we have

$$\int_{q_1}^{u(x)} \frac{dt}{\sqrt{F(\rho) - F(t)}} = \sqrt{2\lambda}x; \; x \in [0, x_0], \tag{2.18}$$

$$\int_{\rho}^{u(x)} \frac{dt}{\sqrt{F(\rho)-F(t)}} = -\sqrt{2\lambda}(x-x_0);\ x \in [x_0, 1]. \tag{2.19}$$

Substituting $x = x_0$ into (2.18) and $x = 1$ into (2.19) gives

$$\int_{q_1}^{\rho} \frac{dt}{\sqrt{F(\rho)-F(t)}} = \sqrt{2\lambda}x_0, \tag{2.20}$$

$$\int_{\rho}^{q_2} \frac{dt}{\sqrt{F(\rho)-F(t)}} = -\sqrt{2\lambda}(1-x_0). \tag{2.21}$$

Now subtraction of (2.21) from (2.20) yields

$$\lambda = \frac{1}{2}\Big(\int_{q_1}^{\rho} \frac{ds}{\sqrt{F(\rho)-F(s)}} + \int_{q_2}^{\rho} \frac{ds}{\sqrt{F(\rho)-F(s)}}\Big)^2. \tag{2.22}$$

From (2.20) and (2.22), it is clear that

$$x_0 = \frac{\int_{q_1}^{\rho} \frac{ds}{\sqrt{F(\rho)-F(s)}}}{\int_{q_1}^{\rho} \frac{ds}{\sqrt{F(\rho)-F(s)}} + \int_{q_2}^{\rho} \frac{ds}{\sqrt{F(\rho)-F(s)}}}.$$

Next assume $\lambda > 0,\ \rho \in (0,1)$, and $q_1, q_2 \in [0, \rho)$ satisfy (2.3) and (2.4). Define $u(x) : [0,1] \to \mathbb{R}$ by

$$\int_{q_1}^{u(x)} \frac{dt}{\sqrt{F(\rho)-F(t)}} = \sqrt{2\lambda}x;\ x \in [0, x_0], \tag{2.23}$$

$$\int_{\rho}^{u(x)} \frac{dt}{\sqrt{F(\rho)-F(t)}} = -\sqrt{2\lambda}(x-x_0);\ x \in [x_0, 1]. \tag{2.24}$$

We will now show that $u(x)$ is a positive solution to (2.2). It is easy to see that the turning point given by $x_0 = \frac{1}{\sqrt{2\lambda}} \int_{q_1}^{\rho} \frac{dt}{\sqrt{F(\rho)-F(t)}}$ is unique for fixed λ, q_1, and ρ values.

The function

$$\frac{1}{\sqrt{2\lambda}}\int_{q_1}^{u}\frac{dt}{\sqrt{F(\rho)-F(t)}},$$

is a differentiable function of u which is strictly increasing from 0 to x_0 as u increases from q_1 to ρ. Thus, for each $x \in [0, x_0]$, there is a unique $u(x)$ such that

$$\int_{q_1}^{u(x)}\frac{dt}{\sqrt{F(\rho)-F(t)}} \;=\; \sqrt{2\lambda}x. \tag{2.25}$$

Moreover, by the Implicit Function theorem, $u(x)$ is differentiable with respect to x. Differentiating (2.25) gives

$$u'(x) \;=\; \sqrt{2[F(\rho)-F(u(x))]};\; x \in (0, x_0]. \tag{2.26}$$

Through a similar argument, $u(x)$ is a differentiable, decreasing function of x for $x \in (x_0, 1)$ with

$$u'(x) \;=\; -\sqrt{2[F(\rho)-F(u(x))]};\; x \in [x_0, 1). \tag{2.27}$$

This implies that we have

$$\frac{-\left[u'(x)\right]^2}{2} \;=\; F(\rho)-F(u(x));\; x \in (0,1).$$

Differentiating again, we have

$$-u''(x) = f(u(x));\; x \in (0,1).$$

Thus, $u(x)$ satisfies the differential equation in (2.2). It only remains to be seen that $u(x)$ satisfies the boundary conditions in (2.2). However, from (2.23) and (2.24) it is clear that $u(0) = q_1$ and $u(1) = q_2$. Since q_1 is a solution of (2.11), we have

$$F(\rho) - F(q_1) = \frac{\gamma^2 g^2(q_1) q_1^2}{2}. \tag{2.28}$$

Substituting $x = 0$ into (2.26) gives

$$u'(0) = \sqrt{2\lambda}\sqrt{F(\rho) - F(q_1)}. \tag{2.29}$$

Combining (2.28) and (2.29) we have

$$u'(0) = \sqrt{\lambda}\gamma g(q_1) q_1.$$

A similar argument shows that

$$u'(1) = -\sqrt{\lambda}\gamma g(q_2) q_2.$$

Hence, $u(x)$ satisfies (2.2) and the proof is complete.

2.3 Finite Element Method for Computing the Numerical Solutions

Here, we provide the variational formulation and a finite element method (see [BS02] and [Cia78]) that we will be using to obtain the numerical solution of (2.1). We restrict our numerical study to the case when $\mu(s) := \sqrt{s}$.

2.3.1 Variational Formulation

Let $V := H^1(\Omega) = \{v \in L_2(\Omega) \mid \nabla v \in L_2(\Omega)\}$, where $\Omega := (0,1) \times (0,1) \subset \mathbb{R}^2$. Then we take any $v \in V$ and multiply both sides of (2.1) by v to obtain

$$(-\Delta u)v = \lambda f(u)v.$$

Then by integration by parts we obtain

$$\int_{\Omega} \nabla u \cdot \nabla v dx - \int_{\partial\Omega} \frac{\partial u}{\partial \eta} v ds = \lambda \int_{\Omega} f(u) v dx.$$

Now the boundary conditions implies that

$$\int_{\Omega} \nabla u \cdot \nabla v dx + \gamma\sqrt{\lambda} \int_{\partial\Omega} u g(u) v ds = \lambda \int_{\Omega} f(u) v dx \qquad \forall v \in V. \tag{2.30}$$

The solution u of (2.30) is generally unknown and thus the numerical solution becomes important. In our study, we take our domain Ω to be the unit square in $\mathbb{R}^2$. Given a triangulation of Ω (see Figure 36), we look for a finite dimensional approximation for u by the finite element method. We will choose the standard Lagrange basis functions as the basis for the set of continuous piecewise linear functions on the unit square based on the triangulation.

2.3.2 Finite Element Method Formulation

Let $V_h := \{v \in C^0(\overline{\Omega}) \ : \ v|_K \in P_1(K) \ \forall \ K \in \mathcal{K}_h\}$, where $\mathcal{K}_h$ is a shape-regular triangulation of Ω. Note that V_h is conforming in the sense that $V_h \subset V$.

The finite element method is to find $u_h \in V_h$ such that

$$\int\limits_{\Omega} \nabla u_h.\nabla v dx + \gamma\sqrt{\lambda}\int\limits_{\partial\Omega} u_h g(u_h) v ds = \lambda \int\limits_{\Omega} f(u_h) v dx \qquad \forall v \in V_h.$$

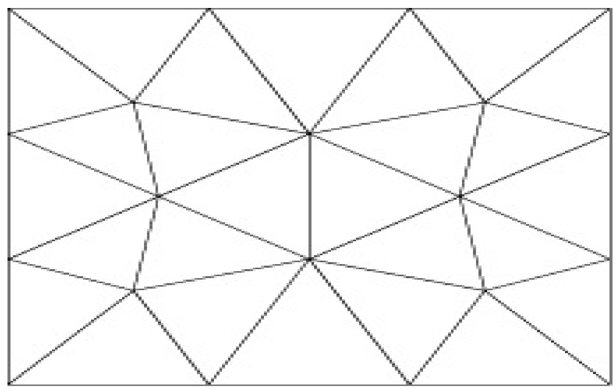

Figure 36. Triangulation ($\mathcal{K}_h$) of the Domain.

Since $V_h = Span\{\phi_i\}_{i=1}^{n_h}$, where $n_h := dim(V_h)$, equation is equivalent to finding $u_h \in V_h$ such that

$$\int\limits_{\Omega} \nabla u_h.\nabla \phi_i dx + \gamma\sqrt{\lambda}\int\limits_{\partial\Omega} u_h g(u_h)\phi_i dx = \lambda \int\limits_{\Omega} f(u_h)\phi_i ds,$$

for all $i = 1, 2, ..., n_h$. Let $u_h := \sum_{j=1}^{n_h} u_j\phi_j$. Then we obtain

$$\sum_{j=1}^{n_h} u_i \int\limits_{\Omega} \nabla\phi_i.\nabla\phi_j dx + \gamma\sqrt{\lambda}\int\limits_{\partial\Omega} (\sum_{j=1}^{n_h} u_j\phi_j) g(\sum_{j=1}^{n_h} u_j\phi_j)\phi_i dx = \lambda \int\limits_{\Omega} f(\sum_{j=1}^{n_h} u_j\phi_j)\phi_i ds \tag{2.31}$$

for all $i = 1, 2, ..., n_h$, which leads to a system of nonlinear equations of the form $G(u) = 0$, where G is a nonlinear function and u is the solution vector representing the coefficients of the expansion of u_h in terms of the basis functions $\{\phi_i\}$. The nonlinear system $G(u) = 0$ can be solved by Newton's method.

CHAPTER III

PROOFS OF THEOREMS 1.4 - 1.7 STATED IN FOCUS 1 AND COMPUTATIONAL RESULTS

3.1 Proof of Theorem 1.4

We first show that (1.8) has no positive solution u_λ for $\lambda < E_{1,\mu}$. Assume to the contrary that u_λ is a positive solution for $\lambda < E_{1,\mu}$. Let σ_λ be the principal eigenvalue and $\theta_\lambda > 0$ be the corresponding normalized eigenfunction of:

$$\begin{cases} -\Delta\theta = (\sigma + \lambda)\theta;\ \Omega, \\ \frac{\partial\theta}{\partial\eta} + \mu(\lambda)\theta = 0;\ \partial\Omega. \end{cases} \tag{3.1}$$

Then we have

$$\int_\Omega [\theta_\lambda \Delta u_\lambda - u_\lambda \Delta\theta_\lambda] dx = \int_{\partial\Omega} \Big[\theta_\lambda \frac{\partial u_\lambda}{\partial\eta} - u_\lambda \frac{\partial\theta_\lambda}{\partial\eta}\Big] dx = 0.$$

Noting $\sigma_\lambda > 0$ for $\lambda < E_{1,\mu}$ by (H_2), and since $f(s) \leq s$ for $s \in [0, r_0)$, we also have

$$\int_\Omega [\theta_\lambda \Delta u_\lambda - u_\lambda \Delta\theta_\lambda] dx = \int_\Omega [-\lambda f(u_\lambda) + (\lambda + \sigma_\lambda)u_\lambda]\theta_\lambda dx \geq \int_\Omega \sigma_\lambda u_\lambda \theta_\lambda dx > 0.$$

This is a contradiction. Hence, there exists no positive solution for $\lambda < E_{1,\mu}$.

We also show that (1.8) has a positive solution u_λ for $\lambda > E_{1,\mu}$. Let $\psi_\lambda := m_\lambda \theta_\lambda$ and $H(s) := (\sigma_\lambda + \lambda)s - \lambda f(s)$. We note that $\sigma_\lambda < 0$ for $\lambda > E_{1,\mu}$ by (H_2). Thus we have $H'(0) = \sigma_\lambda + \lambda - \lambda f'(0) < 0$. This implies that $-\Delta\psi_\lambda = m_\lambda(\sigma_\lambda + \lambda)\theta_\lambda \leq$

$\lambda f(m_\lambda\theta_\lambda)$ in Ω for $m_\lambda \approx 0$. Thus ψ_λ is a subsolution of (1.8). We construct a supersolution Z_λ. If $0 < r_0 < \infty$, it is easy to see that $Z_\lambda \equiv r_0$ is a supersolution. Taking $m_\lambda \approx 0$ so that $\psi_\lambda \leq r_0$, it easily follows that (1.8) has a solution $u_\lambda \in [\psi_\lambda, r_0]$. If $r_0 = \infty$, let $f^*(s) := \max\limits_{r\in[0,s]} f(r)$ and e_λ be the unique positive solution of the following boundary value problem:

$$\begin{cases} -\Delta e = 1;\ \Omega, \\ \frac{\partial e}{\partial \eta} + \mu(\lambda)e = 0;\ \partial\Omega. \end{cases} \tag{3.2}$$

We note that f^* is nondecreasing and sublinear at ∞. Then for each $\lambda > 0$ there exists $M_\lambda > 0$ such that $\frac{1}{\lambda\|e_\lambda\|_\infty} \geq \frac{f^*(M_\lambda\|e_\lambda\|_\infty)}{M_\lambda\|e_\lambda\|_\infty}$. Let $Z_\lambda := M_\lambda e_\lambda$. Then we have

$$-\Delta Z_\lambda = M_\lambda \geq \lambda f^*(M_\lambda\|e_\lambda\|_\infty) \geq \lambda f^*(M_\lambda e_\lambda) \geq \lambda f(Z_\lambda).$$

Further, Z_λ satisfies $\frac{\partial Z_\lambda}{\partial \eta} + \mu(\lambda)Z_\lambda = M_\lambda[\frac{\partial e_\lambda}{\partial \eta} + \mu(\lambda)e_\lambda] = 0$ on $\partial\Omega$. Therefore Z_λ is a supersolution of (1.8). We can also choose $M_\lambda \gg 1$ such that $\psi_\lambda \leq Z_\lambda$. By Lemma 2.1, there exists a positive solution $u_\lambda \in [\psi_\lambda, Z_\lambda]$.

Next we show the uniqueness of a positive solution u_λ for $\lambda > E_{1,\mu}$. Assume to the contrary that there exist two distinct positive solutions u_1 and u_2. By the Green's second identity, we obtain

$$\int\limits_\Omega [u_2\Delta u_1 - u_1\Delta u_2]dx = \int\limits_{\partial\Omega} \Big[u_2\frac{\partial u_1}{\partial \eta} - u_1\frac{\partial u_2}{\partial \eta}\Big]dx = 0.$$

But $\int\limits_{\Omega}[u_2\Delta u_1 - u_1\Delta u_2]dx = \int\limits_{\Omega} -\lambda u_1 u_2 \left[\frac{f(u_1)}{u_1} - \frac{f(u_2)}{u_2}\right] dx < 0$. Here, without loss of generality, we can assume $u_1 \leq u_2$ since ψ_λ is a subsolution for $m_\lambda \approx 0$. This is a contradiction and the proof is complete.

Now we show that there exists a positive solution u_λ for $\lambda > E_{1,\mu}$ and $\lambda \approx E_{1,\mu}$ such that $\|u_\lambda\|_\infty \to 0$ as $\lambda \to E_{1,\mu}^+$. Since $f'' < 0$ on $[0, r_0)$, there exists $A^* > 0$ such that $f''(s) \leq -A^*$ for $s \approx 0$. Let $\hat{Z}_\lambda := \delta_\lambda\theta_\lambda$, where $\delta_\lambda = -\frac{2\sigma_\lambda}{\lambda A^* \min\limits_{x\in\overline{\Omega}} \theta_\lambda}$. We note that $\delta_\lambda > 0$ and $\delta_\lambda \to 0$ as $\lambda \to E_{1,\mu}^+$ since $\sigma_\lambda < 0$, $\sigma_\lambda \to 0$ as $\lambda \to E_{1,\mu}^+$ and $\min\limits_{x\in\overline{\Omega}} \theta_\lambda \not\to 0$ as $\lambda \to E_{1,\mu}^+$. We also note that $f(\hat{Z}_\lambda) = f(0) + f'(0)\hat{Z}_\lambda + \frac{f''(\zeta)}{2}\hat{Z}_\lambda^2 = \hat{Z}_\lambda + \frac{f''(\zeta)}{2}\hat{Z}_\lambda^2$ for some $\zeta \in [0, \hat{Z}_\lambda]$ by Taylor's Theorem. Then we have

$$
\begin{aligned}
-\Delta\hat{Z}_\lambda - \lambda f(\hat{Z}_\lambda) &= \delta_\lambda(\sigma_\lambda + \lambda)\theta_\lambda - \lambda\Big[\delta_\lambda\theta_\lambda + \frac{f''(\zeta)}{2}(\delta_\lambda\theta_\lambda)^2\Big] \\
&\geq \delta_\lambda\theta_\lambda\Big[\sigma_\lambda + \frac{\lambda A^*}{2}\delta_\lambda \min_{x\in\overline{\Omega}} \theta_\lambda\Big] = 0,
\end{aligned}
$$

by our choice of δ_λ. Thus $\hat{Z}_\lambda$ is a supersolution of (1.8) for $\lambda > E_{1,\mu}$ and $\lambda \approx E_{1,\mu}$ such that $\|\hat{Z}_\lambda\|_\infty \to 0$ as $\lambda \to E_{1,\mu}^+$. Choosing $m_\lambda \approx 0$, we also have $\psi_\lambda \leq \hat{Z}_\lambda$. By Lemma 2.1, there exists a positive solution $u_\lambda \in [\psi_\lambda, \hat{Z}_\lambda]$ for $\lambda > E_{1,\mu}$ and $\lambda \approx E_{1,\mu}$ such that $\|u_\lambda\|_\infty \to 0$ as $\lambda \to E_{1,\mu}^+$.

Finally, we show that there exists a positive solution u_λ for $\lambda \gg 1$ such that $\|u_\lambda\|_\infty \to r_0$ as $\lambda \to \infty$. We first consider the case $0 < r_0 < \infty$. We note that the boundary value problem:

$$
\begin{cases}
-\Delta w = \lambda f(w);\ \Omega, \\
\quad w = 0;\ \partial\Omega,
\end{cases}
$$

has a solution w_λ for $\lambda \gg 1$ such that $0 \leq w_\lambda \leq r_0$ and $\|w_\lambda\|_\infty \to r_0$ as $\lambda \to \infty$ (see [CS87]). Further, w_λ satisfies $\frac{\partial w_\lambda}{\partial \eta} + \mu(\lambda) w_\lambda < 0$ on $\partial\Omega$ since $\frac{\partial w_\lambda}{\partial \eta} < 0$ on $\partial\Omega$. Therefore w_λ is a subsolution of (1.8) for $\lambda \gg 1$. Clearly $Z_\lambda \equiv r_0$ is a supersolution. By Lemma 2.1, there exists a solution $u_\lambda \in [w_\lambda, r_0]$ of (1.8) for $\lambda \gg 1$. By the maximum principle, we can easily show that $u_\lambda > 0$ on $\overline{\Omega}$. Hence, (1.8) has a positive solution $u_\lambda \in [w_\lambda, r_0]$ for $\lambda \gg 1$ such that $\|u_\lambda\|_\infty \to r_0$ as $\lambda \to \infty$ (since $\|w_\lambda\|_\infty \to r_0$ as $\lambda \to \infty$).

Next we assume $r_0 = \infty$. Define $g \in C^2([0,\infty))$ such that $g(0) < 0$, $g(s) \leq f(s)$ for $s \in (0,\infty)$ and $\lim_{s\to\infty} g(s) > 0$. Then the boundary value problem:

$$\begin{cases} -\Delta w = \lambda g(w);\ \Omega, \\ \quad w = 0;\ \partial\Omega, \end{cases}$$

has a solution $\overline{w}_\lambda \geq 0$ for $\lambda \gg 1$ such that $\|\overline{w}_\lambda\|_\infty \to \infty$ as $\lambda \to \infty$ (see [CGS93]). It is easy to show that $\overline{w}_\lambda$ is a subsolution of (1.8) for $\lambda \gg 1$. We can also choose $M_\lambda \gg 1$ such that $Z_\lambda = M_\lambda e_\lambda$ $(\geq \overline{w}_\lambda)$ is a supersolution. By Lemma 2.1 and the maximum principle, (1.8) has a positive solution $u_\lambda \in [\overline{w}_\lambda, Z_\lambda]$ for $\lambda \gg 1$ such that $\|u_\lambda\|_\infty \to \infty$ as $\lambda \to \infty$. Hence, Theorem 1.4 is proven.

3.2 Proof of Theorem 1.5

Let $\psi_1 := \psi_\lambda$ and $Z_1 := Z_\lambda$ be as in the proof of Theorem 1.4. Then ψ_1 is a subsolution of (1.8) and Z_1 is a supersolution of (1.8). Now we construct a strict subsolution of (1.8).

Let $\hat{g} \in C^1([0,\infty))$ be such that $\hat{g}$ is nondecreasing on $[0, r_2)$, $0 \le \hat{g}(s) \le f(s)$ on $(0, r_1)$ and $\hat{g}(s) = f(s)$ on $[r_1, r_0)$. Then the following boundary value problem:

$$\begin{cases} -\Delta w = \lambda \hat{g}(w); \ \Omega, \\ \quad w = 0; \ \partial\Omega, \end{cases}$$

has a solution $\hat{w}_\lambda \ge 0$ such that $\|\hat{w}_\lambda\|_\infty \ge b$ for $\lambda \in \left(\frac{2bNC_N}{R^2 f(b)}, \frac{2r_2 N}{f(b)R^2}\right)$ provided (H_4) is satisfied (see [LSS11]). Let $\psi_2 := \hat{w}_\lambda$. Since $\hat{g}(s) \le f(s)$ on $[0, r_0)$ and $\frac{\partial \hat{w}_\lambda}{\partial \eta} < 0$ on $\partial\Omega$, it easily follows that ψ_2 is a strict subsolution for $\lambda \in \left(\frac{2bNC_N}{R^2 f(b)}, \frac{2r_2 N}{f(b)R^2}\right)$.

Next we construct a strict supersolution Z_2 of (1.8) for $\lambda \in \left(\frac{2bNC_N}{R^2 f(b)}, \frac{a}{f^*(a)\|v_{\mu_b}\|_\infty}\right)$. Let $Z_2 := \frac{a v_{\mu_b}}{\|v_{\mu_b}\|_\infty}$. Then we have

$$-\Delta Z_2 = \frac{a}{\|v_{\mu_b}\|_\infty} > \lambda f^*(a) \ge \lambda f(Z_2).$$

Further, Z_2 satisfies $\frac{\partial Z_2}{\partial \eta} + \mu(\lambda) Z_2 > \frac{a}{\|v_{\mu_b}\|_\infty}[\frac{\partial v_{\mu_b}}{\partial \eta} + \mu_b v_{\mu_b}] = 0$ on $\partial\Omega$ since μ is a strictly increasing function and $\lambda > \frac{2bNC_N}{R^2 f(b)}$. Thus Z_2 is a strict supersolution of (1.8) for $\lambda \in \left(\frac{2bNC_N}{R^2 f(b)}, \frac{a}{f^*(a)\|v_{\mu_b}\|_\infty}\right)$.

We note that $\|\psi_2\|_\infty \ge b > a = \|Z_2\|_\infty$ and we can choose ψ_1 and Z_1 such that $\psi_1 \le \psi_2 \le Z_1$ and $\psi_1 \le Z_2 \le Z_1$. By Lemma 2.2 and the maximum principle, there exist at least three positive solutions for $\lambda \in \left(\frac{2bNC_N}{R^2 f(b)}, \min\left\{\frac{a}{f^*(a)\|v_{\mu_b}\|_\infty}, \frac{2r_2 N}{f(b)R^2}\right\}\right)$. Hence, Theorem 1.5 is proven.

3.3 Proof of Theorem 1.6

Clearly $0 < r_0 < \infty$. If $KM < 4$, then $f'' < 0$. It follows that (H_1) is satisfied. Further, we can show that (H_2) is satisfied when $\mu(s) = \sqrt{s}$. Hence, Theorem 1.6 is proven.

3.4 Proof of Theorem 1.7

Let $C_N := \frac{(N+1)^{N+1}}{2N^N}$. For $M \in \left(\frac{8}{3\sqrt{3}}, 2\right)$ and $K \gg 1$, there exist $b > 0$, $c > 0$, $r_0 > 0$, $r_1 > 0$ and $r_2 > 0$ such that $c < r_1 < b < \frac{r_2}{C_N} < \frac{r_0}{C_N} < \infty$, $b \leq \sqrt{KM}$, $r_2 > \frac{K}{4}$, $f(s) > 0$ for $s \in (0, r_0)$, $f(s) < 0$ for $s \in (r_0, \infty)$, f is increasing on $(0, c) \cup (r_1, r_2)$ and f is decreasing on $(c, r_1) \cup (r_2, \infty)$. Further, $\lim_{K\to\infty} f(b) = \infty$ and $\lim_{K\to\infty} \frac{b}{f(b)} = 1$. See [LSS11] for details. Thus (H_1) is satisfied. Next we choose $a \in (r_1, b)$ such that $f(a) = f^*(a) = f(c)$. Then $a \approx 1.5437$ and $\frac{a}{f^*(a)} \approx 11.4445$ for $M \approx 2$ and $K \gg 1$. Noting $v_{\mu_b}(x) = \frac{R^2-|x|^2}{2N} + \frac{R}{N}\sqrt{\frac{f(b)}{m_0 b}}$, where $m_0 = \frac{2NC_N}{R^2}$, we obtain $m_0\|v_{\mu_b}\|_\infty \leq \frac{R^2 m_0}{2N} + \frac{R}{N}\sqrt{\frac{m_0 f(b)}{b}} < \frac{R^2 m_0}{2N} + \frac{2R\sqrt{m_0}}{N}$ for $K \gg 1$. This implies $m_0\|v_{\mu_b}\|_\infty < 6$ for $N = 1$, $m_0\|v_{\mu_b}\|_\infty < 8$ for $N = 2$ and $m_0\|v_{\mu_b}\|_\infty < 9$ for $N = 3$. Thus $\frac{a}{f^*(a)}/\frac{b}{f(b)} > m_0\|v_{\mu_b}\|_\infty = \frac{2NC_N\|v_{\mu_b}\|_\infty}{R^2}$ for $K \gg 1$. Therefore $(H_3) - (H_4)$ are satisfied. We also note that $m_0 = \frac{4}{R^2} > \frac{8A_1}{5}$ for $N = 1$, $m_0 = \frac{27}{2R^2} > \frac{8A_1}{5}$ for $N = 2$ and $m_0 = \frac{256}{9R^2} > \frac{8A_1}{5}$ for $N = 3$, where A_1 is the principal eigenvalue of (1.6). This implies $\frac{2bNC_N}{R^2 f(b)} = \frac{m_0 b}{f(b)} > \frac{5m_0}{8} > A_1 > E_1(1,1)$ for $M \in \left(\frac{8}{3\sqrt{3}}, 2\right)$ and $K \gg 1$. Thus (H_5) is satisfied. Further, we can easily show that (H_2) is satisfied when $\mu(s) = \sqrt{s}$. Hence, Theorem 1.7 is proven (by Theorem 1.5).

3.5 Computational Results

Finally, we provide some bifurcation diagrams that we have obtained for various values of K and M. Here, we briefly explain how we obtain numerical bifurcation diagrams. Let $\gamma > 0$ be fixed and let $x_i = \frac{ir_0}{n+1}$; $i = 1, ..., n$ for some $n \geq 1$. We note that in this case $q_1 = q_2$. Letting $\rho = x_1$, we numerically solve the equation (2.4) for q using the FindRoot command in Mathematica. The values of q and ρ are substituted into (2.3) to find the corresponding value of λ. Repeating this procedure for $\rho = x_i$, $i = 2, ..., n$, we obtain (λ, ρ) points for the bifurcation diagram.

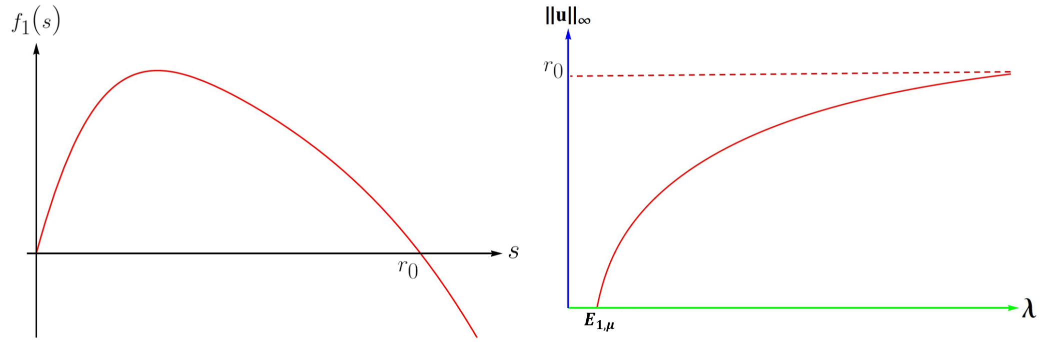

(a) $f(s) = f_1(s) = s - \frac{s^2}{3} - \frac{s^2}{1+s^2}$

(b) Exact Bifurcation Diagram for (1.10) When $f = f_1$

Figure 37. $f = f_1$ and the Corresponding Bifurcation Diagram for (1.10) When $\mu(s) = \sqrt{s}$.

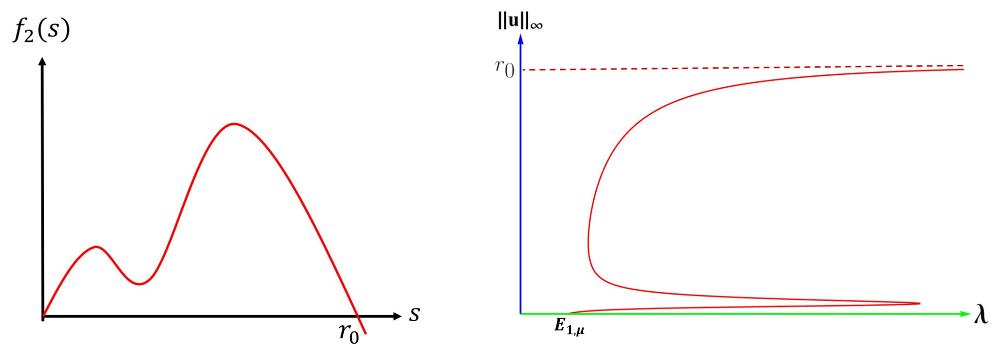

(a) $f(s) = f_2(s) = s - \frac{s^2}{30} - \frac{9s^2}{5+5s^2}$

(b) Exact Bifurcation Diagram for (1.10) When $f = f_2$

Figure 38. Graph of $f = f_2$ and the Corresponding Exact Bifurcation Diagram for (1.10) When $\mu(s) = \sqrt{s}$.

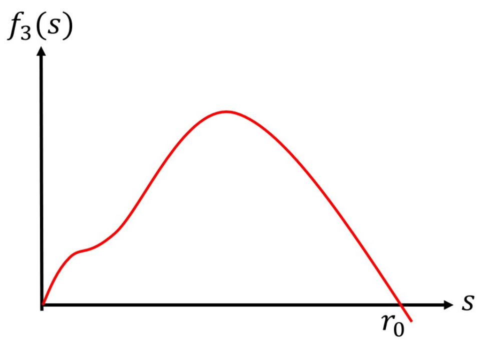

(a) $f(s) = f_3(s) = s - \frac{s^2}{30} - \frac{s^2}{2+2s^2}$

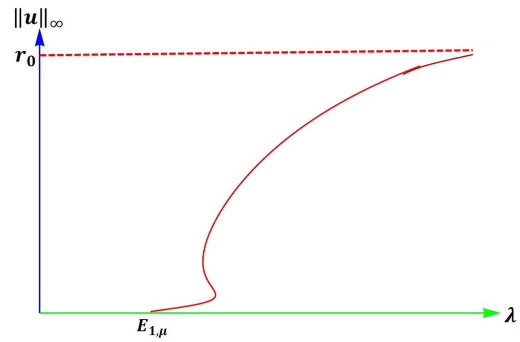

(b) Exact Bifurcation Diagram for (1.10) When $f = f_3$

Figure 39. $f = f_3$ and the Corresponding Bifurcation Diagram for (1.10) When $\mu(s) = \sqrt{s}$.

Here, we observe that the exact bifurcation diagram described in Theorem 1.6 occurs when $K = 3$ and $M = 1$ (see Figure 37). We further observe that the bifurcation diagrams of (1.10) are in fact exactly s-shaped for certain values of K and M. See Figure 38 for the exact bifurcation diagram for the case when $K = 30$ and $M = \frac{9}{5}$ and Figure 39 for the exact bifurcation diagram for the case when $K = 30$ and $M = \frac{1}{2}$.

CHAPTER IV

PROOFS OF THEOREMS 1.8 - 1.12 STATED IN FOCUS 2 AND COMPUTATIONAL RESULTS

4.1 Proof of Theorem 1.8

Let $\lambda \leq E_1(\gamma, \epsilon)$. Assume to the contrary that (1.11) has a positive solution u. Then there exist a unique $\epsilon_\lambda \leq \epsilon$ such that λ is the principal eigenvalue of the boundary value problem:

$$\begin{cases} -\Delta e = Ee; \ x \in \Omega, \\ \frac{\partial e}{\partial \eta} + \gamma \epsilon_\lambda \sqrt{E} e = 0; \ x \in \partial\Omega, \end{cases} \tag{4.1}$$

and equality holds if and only if $\lambda = E_1(\gamma, \epsilon)$. This easily follows from the behavior of $\frac{\kappa^2}{\gamma^2 \epsilon^2}$ as ϵ varies (see Figure 40). See also [GMRS18].

Let $e > 0$ be the corresponding normalized eigenfunction for the principal eigenvalue λ in (4.1). Then we have

$$\int_\Omega [(-\Delta u)e + (\Delta e)u] \ dx = \int_\Omega \lambda u(1-u)e - \lambda eu \ dx = -\int_\Omega \lambda e u^2 \ dx < 0.$$

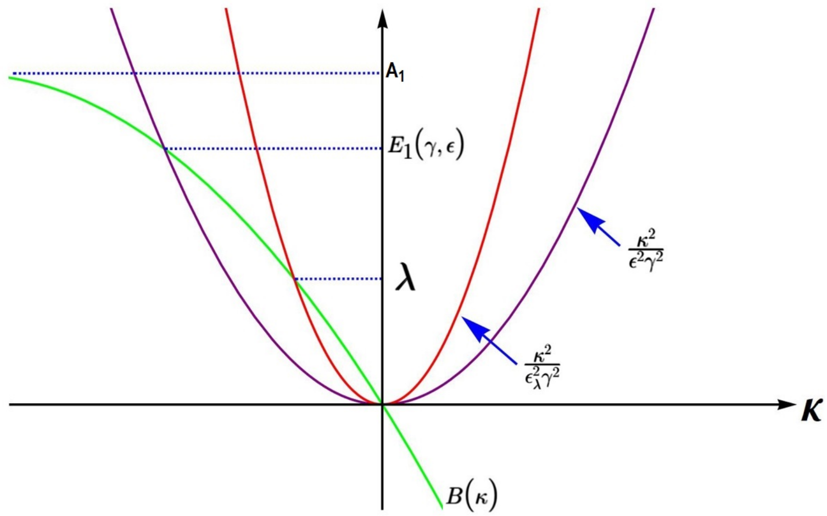

Figure 40. Plot that Illustrates the Existence of ϵ_λ.

However, by the Green's second identity we have

$$\begin{aligned}\int_\Omega [(-\Delta u)e + (\Delta e)u]\ dx &= \int_{\partial\Omega} \Big[-\frac{\partial u}{\partial \eta}e + \frac{\partial e}{\partial \eta}u\Big]\ ds \\ &= \int_{\partial\Omega} \Big[\gamma\sqrt{\lambda}[(A-u)^2+\epsilon]ue - \gamma\epsilon_\lambda\sqrt{\lambda}eu\Big]\ ds \\ &\geq \int_{\partial\Omega} \gamma(\epsilon-\epsilon_\lambda)\sqrt{\lambda}ue\ ds \\ &\geq 0.\end{aligned}$$

This is a contradiction since $\epsilon_\lambda \leq \epsilon$. Hence, Theorem 1.8 is proven.

4.2 Proof of Theorem 1.9

Let $\lambda > E_1(\gamma, A^2+\epsilon)$. It is easy to see that $\phi \equiv 1$ is a supersolution for (1.11). Next we construct a subsolution for (1.11).

Let μ_λ be the principal eigenvalue and $z > 0$ be the corresponding normalized eigenfunction for the boundary value problem:

$$\begin{cases} -\Delta z = (\lambda + \mu) z; \;\; x \in \Omega, \\ \frac{\partial z}{\partial \eta} + [\gamma\sqrt{\lambda}(A^2 + \epsilon) - \mu] z = 0; \;\; x \in \partial\Omega. \end{cases} \tag{4.2}$$

We note that $\mu_\lambda < 0$ for $\lambda > E_1(\gamma, A^2 + \epsilon)$ (see [GMPS19]) and $\min_{x \in \overline{\Omega}} z(x) > 0$. Let $\psi := \alpha_\lambda z$ where $\alpha_\lambda > 0$ will be chosen later. Then ψ satisfies

$$-\Delta \psi = \alpha_\lambda(\lambda + \mu_\lambda) z \leq \lambda \alpha_\lambda z (1 - \alpha_\lambda z) = \lambda \psi (1 - \psi),$$

for $x \in \Omega$ provided $\mu_\lambda + \lambda \alpha_\lambda z \leq 0$. Further, ψ satisfies

$$\frac{\partial \psi}{\partial \eta} = \alpha_\lambda[-\gamma\sqrt{\lambda}(A^2 + \epsilon) + \mu_\lambda] z \leq -\alpha_\lambda \gamma \sqrt{\lambda}[(A - \alpha_\lambda z)^2 + \epsilon] z = -\gamma\sqrt{\lambda}[(A - \psi)^2 + \epsilon]\psi,$$

for all $x \in \partial\Omega$ provided $\gamma\sqrt{\lambda}[(A - \alpha_\lambda z)^2 - A^2] + \mu_\lambda \leq 0$. Since $\mu_\lambda < 0$, choosing $\alpha_\lambda \approx 0$, it follows that ψ is a subsolution for (1.11) and $\psi \leq \phi$ in Ω. Hence, for $\lambda > E_1(\gamma, A^2 + \epsilon)$, (1.11) has a positive solution u such that $\psi \leq u \leq \phi$, and Theorem 1.9 is proven.

4.3 Proof of Theorem 1.10

Let $\lambda < E_1(\gamma, A^2 + \epsilon)$. It is easy to see that $\phi_1 \equiv 1$ is a supersolution and $\psi_1 \equiv 0$ is a subsolution for (1.11). We now construct a strict supersolution for (1.11). Let μ_λ be the principal eigenvalue and $z > 0$ be the corresponding normalized eigenfunction for (4.2).

We note that $\mu_\lambda > 0$ for $\lambda < E_1(\gamma, A^2+\epsilon)$ (see [GMPS19]). Let $\phi_2 := \beta_\lambda z$ for $\beta_\lambda \in (0, A)$. Then ϕ_2 satisfies

$$-\Delta\phi_2 = \beta_\lambda(\lambda + \mu_\lambda)z \geq \lambda\beta_\lambda z(1-\beta_\lambda z) = \lambda\phi_2(1-\phi_2),$$

for $x \in \Omega$. Further, ϕ_2 satisfies

$$\frac{\partial\phi_2}{\partial\eta} = \beta_\lambda[-\gamma\sqrt{\lambda}(A^2+\epsilon)+\mu_\lambda]z > -\beta_\lambda\gamma\sqrt{\lambda}[(A-\beta_\lambda z)^2+\epsilon]z = -\gamma\sqrt{\lambda}[(A-\phi_2)^2+\epsilon]\phi_2,$$

for $x \in \partial\Omega$ provided $\gamma\sqrt{\lambda}[(A-\beta_\lambda z)^2 - A^2] + \mu_\lambda > 0$. Since $\mu_\lambda > 0$, choosing $\beta_\lambda \approx 0$, it follows that ϕ_2 is a strict supersolution for (1.11).

We next construct a strict subsolution for (1.11). For each $\epsilon \in (0, \epsilon_\gamma^*)$, there exists $\lambda_* < E_1(\gamma, A^2)$ such that $(w_\lambda^* - A)^2 > \epsilon$ for $\lambda \in (\lambda_*, E_1(\gamma, 2A^2))$. We note that $E_1(\gamma, A^2+\epsilon) < E_1(\gamma, 2A^2)$ since $\epsilon < \epsilon_\gamma^* \leq A^2$. Let $\psi_2 := w_\lambda$ for $\lambda \in (\lambda_*, E_1(\gamma, A^2+\epsilon))$. Then $\frac{\partial w_\lambda}{\partial\eta} = -2\gamma\sqrt{\lambda}(A-w_\lambda)^2 w_\lambda < -\gamma\sqrt{\lambda}[(A-w_\lambda)^2+\epsilon]w_\lambda$ on $\partial\Omega$, and hence ψ_2 is a strict subsolution. We note that $\|\psi_2\|_\infty > A$ and $\|\phi_2\|_\infty < A$. By Lemma 2.2, we obtain solutions u, u_* and u^* such that $u \in [\psi_1, \phi_2]$, $u_* \in [\psi_2, \phi_1]$ and $u^* \in [\psi_1, \phi_1] \setminus ([\psi_1, \phi_2] \cup [\psi_2, \phi_1])$. Clearly u_* and u^* are positive solutions. Further, $u_* \in \Gamma$ since $u_* \geq \psi_2 > A$ on $\overline{\Omega}$.

Next in Γ, we show that (1.11) has a unique positive solution. Assume to the contrary that in Γ there exist two distinct positive solutions u and v. Without loss of generality, we assume $u \leq v$ since $\phi_1 \equiv 1$ is a global supersolution. Therefore we have

$$\int_\Omega [(-\Delta v)u + (\Delta u)v]\; dx = \int_\Omega \lambda uv(u-v)\; dx < 0.$$

However, by the Green's second identity we have

$$\begin{aligned}\int_{\Omega}[(-\Delta v)u + (\Delta u)v]\ dx &= \int_{\partial\Omega}\Big[-\frac{\partial v}{\partial\eta}u + \frac{\partial u}{\partial\eta}v\Big]\ ds\\ &= \int_{\partial\Omega}\gamma\sqrt{\lambda}uv[(A-v)^2 - (A-u)^2]\ ds\\ &= \int_{\partial\Omega}\gamma\sqrt{\lambda}uv(u-v)(2A-u-v)\ ds \geq 0,\end{aligned}$$

which is a contradiction. Thus, in Γ, there exists a unique positive solution, which is u_*, and u^* is a positive solution which does not belong to Γ. Hence, Theorem 1.10 is proven.

4.4 Proof of Theorem 1.11

Let u be a positive solution such that $u(0) = q_1$ and $u(1) = q_2$. Assume $x_0 < \frac{1}{2}$. Since u is symmetric about x_0 and u is concave, $q_1 > q_2$, and hence $|u'(0)| < |u'(1)|$. By the boundary conditions we have $\gamma\sqrt{\lambda}[(A-q_1)^2+\epsilon]q_1 < \gamma\sqrt{\lambda}[(A-q_2)^2+\epsilon]q_2$. Let $G(q) := \gamma\sqrt{\lambda}[(A-q)^2+\epsilon]q$. It is easy to show that if $\epsilon > \frac{A^2}{3}$ then $G'(q) > 0$. This implies $\gamma\sqrt{\lambda}[(A-q_1)^2+\epsilon]q_1 > \gamma\sqrt{\lambda}[(A-q_2)^2+\epsilon]q_2$. This is a contradiction. A similar contradiction can be obtained when $x_0 > \frac{1}{2}$. Hence, the solution is symmetric if $\epsilon > \frac{A^2}{3}$, and Theorem 1.11 is proven.

4.5 Proof of Theorem 1.12

Let u be a positive solution such that $u(0) = q_1$ and $u(1) = q_2$. To show that the solution is symmetric, we need to show $q_1 = q_2$. By Theorem 2.3, this follows by showing that for any fixed $\rho \in (0,1)$,

$$\frac{\sqrt{F(\rho)-F(q)}}{q[(A-q)^2+\epsilon]} = \frac{\gamma}{\sqrt{2}} \tag{4.3}$$

has only one solution $q \in (0, \rho)$. Let $H(q) := \frac{\sqrt{F(\rho)-F(q)}}{q[(A-q)^2+\epsilon]}$. It is easy to see that $\lim_{q \to 0^+} H(q) = \infty$ and $H(\rho) = 0$. Further, we have

$$H'(q) = \frac{-qf(q)[(A-q)^2+\epsilon] - 2[F(\rho)-F(q)][(A-q)(A-3q)+\epsilon]}{2q^2[(A-q)^2+\epsilon]^2\sqrt{F(\rho)-F(q)}}.$$

Thus we obtain $\lim_{q \to 0^+} H'(q) = \lim_{q \to \rho} H'(q) = -\infty$. This implies (4.3) has only one solution $q \in (0, \rho)$ for $\gamma \gg 1$ or $\gamma \approx 0$ (see Figure 41 for an illustration). Hence, Theorem 1.12 is proven.

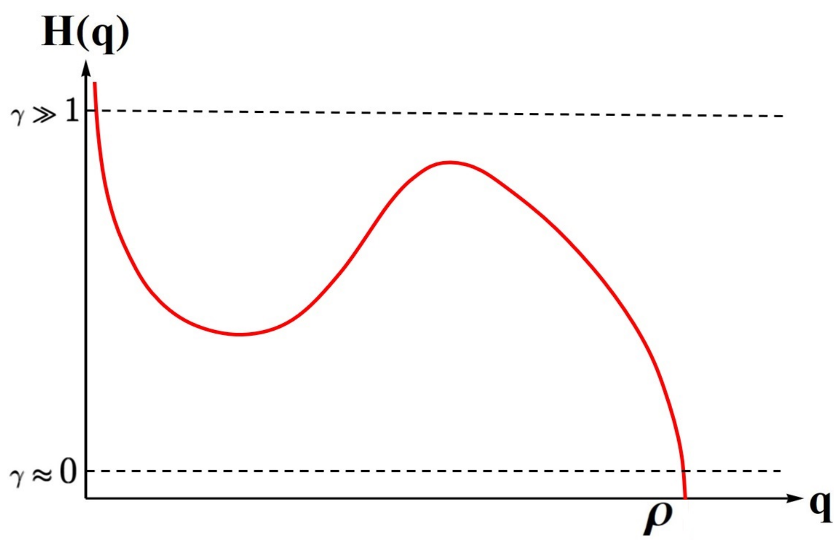

Figure 41. The Graph of $H(q)$.

4.6 Computational Results

Finally, we present some bifurcation curves for a couple of parameter selections. Here, we briefly explain how we obtain numerical bifurcation diagrams. Let $\gamma > 0$ be fixed and let $x_i = \frac{i}{n+1}$; $i = 1, ..., n$ for some $n \geq 1$. Letting $\rho = x_1$, we numerically solve the equation (2.4) for q_1 and q_2 using the FindRoot command in Mathematica.

The values of q_1, q_2, and ρ are substituted into (2.3) to find the corresponding value of λ. Repeating this procedure for $\rho = x_i$, $i = 2, ..., n$, we obtain (λ, ρ) points for the bifurcation diagram.

Example 4.1. Let $\epsilon = 0.1$ and $A = 0.5$. We note that by Theorem 1.11, every positive solution of (1.14) is symmetric. Here, we provide bifurcation curves numerically generated via Mathematica for various γ values. See Figure 42 consisting of 6 bifurcation curves. The first five are in the ascending order of γ from left to right, and the last one is the bifurcation curve with Dirichlet boundary conditions.

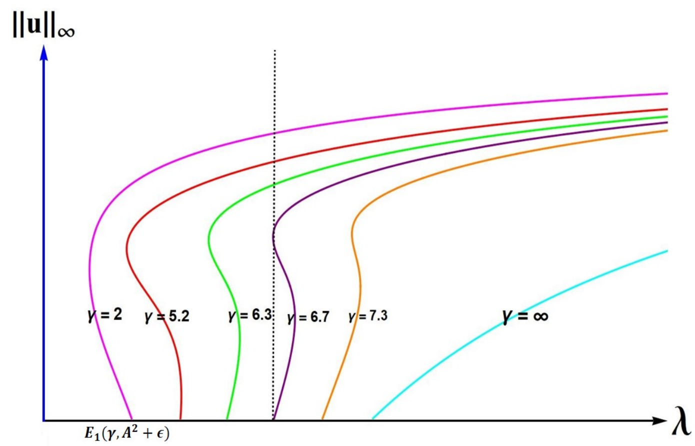

Figure 42. Evolution of Bifurcation Diagrams for (1.14) as γ Varies When $\epsilon = 0.1$ and $A = 0.5$.

Example 4.2. Here, we present an example where we get both symmetric and non-symmetric solutions of (1.14) for certain values of γ when $\epsilon = 0.01$ and $A = 0.8$ (see Figure 43). We observe that solutions are symmetric for $\gamma = 1$, $\gamma = 23$ and $\gamma = 25$ (see (a), (f) and (g) in Figure 43). We also find that for some γ values, (4.3) has three distinct q-values, say q_1, q_2 and q_3, for a certain range of ρ values.

This implies that there exist three symmetric solutions such that $\|u\|_\infty = \rho$ and $u(0) = u(1) = q_i$ for $i = 1, 2, 3$ and six nonsymmetric solutions such that $\|u\|_\infty = \rho$, $u(0) = q_i$ and $u(1) = q_j$ for $i, j = 1, 2, 3$ and $i \neq j$ (Note: In general, if (4.3) has n $q-$value solutions then there are n^2 total solutions). See (c), (d) and (e) in Figure 43 for bifurcation diagrams when $\gamma = 6$, $\gamma = 10$ and $\gamma = 16$, respectively. Here, the bifurcation curves for symmetric solutions are in red and the bifurcation curves for non-symmetric solutions are in green (Note: green points represent two solutions each while red represents only one solution each). Note that (h) in Figure 43 is the bifurcation curve with Dirichlet boundary conditions i.e., the boundary conditions is $u(0) = 0 = u(1)$. We observe that bifurcation curves of (1.14) approach the bifurcation curve with Dirichlet boundary conditions when $\gamma \longrightarrow \infty$. However, for a fixed $\gamma > 3$, we observe that there always exists a range of λ in which there exists at least three solutions. A similar scenario can be observed for the case when $\epsilon = 0.01$ and $A = 0.5$ (see Figure 44).

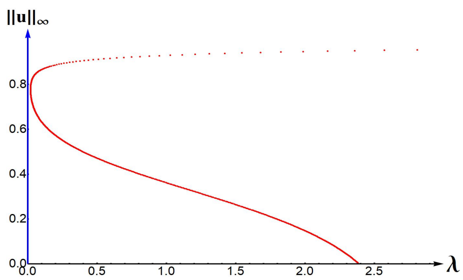

(a) $\gamma = 1$

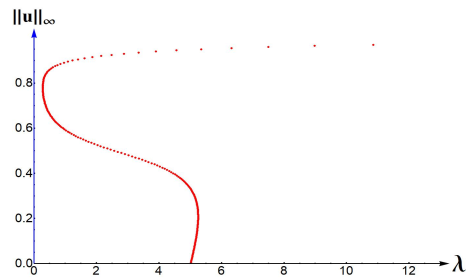

(b) $\gamma = 3$

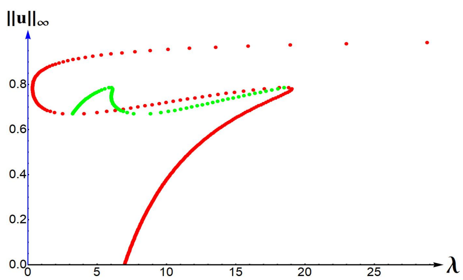

(c) $\gamma = 6$

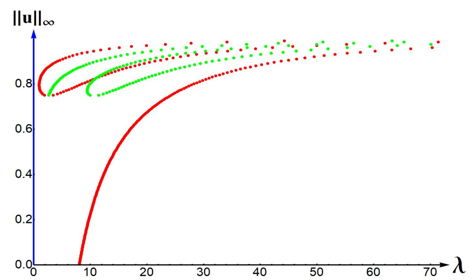

(d) $\gamma = 10$

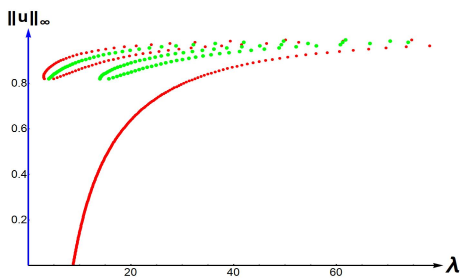

(e) $\gamma = 16$

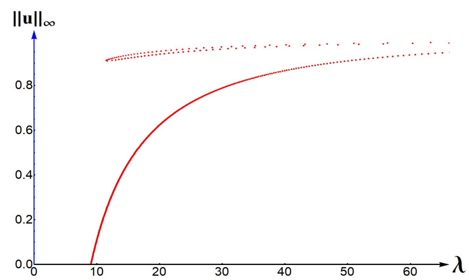

(f) $\gamma = 23$

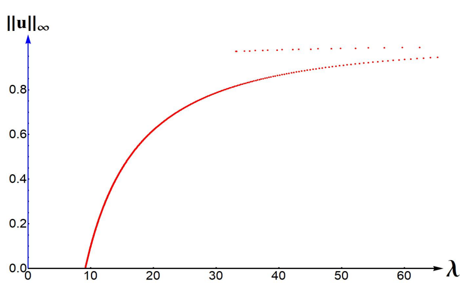

(g) $\gamma = 25$

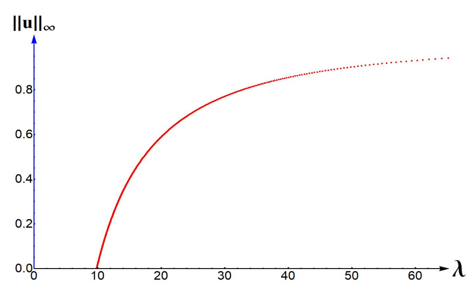

(h) $\gamma = \infty$

Figure 43. Bifurcation Diagrams for (1.14) for Several Values of γ, When $\epsilon = 0.01$ and $A = 0.8$. Symmetric Solutions are in Red and Non-symmetric Solutions are in Green.

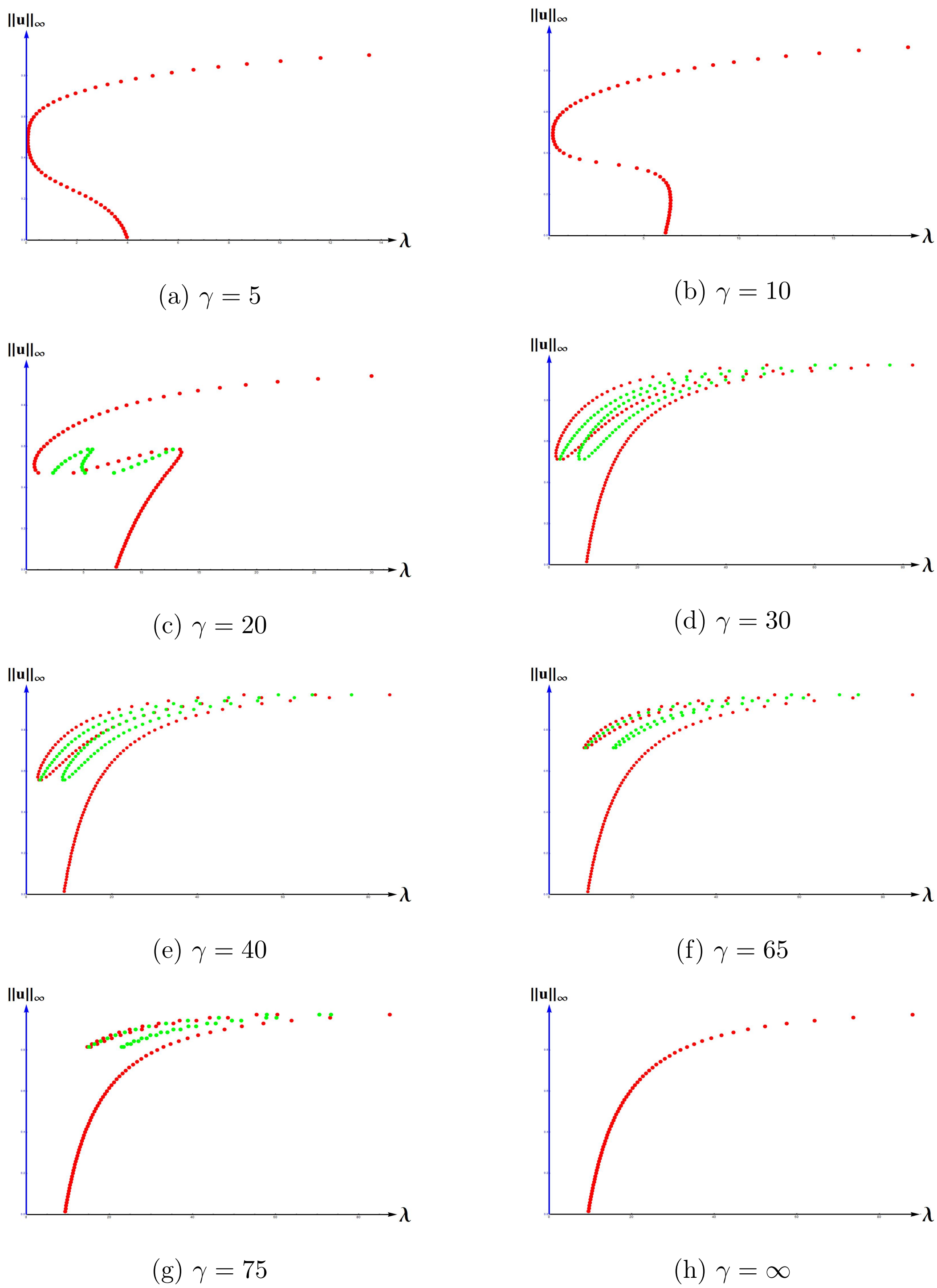

(a) $\gamma = 5$ (b) $\gamma = 10$

(c) $\gamma = 20$ (d) $\gamma = 30$

(e) $\gamma = 40$ (f) $\gamma = 65$

(g) $\gamma = 75$ (h) $\gamma = \infty$

Figure 44. Bifurcation Diagrams for (1.14) for Several Values of γ, When $\epsilon = 0.01$ and $A = 0.5$. Symmetric Solutions are in Red and Non-symmetric Solutions are in Green.

When $\epsilon = 0.1$ and $A = 0.5$ (in this case $\epsilon > \frac{A^2}{3}$ and we have all solutions are symmetric by Theorem 1.11), we note that the shapes of the bifurcation diagrams predicted in Theorem 1.10 are in fact exact and as γ increases the bifurcation diagrams shift to right. In particular, the patch-level Allee effect is lost when $\gamma > 6.7$ (see Figure 42). When $\epsilon = 0.01$ and $A = 0.8$ (in this case $\epsilon < \frac{A^2}{3}$), we observe both symmetric and non-symmetric solutions depending on the value of γ.

CHAPTER V

PROOFS OF THEOREMS 1.13 - 1.14 STATED IN FOCUS 3 AND COMPUTATIONAL RESULTS

5.1 Proof of Theorem 1.13

First let $0 < \lambda < \overline{E}_1$. Consider the eigenvalue problem (see [GMRS18]):

$$\begin{cases} -\Delta\theta - \lambda\theta = \sigma\theta; \ \Omega, \\ \frac{\partial\theta}{\partial\eta} + \gamma\sqrt{\lambda}K\theta = 0; \ \partial\Omega, \end{cases} \tag{5.1}$$

where $K > 0$ is a constant. Let σ_λ be the principal eigenvalue and θ_λ be the normalized eigenfunction such that $\theta_\lambda > 0; \ \overline{\Omega}$. Let $K := A^2 + \epsilon$ and $\delta_\lambda := \frac{2\sigma_\lambda}{\lambda A^* \min_{\overline{\Omega}} \theta_\lambda}$, where $A^* > 0$ is such that $f''(s) > A^*$ for $s \approx 0$. Note that $\delta_\lambda > 0$ (since $\sigma_\lambda > 0$) for $\lambda < \overline{E}_1$ and $\delta_\lambda \longrightarrow 0$ (since $\sigma_\lambda \longrightarrow 0$ and $\min_{\overline{\Omega}} \theta_\lambda \not\longrightarrow 0$) as $\lambda \longrightarrow \overline{E}_1$. Let $\psi := \delta_\lambda\theta_\lambda$. Clearly $\|\psi\|_\infty \longrightarrow 0$ when $\lambda \longrightarrow \overline{E}_1$. Further, by Taylor's Theorem, in Ω, we obtain (for some $\zeta \in [0, \psi]$):

$$-\Delta\psi - \lambda f(\psi) = (\sigma_\lambda + \lambda)\psi - \lambda\Big[\psi + \frac{f''(\zeta)}{2}\psi^2\Big] < \psi\Big[\sigma_\lambda - \frac{\lambda A^*}{2}\delta_\lambda \min_{\overline{\Omega}} \theta_\lambda\Big] = 0,$$

for $\lambda < \overline{E}_1$ and $\lambda \approx \overline{E}_1$. Also, on $\partial\Omega$, we obtain (assuming $\lambda \approx \overline{E}_1$ so that $\|\psi\|_\infty < 2A$):

$$\frac{\partial\psi}{\partial\eta} + \gamma\sqrt{\lambda}[(A-\psi)^2 + \epsilon]\psi < \frac{\partial\psi}{\partial\eta} + \gamma\sqrt{\lambda}[A^2 + \epsilon]\psi = 0.$$

Thus ψ is a strict subsolution of (1.15) for $\lambda < \overline{E}_1$ and $\lambda \approx \overline{E}_1$. It is easy to verify that $Z \equiv 1$ is a supersolution for any λ, and hence by Lemma 2.1 there exists $\overline{\lambda} = \overline{\lambda}(A, \gamma, \epsilon) < \overline{E}_1$ such that (1.15) has a positive solution for $\lambda \in [\overline{\lambda}, \overline{E}_1)$. Next let $\lambda \geq \overline{E}_1$. Consider the eigenvalue problem (see [GMRS18]):

$$\begin{cases} -\Delta\phi - \lambda\phi = \mu\phi; \ \Omega, \\ \frac{\partial\phi}{\partial\eta} + \gamma\sqrt{\lambda}(A^2 + \epsilon)\phi = \mu\phi; \ \partial\Omega. \end{cases} \tag{5.2}$$

Let μ_λ be the principal eigenvalue and ϕ_λ be the normalized eigenfunction such that $\phi_\lambda > 0; \ \overline{\Omega}$. Then $\mu_\lambda \leq 0$ for $\lambda \geq \overline{E}_1$. Let $\tilde{\psi} := \beta\phi_\lambda$ for $\beta \in (0, 1)$. Recall that $f(0) = 0, \ f'(0) = 1$ and $f''(0) > 0$. Hence, for $\beta \approx 0$, in Ω, we have:

$$-\Delta\tilde{\psi} - \lambda f(\tilde{\psi}) = (\lambda + \mu_\lambda)\tilde{\psi} - \lambda f(\tilde{\psi}) \leq 0,$$

since $H(s) := (\lambda + \mu_\lambda)s - \lambda f(s)$ satisfies $H(0) = 0, \ H'(0) = \mu_\lambda \leq 0$ and $H''(0) = -\lambda f''(0) < 0$. Also, on $\partial\Omega$, assuming $\beta \approx 0$ so that $\|\tilde{\psi}\|_\infty < 2A$, we have:

$$\frac{\partial\tilde{\psi}}{\partial\eta} + \gamma\sqrt{\lambda}[(A - \tilde{\psi})^2 + \epsilon]\tilde{\psi} \leq \frac{\partial\tilde{\psi}}{\partial\eta} + \gamma\sqrt{\lambda}[A^2 + \epsilon]\tilde{\psi} = \mu_\lambda\tilde{\psi} \leq 0.$$

Hence, for $\beta \approx 0$, $\tilde{\psi}$ is a subsolution for $\lambda \geq \overline{E}_1$. Again using the supersolution $Z \equiv 1$ and Lemma 2.1, there exists a positive solution for (1.15) when $\lambda \geq \overline{E}_1$. Combining the above two cases, we conclude that (1.15) has a positive solution for all $\lambda \geq \overline{\lambda}$.

Now we will show that there exists a positive solution u_λ of (1.15) for $\lambda \gg 1$ such that $\|u_\lambda\|_\infty \longrightarrow 1$ as $\lambda \longrightarrow \infty$. Consider the boundary value problem:

$$\begin{cases} -\Delta w = \lambda f(w);\ \Omega, \\ \quad w = 0;\ \partial\Omega. \end{cases} \tag{5.3}$$

In [SS06], it was established that there exists $\lambda^* \in (0, A_1)$ such that (5.3) has a positive solution $w_\lambda \in [0,1]$ for $\lambda \geq \lambda^*$, and $\|w_\lambda\|_\infty \longrightarrow 1$ as $\lambda \longrightarrow \infty$. Now by the Hopf's maximum principle $\frac{\partial w_\lambda}{\partial \eta} < 0$ on $\partial\Omega$, and hence w_λ is a strict subsolution for (1.15). Again using the supersolution $Z \equiv 1$ and Lemma 2.1, (1.15) has a positive solution $u_\lambda \in [w_\lambda, 1]$ for $\lambda \geq \lambda^*$, and since $\|w_\lambda\|_\infty \longrightarrow 1$ as $\lambda \longrightarrow \infty$, we obtain $\|u_\lambda\|_\infty \longrightarrow 1$ as $\lambda \longrightarrow \infty$.

Next we will show that there exists at least two positive solutions for $\lambda \in [\overline{\lambda}, \overline{E}_1)$. Consider the eigenvalue problem (5.2) with μ_λ and $\phi_\lambda > 0$; $\overline{\Omega}$ as before. Then $\mu_\lambda > 0$ for $\lambda < \overline{E}_1$ (see [GMRS18]). Let $Z_1 := \beta_1\phi_\lambda$ with $\beta_1 > 0$. For $\beta_1 \approx 0$, in Ω, we have

$$-\Delta Z_1 - \lambda f(Z_1) = (\lambda + \mu_\lambda)Z_1 - \lambda f(Z_1) > 0,$$

since $H_1(s) := (\lambda + \mu_\lambda)s - \lambda f(s)$ satisfies $H_1(0) = 0$ and $H_1'(0) = \mu_\lambda > 0$. Also, on $\partial\Omega$, choosing $\beta_1 \approx 0$ so that $|\gamma\sqrt{\lambda}[(A - Z_1)^2 - A^2]| < \mu_\lambda$, we have:

$$\begin{aligned} \frac{\partial Z_1}{\partial \eta} + \gamma\sqrt{\lambda}[(A - Z_1)^2 + \epsilon]Z_1 &= \frac{\partial Z_1}{\partial \eta} + \gamma\sqrt{\lambda}[A^2 + \epsilon]Z_1 + \gamma\sqrt{\lambda}[(A - Z_1)^2 - A^2]Z_1 \\ &= \Big\{\mu_\lambda + \gamma\sqrt{\lambda}\big[(A - Z_1)^2 - A^2\big]\Big\}Z_1 > 0. \end{aligned}$$

Hence, for $\beta_1 \approx 0$, Z_1 is a strict supersolution for $\lambda < \overline{E}_1$. Now for $\lambda \in [\overline{\lambda}, \overline{E}_1)$ we have the solution $\psi_0 \equiv 0$ (hence a subsolution), strict subsolution $\psi = \delta_\lambda \theta_\lambda$ (≤ 1), strict supersolution $Z_1 = \beta_1 \phi_\lambda$ (with $\beta_1 \approx 0$ so that $\psi \nleq Z_1$ and $Z_1 \leq 1$), and the supersolution $Z \equiv 1$. Hence, by Lemma 2.2, for $\lambda \in [\overline{\lambda}, \overline{E}_1)$ there exists at least two positive solutions u_1, u_2 with $u_1 \in [\psi, Z]$ and $u_2 \in [0, Z] \backslash \{[0, Z_1] \cup [\psi, Z]\}$.

Finally, we will show that for $\lambda \approx 0$, (1.15) has no positive solutions. Recall $\sigma_\lambda, \theta_\lambda$ in (5.1) with $K = \epsilon$. Suppose u is a positive solution of (1.15), By Green's second identity we obtain:

$$L = \int_\Omega [(\Delta u)\theta_\lambda - (\Delta \theta_\lambda) u] dx = \int_{\partial\Omega} -\gamma\sqrt{\lambda}(A-u)^2 u \theta_\lambda ds \leq 0.$$

However, $L = \int_\Omega [-\lambda f(u) + (\lambda + \sigma_\lambda)u]\theta_\lambda dx \geq \int_\Omega [\sigma_\lambda - (M-1)\lambda] u\theta_\lambda dx$, where $M > 0$ is such that $f(s) \leq Ms$ for $s \in [0, \infty)$. But $\frac{\sigma_\lambda}{\lambda} \longrightarrow \infty$ as $\lambda \longrightarrow 0$ (see [FMSS]), and hence $L > 0$ for $\lambda \approx 0$, which is a contradiction. Thus (1.15) has no positive solutions for $\lambda \approx 0$. Hence, Theorem 1.13 is proven.

5.2 Proof of Theorem 1.14

We first recall that (see [GMRS18]) $E_1(\gamma, D)$ is increasing both in γ and D, and $\lim_{\gamma \to \infty} E_1(\gamma, D) = \lim_{D \to \infty} E_1(\gamma, D) = A_1$. Let $\tilde{\lambda} > A_1$. Here, we will discuss the existence of three positive solutions when $\lambda \in [\overline{E}_1, \tilde{\lambda}]$. Let $\Gamma \supset \Omega$, $\Gamma \approx \Omega$ be such that the boundary value problem (see [SS06]):

$$-\Delta w = \tilde{\lambda} f(w);\ \Gamma,$$
$$w = 0;\ \partial\Gamma,$$

has a positive solution $w_{\tilde{\lambda}} = Z_1$ (say) such that $Z_1 \in (0, \frac{A}{2})$; $\partial\Omega$. This is possible since (5.3) has a positive solution for $\lambda \geq \lambda^* \in (0, A_1)$. Let $C := \min_{\partial\Omega} Z_1$. Choose $\gamma^*(\tilde{\lambda}) > 0$ such that for $\gamma > \gamma^*$

$$E_1(\gamma, A^2) > \tfrac{A_1}{2}, \tag{5.4}$$

($\Rightarrow E_1(\gamma, A^2 + \epsilon) > \frac{A_1}{2}$) and

$$\tfrac{\partial Z_1}{\partial \eta} + \gamma\sqrt{\tfrac{A_1}{2}}\tfrac{A^2}{4}C > 0;\ \partial\Omega, \tag{5.5}$$

($\Rightarrow \frac{\partial Z_1}{\partial \eta} + \gamma\sqrt{\frac{A_1}{2}}(\frac{A^2}{4} + \epsilon)C > 0;\ \partial\Omega$) hold. Now for $\lambda \in [\frac{A_1}{2}, \tilde{\lambda}]$ we have:

$$-\Delta Z_1 = \tilde{\lambda} f(Z_1) \geq \lambda f(Z_1);\ \Omega,$$

and

$$\frac{\partial Z_1}{\partial \eta} + \gamma\sqrt{\lambda}[(Z_1 - A)^2 + \epsilon]Z_1 \geq \frac{\partial Z_1}{\partial \eta} + \gamma\sqrt{\frac{A_1}{2}}\Big(\frac{A^2}{4} + \epsilon\Big)C > 0;\ \partial\Omega.$$

Thus Z_1 is a strict supersolution for (1.15) when $\lambda \in [\frac{A_1}{2}, \tilde{\lambda}]$. Next consider the boundary value problem:

$$\begin{cases} -\Delta v = \lambda v(1 - v);\ \Omega, \\ \frac{\partial v}{\partial \eta} + 2\gamma\sqrt{\lambda}(A - v)^2 v = 0;\ \partial\Omega. \end{cases} \tag{5.6}$$

For each $\lambda > 0$, (5.6) has a unique solution $v_\lambda \in [A, 1];\ \overline{\Omega}$ (see [GMPS19]). Further, by the Hopf's maximum principle $v_\lambda > A;\ \partial\Omega$.

Let $c_\lambda := \min_{\partial\Omega} v_\lambda$ and $\epsilon^*(\tilde{\lambda},\gamma) := \min_{\lambda\in[\overline{E}_1,\tilde{\lambda}]} (c_\lambda - A)^2$. Let $\psi_2 := v_\lambda$. Then for $\epsilon < \epsilon^*$, ψ_2 satisfies (for $\lambda \in [\overline{E}_1, \tilde{\lambda}]$):

$$-\Delta\psi_2 = \lambda\psi_2(1-\psi_2) \leq \lambda f(\psi_2);\ \Omega,$$

(since $\frac{a+\psi_2}{a} > 1$), and

$$\frac{\partial\psi_2}{\partial\eta} + \gamma\sqrt{\lambda}[(\psi_2 - A)^2 + \epsilon]\psi_2 = \gamma\sqrt{\lambda}[\epsilon - (\psi_2 - A)^2] < \gamma\sqrt{\lambda}[\epsilon - \epsilon^*] < 0;\ \partial\Omega,$$

(since $\frac{\partial\psi_2}{\partial\eta} + 2\gamma\sqrt{\lambda}(\psi_2 - A)^2\psi_2 = 0;\ \partial\Omega$). Thus ψ_2 is a strict subsolution for $\lambda \in [\overline{E}_1, \tilde{\lambda}]$.

Now let $\psi_1 = \tilde{\psi}(= \beta\phi)$ where $\tilde{\psi}$ is as in the proof of Theorem 1.13. Note that when $\beta \approx 0$, ψ is a subsolution for $\lambda \geq \overline{E}_1$. Finally, take $Z_2 \equiv 1$ which is a supersolution for $\lambda > 0$. Now choosing $\beta \approx 0$, we can make sure $Z_1, \psi_2 \in [\psi_1, Z_2]$. Further, note that $\|\psi_2\|_\infty \geq A$ while $\|Z_1\|_\infty \leq \frac{A}{2}$. Hence, by Lemma 2.2, (1.15) has at least three positive solutions when $\lambda \in [\overline{E}_1, \tilde{\lambda}]$, and Theorem 1.14 is proven.

5.3 Computational Results

Finally, we present some bifurcation diagrams that we have obtained for (1.16). We employ a similar procedure as described in Chapter IV to compute numerical bifurcation diagrams.

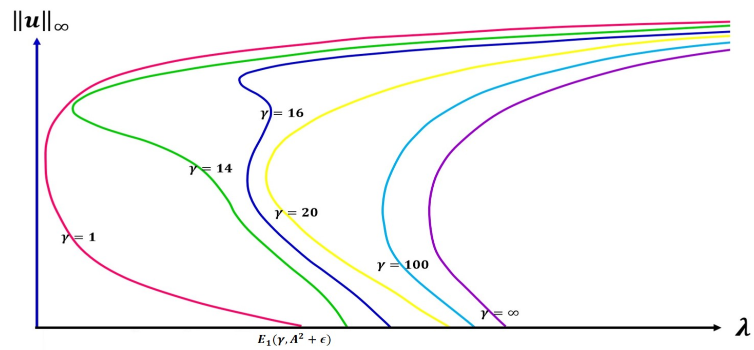

Figure 45. Evolution of the Bifurcation Diagrams for (1.16) as γ Varies, Using $\epsilon = 0.084$ and $A = 0.5$.

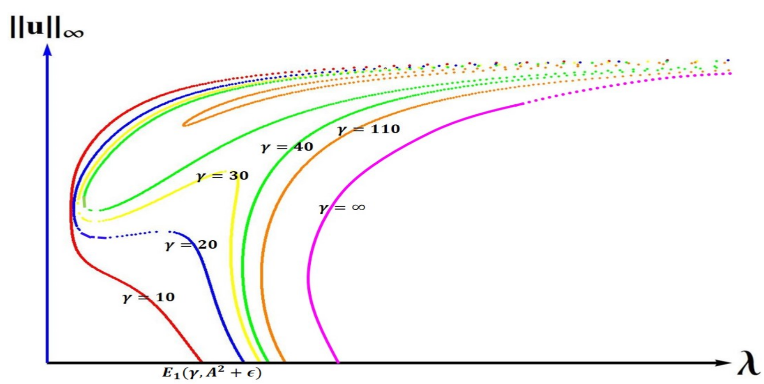

Figure 46. Evolution of the Bifurcation Diagrams for (1.16) as γ Varies, Using $\epsilon = 0.01$ and $A = 0.5$.

When $\epsilon = 0.084$, the hypothesis of Theorem 1.11 is satisfied, and hence all positive solutions of (1.16) are symmetric. In this case we note that the exact bifurcation diagram predicted via Theorem 1.13 occurs for certain γ values (see Figure 45). We also observe that the solution is unique for $\lambda > E_1(\gamma, A^2 + \epsilon)$.

When $\epsilon = 0.01$, the hypothesis of Theorem 1.11 is not satisfied. In this case, we note that both symmetric and non-symmetric solutions occur for certain γ values and the bifurcation diagrams corresponding to all solutions are more than that was predicted via Theorem 1.14 (see Figure 47).

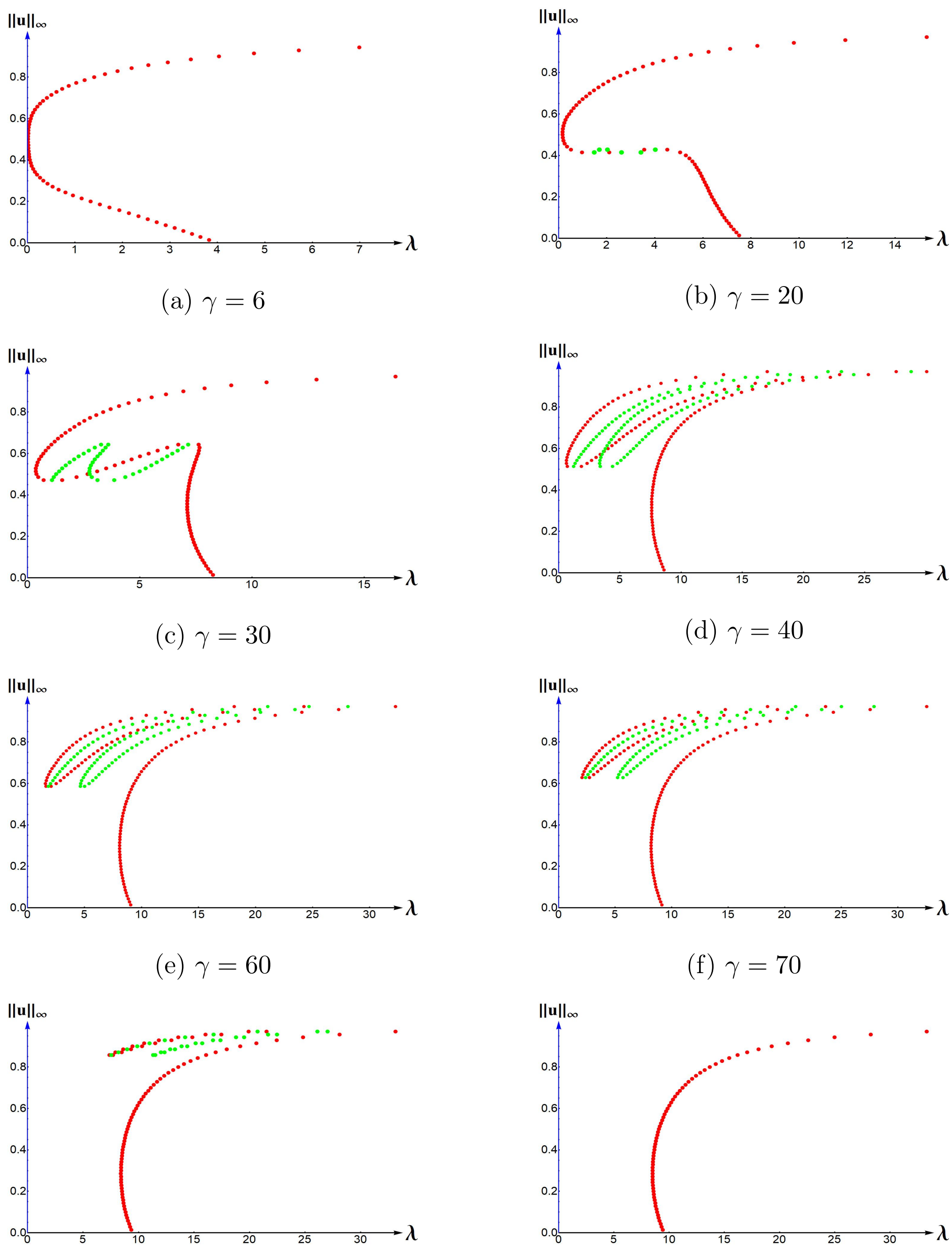

(a) $\gamma = 6$

(b) $\gamma = 20$

(c) $\gamma = 30$

(d) $\gamma = 40$

(e) $\gamma = 60$

(f) $\gamma = 70$

(g) $\gamma = 120$

(h) $\gamma = \infty$

Figure 47. Bifurcation Diagrams for (1.16) for Several Values of γ, When $\epsilon = 0.01$ and $A = 0.5$. Symmetric Solutions are in Red and Non-symmetric Solutions are in Green.

CHAPTER VI

PROOFS OF THEOREMS 1.15, 1.18 - 1.20 STATED IN FOCUS 4 AND COMPUTATIONAL RESULTS

6.1 Proof of Theorem 1.15

Let $\lambda < E_1(\gamma, 1)$. By Lemma 1.17, we see that the zero solution is asymptotically stable if the principal eigenvalue σ_1^* of (1.22) with $u \equiv 0$ is positive. Note that, for $\lambda < E_1(\gamma, 1)$, the zero solution is isolated since λ is not a bifurcation point on the solution curve $(\mu, 0)$. Let $\mu_1 = \mu_1(\beta)$ be the principal eigenvalue of:

$$\begin{cases} -\phi'' = \mu\phi; \ x \in (0,1), \\ -\phi'(0) = -\beta\phi(0), \\ \phi'(1) = -\beta\phi(1), \end{cases}$$

where $\beta \geq 0$. Then $\mu_1(\beta)$ is a strictly increasing concave function which passes through the origin and is bounded above by A_1 (see [RR19] and [CGS19]).

Let $\beta := \gamma\sqrt{\lambda}g(0)$. Since $\mu_1(\beta)$ is a strictly increasing concave function of β and $\frac{\beta^2}{\gamma^2 g(0)^2}$ is a strictly increasing convex function of β which passes through the origin, they intersect at exactly two points, namely at $(0,0)$, and at $(\beta^*, \mu_1(\beta^*))$ for some $\beta^* > 0$ (see Figure 48). From (1.20), we can easily see that $\mu_1(\beta^*) = E_1(\gamma, 1)$ and $\beta^* = \gamma\sqrt{E_1(\gamma, 1)}g(0)$. Further, $\lambda + \sigma_1^* = \mu_1(\gamma\sqrt{\lambda}g(0))$, where σ_1^* is the principle eigenvalue of (1.22). Thus, if $\lambda < E_1(\gamma, 1)$, then $\gamma\sqrt{\lambda}g(0) < \beta^*$ and $\mu_1(\gamma\sqrt{\lambda}g(0)) > \lambda$, implying $\sigma_1^* > 0$. By Lemma 1.17 the zero solution is asymptotically stable if $\lambda < E_1(\gamma, 1)$.

Next, let $\lambda > E_1(\gamma, 1)$. By Lemma 1.17, the zero solution is unstable if the principle eigenvalue σ_1^* of (1.22) is negative. But when $\lambda > E_1(\gamma, 1)$, $\gamma\sqrt{\lambda}g(0) > \beta^*$ and $\mu_1(\gamma\sqrt{\lambda}g(0)) < \lambda$ implying $\sigma_1^* < 0$ (see Figure 48). Hence, Theorem 1.15 is proven.

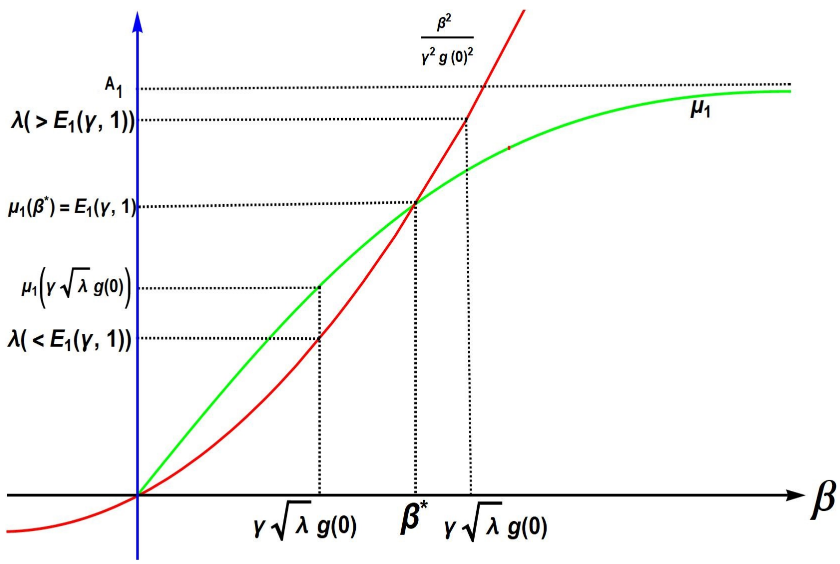

Figure 48. Graphs of β vs $\mu_1(\beta)$ and $\frac{\beta^2}{\gamma^2(g(0))^2}$.

6.2 Proof of Theorem 1.18

Assume that $\gamma > 0$, $a \in (0, 1)$, and $\lambda < E_1(\gamma, 1)$, are given and $u_1(x)$ is a positive solution of (1.18). By Theorem 1.15, the trivial steady state, $u(x) \equiv 0$, of (1.17) is asymptotically stable. Since $f(s) < 0$ for all $s > 1$, any constant $M \geq 1$ is a supersolution for (1.18) and a strict supersolution if $M > 1$ (see Definition 4.1 of [Pao92]). Thus, any positive solution, $u(x)$, of (1.18) must satisfy $0 < u(x) < 1$ for $x \in [0, 1]$. Now, since $u_1(x)$ is a positive solution of (1.18), it is also a subsolution and satisfies $u_1(x) \leq 1$. For any $u_0(x)$ such that $u_1(x) \leq u_0(x) \leq 1$ for $x \in (0, 1)$, Theorem

6.6 of [Pao92] guarantees that the solution of (1.17), $u(t,x)$, with $u(0,x) = u_0(x)$ for $x \in (0,1)$ must satisfy $0 < u_1(x) < u(t,x) < 1$ for all $x \in [0,1], t \geq 0$. It is now clear that the model (1.17) will predict extinction for initial population densities, $u_0(x)$, with $\|u_0\|_\infty \approx 0$, whereas the model will predict persistence for $u_0(x)$ satisfying $u_1(x) \leq u_0(x) \leq 1$ for $x \in (0,1)$. This establishes a patch-level Allee effect. Hence, Theorem 1.18 is proven.

6.3 Proof of Theorem 1.19

Let $u(x)$ be a positive solution of (1.18) such that $q_1 = u(0)$ and $q_2 = u(1)$. From Theorem 2.3, q_1, q_2 must satisfy $2[F(\rho) - F(q_1)] = \gamma^2 g(q_1)^2 q_1^2$ and $2[F(\rho) - F(q_2)] = \gamma^2 g(q_2)^2 q_2^2$. Hence, $g(q_1)^2 q_1^2 [F(\rho) - F(q_2)] = g(q_2)^2 q_2^2 [F(\rho) - F(q_1)]$, or equivalently,

$$\frac{h(q_1)^2}{h(q_2)^2} = \frac{g(q_1)^2 q_1^2}{g(q_2)^2 q_2^2} = \frac{[F(\rho) - F(q_1)]}{[F(\rho) - F(q_2)]}. \tag{6.1}$$

Since $F(s)$ is increasing for $s \in (0,1)$, (6.1) can hold only if $q_1 = q_2$. Hence, Theorem 1.19 is proven.

6.4 Proof of Theorem 1.20

To prove (a), we first note that:

$$h'(s) = g(s) + sg'(s) = \tfrac{M_1 + m(s) + sm'(s)}{M_1}. \tag{6.2}$$

Thus, if $m'(s) \geq 0$, then we must have $h'(s) > 0$ for $s \in (0,1)$, and (i) and (ii) hold by Theorem 1.19. To show (iii), we again calculate $h'(s)$ as

$$h'(s) = \frac{3s^2 - 4M_3 s + M_1 M_2}{M_1 M_2}. \tag{6.3}$$

It is easy to see that if $4M_3^2 - 3M_1M_2 < 0$, or equivalently, $M_1M_2 > \frac{4M_3^2}{3}$, then we must have that $h'(s) > 0$ for $s \in (0,1)$, and hence (iii) holds by Theorem 1.19.

To show (b), we calculate $h'(s)$ when $m(s) = \frac{s^2 - 2M_3 s}{M_2}$ for $M_3 \geq 0$:

$$h'(s) = \frac{M_1 M_2 (M_1 M_2 - s^2)}{(s^2 - 2M_3 s + M_1 M_2)^2}. \tag{6.4}$$

Hence, if $M_1M_2 > 1$, then $h'(s) > 0$ for $s \in (0,1)$, and hence (b) holds by Theorem 1.19. Hence, Theorem 1.20 is proven.

6.5 Computational Results

Finally, we present our numerical results including bifurcation diagrams that we have obtained for (1.18). We use a similar procedure as described in Chapter IV to compute numerical bifurcation diagrams.

6.5.1 Structure of Positive Steady States of (1.15) as the effective matrix hostility parameter Varies

Recall from Theorem 1.18 that if there exists a range of $\lambda < E_1(\gamma, 1)$ for which a positive solution of (1.18) exists then the model will predict an Allee effect at the patch-level for patch sizes corresponding to these $\lambda-$values. In this Allee effect case, the population density must surpass a certain threshold in order for persistence to be predicted. Since our growth rate $f(u)$ is taken to be of a weak Allee effect form, we would expect model predictions of an Allee effect at the patch-level in the case of a DIE. We are particularly interested in model predictions of bi-stability scenarios other than a patch-level Allee effect in the case of density dependent emigration. We will present an evolution of the bifurcation curves for all five DDE forms as γ increases for the cases 1) where the forms of DDE are relatively weak and parameter values are $a = 0.5$, $M_1M_2 = 1.1$ and $M_3 = 0.5$ (see Figure 49), where the forms of DDE are relatively strong and pronounced with parameter values $a = 0.5$, $M_1M_2 = 0.08$ and $M_3 = 0.25$ (see Figure 50). In both cases, an a-value of 0.5 gives a substantial weak Allee effect, i.e. the per-capita growth rate will increase for u-values in $[0, 0.25)$. Note that the presentation of an exploration of the entire parameter space would be quite challenging and is outside of the scope of this work.

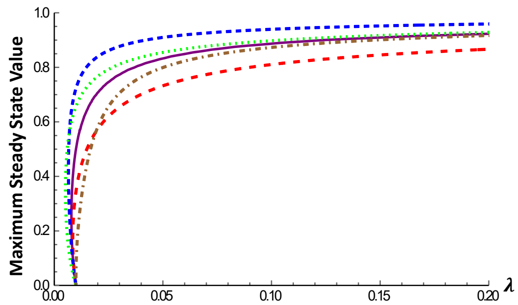

(a) $\gamma = 0.05$

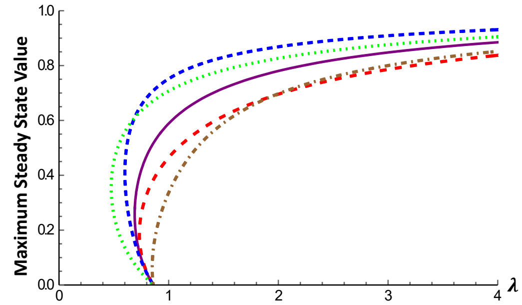

(b) $\gamma = 0.5$

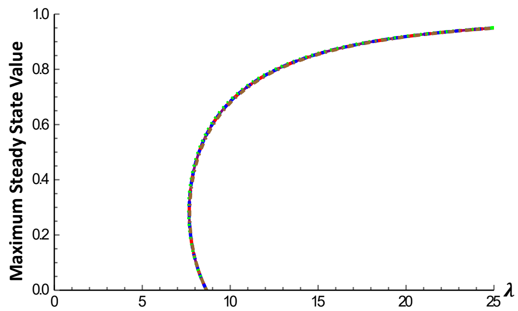

(c) $\gamma = 10$

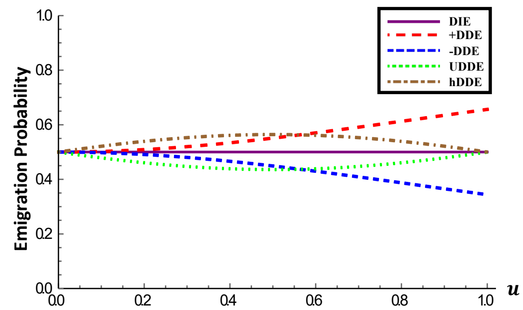

(d) Graph of u vs emigration probability

Figure 49. Bifurcation Curves of Positive Solutions of (1.18) for all Five DDE Forms When $a = 0.5$, $M_1M_2 = 1.1$, and $M_3 = 0.5$ for Various γ-values. This Choice of M_1, M_2, and M_3 Yield DDE Forms That are Weakly Related to Density and Somewhat Similar in Shape to DIE, and an M_3-value of 0.5 Causes the Minimum Emigration Probability and Maximum Emigration Probability of UDDE and hDDE, Respectively, to Both Occur at $u = 0.5$.

As shown in both Figures 49 and 50, the bifurcation curves' starting value, $E_1(\gamma, 1)$, satisfies $E_1(0, 1) = 0$, $E_1(\gamma, 1)$ is strictly increasing in γ, and $E_1(\gamma, 1) \to \pi^2$ as $\gamma \to \infty$ (see [RR19] or [GMRS18], for example).

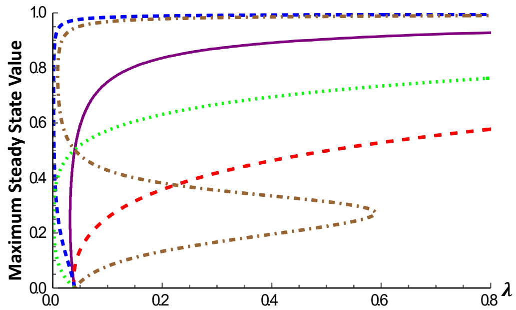

(a) $\gamma = 0.1$

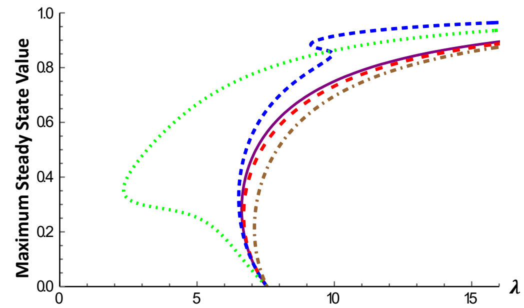

(b) $\gamma = 5$

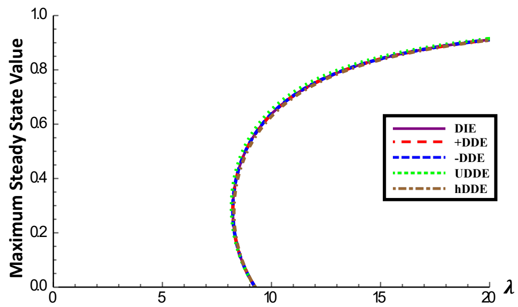

(c) $\gamma = 20$

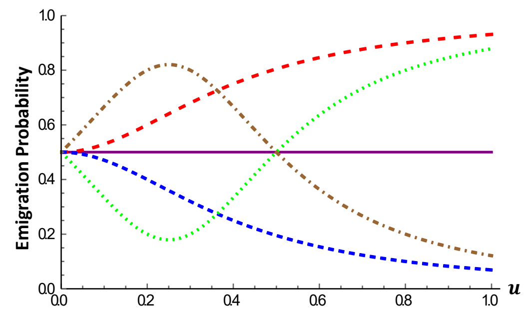

(d) Graph of u vs emigration probability

Figure 50. Bifurcation Curves of Positive Solutions of (1.18) for All Five DDE Forms When $a = 0.5$, $M_1M_2 = 0.08$, and $M_3 = 0.25$ for Various γ-values. This Choice of M_1, M_2, and M_3 Yield DDE Forms That are Quite Different in Shape From the DIE Form, and an M_3-value of 0.25 Causes the Minimum Emigration Probability and Maximum Emigration Probability of UDDE and hDDE, Respectively, to Both Occur at $u = 0.25$.

The positive relationship between density and emigration probability in +DDE and initially in hDDE cause the maximum steady state values of these two forms to be much less than the DIE case, whereas the negative relationship in -DDE and initially in UDDE cause an increase in maximum steady state values as compared with the DIE form. The difference in maximum steady state values appears to be greatest for intermediate values of γ and the least when γ is large. Notice that as $\gamma \to \infty$, i.e. when the matrix is completely hostile, the +DDE, -DDE, UDDE, and hDDE curves all converge to the DIE form as illustrated in Figures 49(c) and 50(c). A patch-level Allee effect is present in all values of γ for Figure 49, but the initial positive relationship between density and emigration probability of hDDE is able to completely counteract the patch-level Allee effect in 50(a), even though the +DDE case does not. This discrepancy is due to the positive relationship being much stronger (at least initially) in the hDDE case versus the +DDE case, as shown in Figure 50(d). In Figure 49, the only bi-stability of steady states predicted by the model is the aforementioned patch-level Allee effect. In contrast, Figure 50 shows examples of other types of bi-stability in the case of hDDE in (a) and -DDE in (b). Though not shown here, a similar non-Allee effect bi-stability also appeared in the UDDE case for the same parameter values in Figure 50. In fact, any S-shaped bifurcation curve (or even a more complicated shape) occurring for $\lambda > E_1(\gamma, 1)$ will not qualify as a patch-level Allee effect since by Theorem 1.15, the trivial steady state, $u(x) \equiv 0$, is unstable. In both cases, model predictions of persistence vary over a wide range as the effective matrix hostility, as measured in the composite parameter γ, varied.

6.5.2 Allee Effect Region Length

In this section, we explore the relationship between DDE form and the strength of the patch-level Allee effect predicted by the model (1.17). In order to accomplish this, we study the length of the AER, defined as $E_1(\gamma, 1) - \lambda_m(\gamma)$, for fixed values of M_1, M_2, M_3, and a (see Figure 51). We calculate $\lambda_m(\gamma)$ by employing Theorem 2.3

and Mathematica (Wolfram Inc., ver. 12.0) to numerically generate the bifurcation curve of positive solutions of (1.18). The smallest λ-value on the curve is then λ_m. Using the Mathematica command `NDEigensystem`, we numerically estimate the value of $E_1(\gamma, 1)$. If $\lambda_m(\gamma) < E_1(\gamma, 1)$, then for $\lambda \in (\lambda_m(\gamma), E_1(\gamma, 1))$, there is at least one positive solution, and by Theorem 1.18 the model predicts a patch-level Allee effect. However, if $\lambda_m(\gamma) \geq E_1(\gamma, 1)$, then no such patch-level Allee effect can exist, since by Theorem 1.15, the trivial steady state is unstable for $\lambda \geq E_1(\gamma, 1)$. In what follows, we will first compare the length of the AER for all the DDE forms given in Table 1 and then explore the possibility of the +DDE form counteracting a patch-level Allee effect.

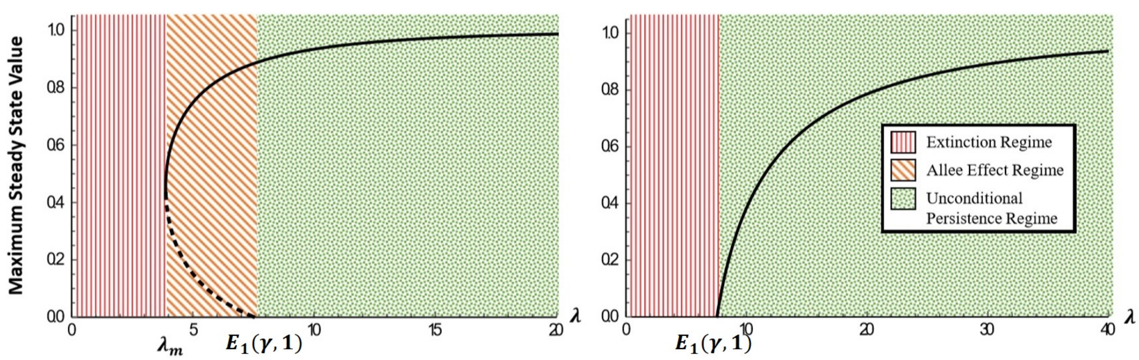

Figure 51. Bifurcation-stability Curves of Population Persistence with λ Proportional to Patch Size Squared. In These Diagrams, the Population Shows a Patch-level Allee effect (left) and No Patch-level Allee Effect (right). Solid Curves Correspond to Stable Steady States and Dashed Curves Correspond to Unstable Steady States. Note that the Trivial Steady State is Stable to the Left of $E_1(\gamma, 1)$ and Unstable to the Right of $E_1(\gamma, 1)$.

6.5.2.1 Qualitative Connection Between AER Length and DDE Form

Choosing $M_3 = 0.25$ and $a = 0.5$, we computed the AER length for different γ-values for each of the five DDE forms. This choice of a will ensure a substantial weak Allee effect, i.e. the per-capita growth rate will increase for u-values in $[0, 0.25)$, whereas, $M_3 = 0.25$ will cause the minimum and maximum emigration probabilities to occur at $u = 0.25$ for UDDE and hDDE, respectively. We evaluated many other parameter values for M_3 and a but obtained similar results. Although a full exploration of the entire parameter space is outside the scope of this work, we aim to provide a qualitative connection between the form of DDE and length of AER as the effective matrix hostility is varied via γ. Figures 52 - 54 illustrate this connection for $M_1M_2 = 0.1, 0.5$, and 1. These M_1M_2-values produce DDE forms that are somewhat different from DIE when $M_1M_2 \approx 0$ to almost identical to DIE when M_1M_2 is large.

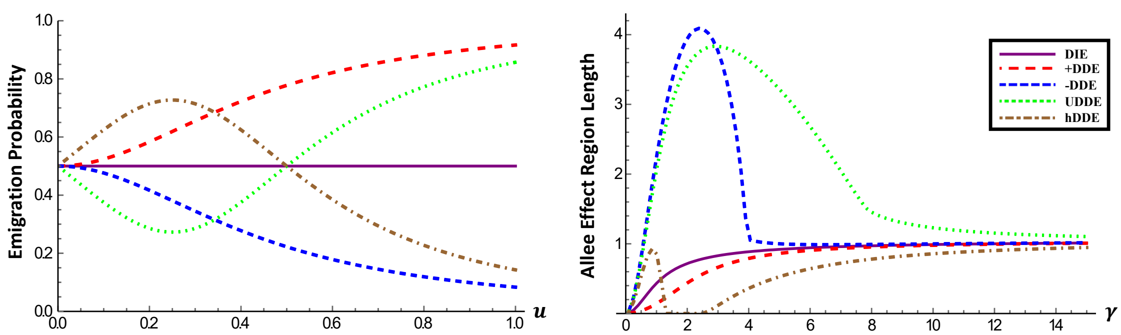

Figure 52. Graph of u vs Emigration Probability (left) and γ vs AER Length (right) for $M_1M_2 = 0.1, M_3 = 0.25$, and $a = 0.5$.

In all three cases of M_1M_2-values, the model always exhibited a patch-level Allee effect in the DIE, +DDE, -DDE, and UDDE cases.

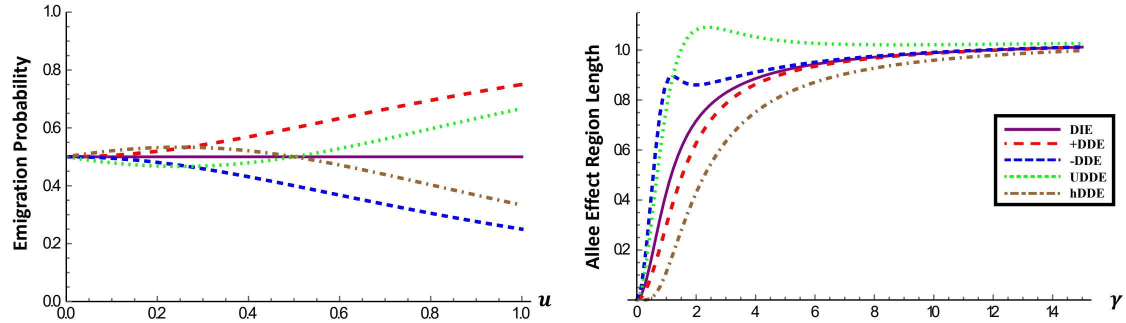

Figure 53. Graph of u vs Emigration Probability (left) and γ vs AER Length (right) for $M_1M_2 = 0.5, M_3 = 0.25$, and $a = 0.5$.

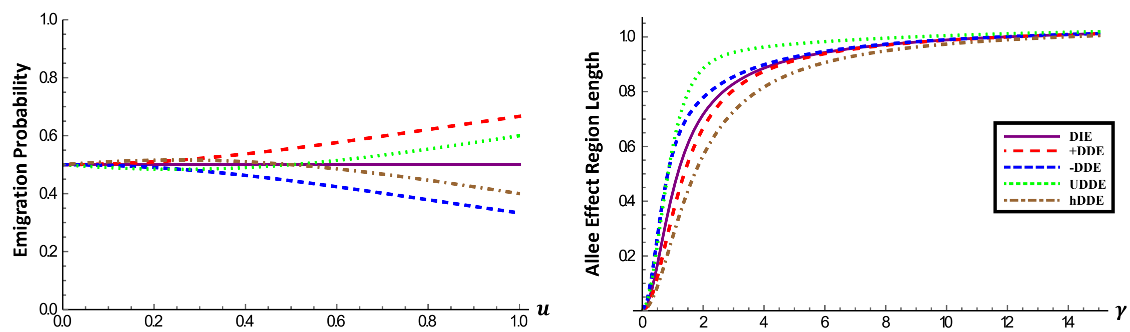

Figure 54. Graph of u vs Emigration Probability (left) and γ vs AER Length (right) for $M_1M_2 = 1, M_3 = 0.25$, and $a = 0.5$.

Also, when γ is large, the length of the AER is virtually identical to DIE across all DDE forms. The AER length approached zero in all DDE forms and in all parameter choices as γ approached zero. The +DDE form partially counteracted the patch-level Allee effect by slightly lowering the AER length for all γ-values, though for these parameter choices, the +DDE relationship was not strong enough to fully counteract the patch-level Allee effect. In contrast, the hDDE form, which is initially a positive relationship between density and emigration rate, was able to completely counteract the patch-level Allee effect for γ approximately in $[1.5, 2.5]$ in Figure 52 and in $(0, 0.5]$ in Figure 53. This discrepancy between the +DDE and hDDE forms is due to the positive relationship in the hDDE being clearly stronger than the one in +DDE in both Figures 52 and 53. Due to switching from a positive relationship to a strong negative one, a patch-level Allee effect reappeared for $\gamma < 1.5$ for hDDE in Figure 52. However, this switch in the relationship in hDDE was not sufficient to allow the patch-level Allee effect to reappear in Figure 53.

In all three Figures, both -DDE and UDDE forms caused an increase in length of the AER as compared to the DIE case. In fact, in Figures 52 and 53, the AER length initially increased as γ decreased but then began to decrease as γ became small for both -DDE and UDDE, even boasting a peak value of almost four-times the DIE AER length in Figure 52. In Figure 54, all DDE forms had strictly decreasing AER length as γ decreased. Interestingly, in Figure 52, the AER length for -DDE exhibited a steep increase from around one for $\gamma \approx 4$ to around four for $\gamma \approx 2.5$. A positive relationship between density and emigration rate at least partially counteracted the patch-level Allee effect for +DDE and hDDE forms, whereas the negative relationship enhanced the patch-level Allee effect for -DDE and UDDE forms. Also, this counteraction and enhancement of the patch-level Allee effect is dependent upon the effective matrix hostility of the surrounding patch matrix, as measured by the parameter γ.

6.5.2.2 Counteracting a Patch-Level Allee Effect with +DDE

Our analysis of the structure of positive steady states for the model indicates that DDE forms containing a negative slope can increase the strength of the patch-level Allee effect as measured by the AER length, whereas, a positive slope can counteract the patch-level Allee effect. Even though both +DDE and hDDE have the potential to completely counteract a patch-level Allee effect for small patch sizes, the hDDE form's negative slope for $u > M_3$ will allow the patch-level Allee effect to reappear as the patch size approaches zero (see Figure 52). Thus, we chose to focus on +DDE in an attempt to quantify when a patch-level Allee effect will be completely counteracted by a DDE relationship containing a positive slope. To that end, we again employed Theorem 2.3 and Mathematica (Wolfram Inc., ver. 12.0) to numerically generate bifurcation curves of positive solutions for (1.18) for fixed sets of parameter values. To establish the existence of a patch-level Allee effect in the +DDE case, it suffices to show that the slope of the bifurcation curve is negative for $\rho \approx 0$, i.e. we consider $\lambda = \lambda(\rho)$ (ρ denotes the maximum steady state value) and numerically calculate $\lambda'(0)$. Figure 55 illustrates the parts of the parameter space for which a patch-level Allee effect is predicted by the model, i.e $\lambda'(0) < 0$, (Region I) and parts where a patch-level Allee effect is not predicted, $\lambda'(0) > 0$, (Region II) for the case of $a = 9$. Notice that the boundary between Regions I and II is comprised of the M_1M_2- and γ-values such that $\lambda'(0) = 0$.

There is clearly a maximal M_1M_2-value, such that for M_1M_2 larger than this value the model will predict a patch-level Allee effect for all $\gamma > 0$. In contrast, it appears that for any $\gamma > 0$, there is always a small range of M_1M_2-values such that no patch-level Allee effect is present.

Figure 56 compares the boundary curve separating parameter space into Region I and II for $a = 0.5, 0.75$, and 0.9. Recall that $a \in (0, 1)$ measures the strength of the demographic weak Allee effect in the model via the per-capita growth rate.

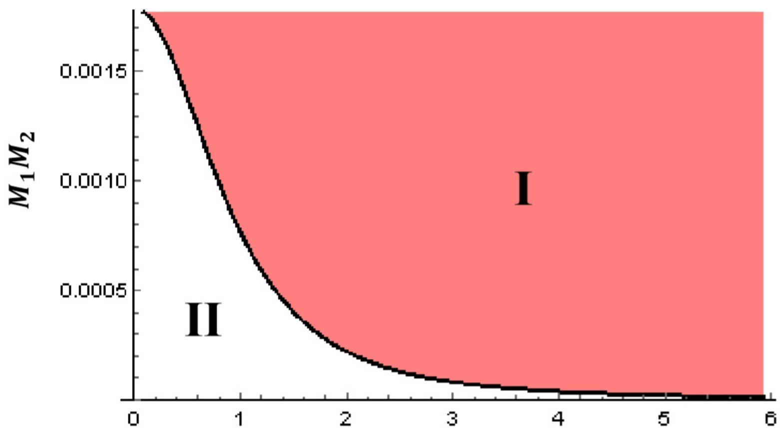

Figure 55. The Model Predicts a Patch-level Allee Effect for Parameters in Region I and No Patch-level Allee Effect in Region II. Note That $a = 0.9$ Indicates a Mild Weak Allee Effect in Per-capita Growth Rate, Whereas, Small Values of M_1M_2 Cause a Very Rapid Ascent for the Emigration Probability From 0.5 to Close to 1.

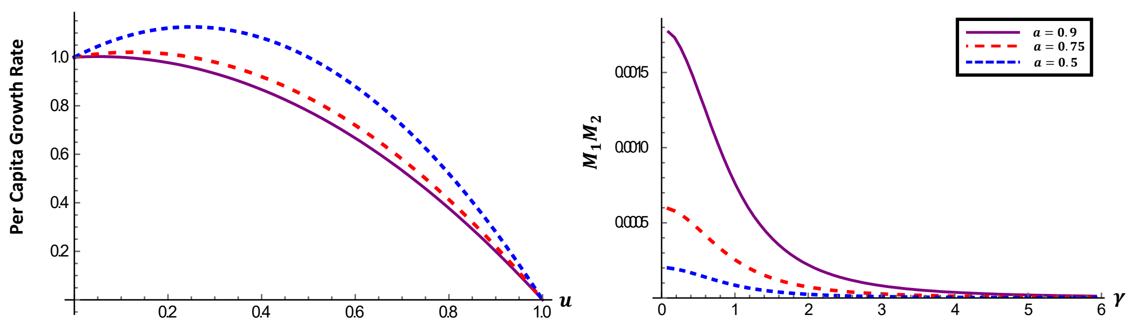

Figure 56. Graph of u vs Per-capita Growth Rate (left) and the Boundary Between a Model Prediction of a Patch-level Allee Effect and No Patch-level Allee Effect for γ vs M_1M_2 (right). Note That the Area of Parameter Space Lying Above the Curves in the (right) is a Patch-level Allee Effect Region, Whereas the Area Below is Not.

Thus, the demographic Allee effect varies from almost not present for $a \approx 1$ to substantial for $a \approx 0$ (see Figure 56 (left)). Figure 56 shows that for smaller a-values, the +DDE response must become correspondingly stronger as indicated in the smaller M_1M_2-values. Figure 57 illustrates this point for fixed $\gamma = 0.59275$ and $a = 0.75$, in which we compare the +DDE forms from Regions I and II.

Notice that for M_1M_2-values that are sufficiently small (corresponding to solid curves in Figure 57) the positive relationship between density and emigration probability is strong enough to completely counteract the demographic Allee effect in the per-capita growth rate to produce no patch-level Allee effect. In contrast, the remaining dashed curves in Figure 57 represent +DDE forms that only partially counteract the patch-level Allee effect. Figure 58 further illustrates this point by comparing the actual bifurcation curves for +DDE forms belonging to Region I (dashed) and Region II (solid). Notice that, initially, the Region I +DDE form bifurcation curves all decrease in λ (i.e. $\lambda'(0) < 0$), while the Region II +DDE form bifurcation curves increase in λ (i.e. $\lambda'(0) > 0$), both as the maximum steady state value increases.

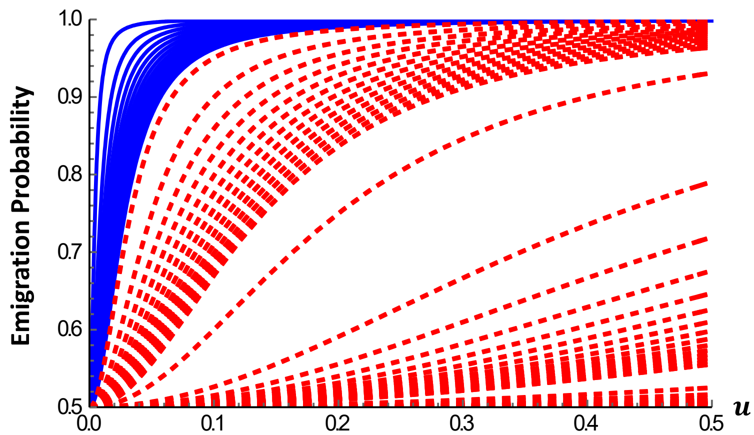

Figure 57. Comparison of +DDE Forms (u vs emigration probability) That Produce a Patch-level Allee Effect (dashed curves) and Forms That Counteract a Patch-level Allee Effect (solid curves) for $a = 0.75$ and $\gamma = 0.59275$.

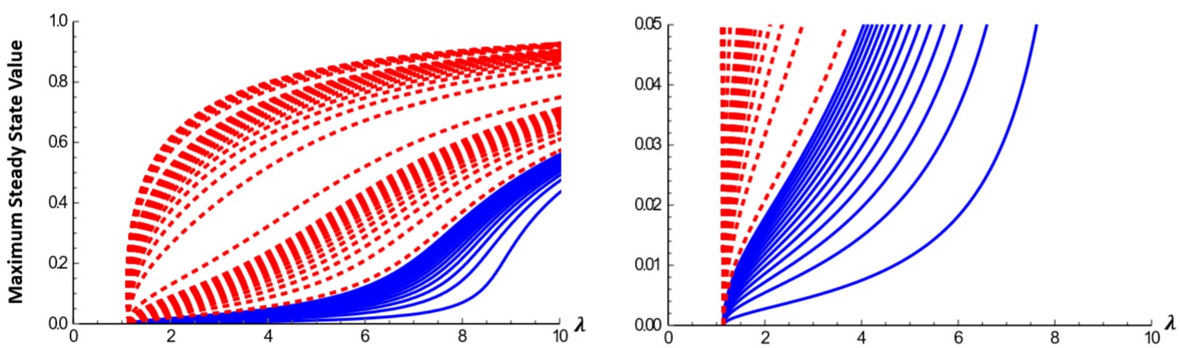

Figure 58. Comparison of Bifurcation Curves of Positive Solutions to (1.18) for the +DDE Forms Shown in Figure 57 (right) and the Same Graph but with Smaller Graphing Window. Note That $a = 0.75$ and $\gamma = 0.59275$.

CHAPTER VII

COMPUTATIONALLY GENERATED BIFURCATION CURVES IN DIMENSION N=2 FOR MODELS STATED IN FOCUS 5

For a fixed $\gamma > 0$ we will compute the numerical solution u_h (described in 2.31) for a sequence of λ values in order to depict a discrete bifurcation diagram. To achieve this, we will use the continuation method (see [Mei00] and [Sey10]), that is, starting from one numerical solution u_{h,λ_1}, we generate u_{h,λ_2}, u_{h,λ_3}, ... based on the increment of $\Delta\lambda$. For an appropriate choice of $\Delta\lambda$, the previous numerical solution u_{h,λ_k} serves as a good initial guess for the next numerical solution $u_{h,\lambda_{k+1}}$.

The main difficulty we are facing in solving the nonlinear system is that our solution does not converge near the turning points in the bifurcation curve since the sup-norm of the solution varies so rapidly near turning points making the Jacobian singular. To overcome this difficulty, we employ a Pseudo-Arclength method. Namely, we parameterize a branch of the bifurcation curve using arc length (see [Sey10]). In this method, we treat the parameter λ also as an unknown parametrized by the arc length, and we solve a nonlinear system of the form (treating λ in 2.31 as an unknown):

$$G(u, \lambda) = 0. \tag{7.1}$$

Let $u = (u_1, u_2, ..., u_n, \lambda)$ be the unknown solution which is to be found. We note that the arc length satisfies the following equation:

$$\left(\frac{du_1}{ds}\right)^2 + \left(\frac{du_2}{ds}\right)^2 + ... + \left(\frac{du_n}{ds}\right)^2 + \left(\frac{d\lambda}{ds}\right)^2 = 1.$$

From the above equation we obtain

$$\sum_{n=1}^{n}(u_i - u_i(s_j))^2 + (\lambda - \lambda(s_j))^2 - (s - s_j)^2 = 0.$$

Let $(u^j, \lambda_j) = (u(s_j), \lambda(s_j))$ is the solution previously calculated during continuation. In [Kel77] "pseudo arclength" was proposed, that is, for $0 < \zeta < 1$,

$$\zeta \sum_{n=1}^{n}(u_i - u_i(s_j))^2 + (1 - \zeta)(\lambda - \lambda(s_j))^2 - (s - s_j)^2 = 0. \tag{7.2}$$

Equation (7.1) together with (7.2) will provide us a system of $n_h + 1$ equations with $n_h + 1$ unknowns which we will solve to find the numerical solution. Whenever we find a solution, we track down the lambda value and the maximum of the solution as a pair to generate our bifurcation diagram.

Now we provide the evolution of bifurcation diagrams of (1.23) with respect to γ.

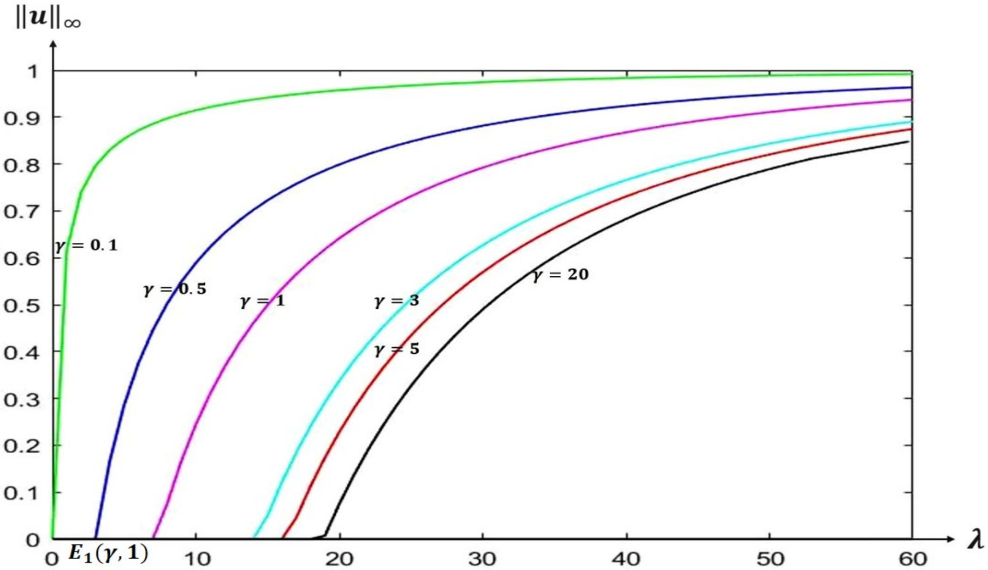

Figure 59. Evolution of Bifurcation Diagrams of (1.23) with Respect to γ.

Next we provide the evolution of bifurcation diagrams of (1.24) with respect to γ for the case when $\epsilon = 0$.

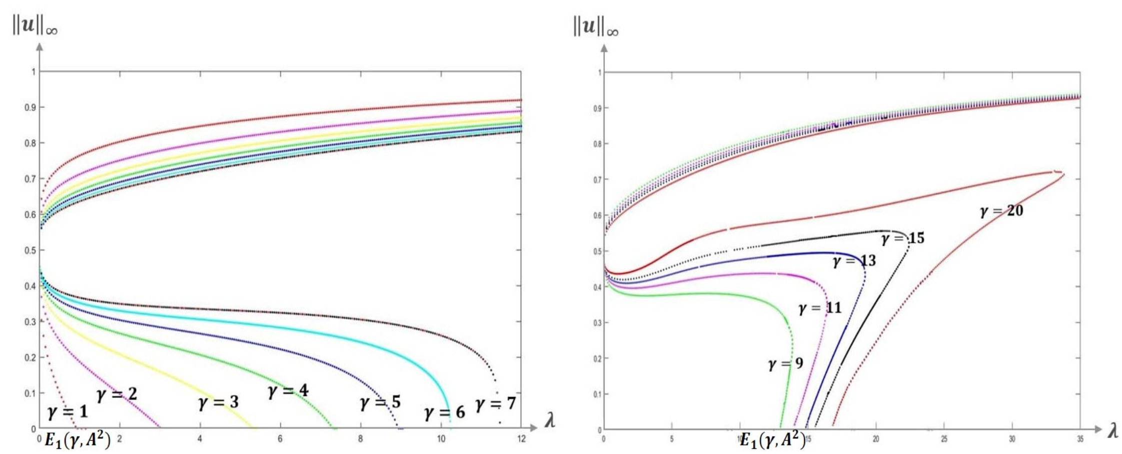

Figure 60. Evolution of Bifurcation Diagrams of (1.24) with Respect to γ When $A = 0.5$ and $\epsilon = 0$.

Finally, we provide the evolution of bifurcation diagrams of (1.24) with respect to γ for the case when $\epsilon > 0$.

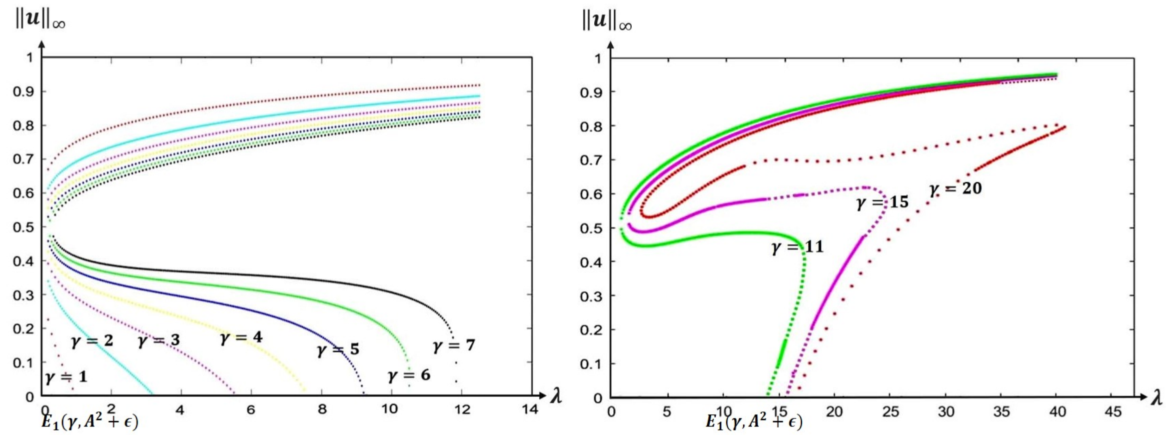

Figure 61. Evolution of Bifurcation Diagrams of (1.24) with Respect to γ When $A = 0.5$ and $\epsilon = 0.01$.

We observe that the exact bifurcation diagram of (1.23) described in Theorem 1.1 occurs for each fixed γ, and the bifurcation curve shifts to the right as γ increases (see Figure 59). Further, our study shows that when $\epsilon = 0$, the bifurcation diagrams of (1.24) are as predicted in Theorem 1.2 for $\gamma \approx 0$, and when γ is large, the bifurcation diagrams of (1.24) are as predicted in Theorem 1.3 (see Figure 60). When $\epsilon > 0$ is small, the bifurcation diagrams of (1.24) are as predicted in Theorem 1.10 for certain γ values (see Figure 61 and 62).

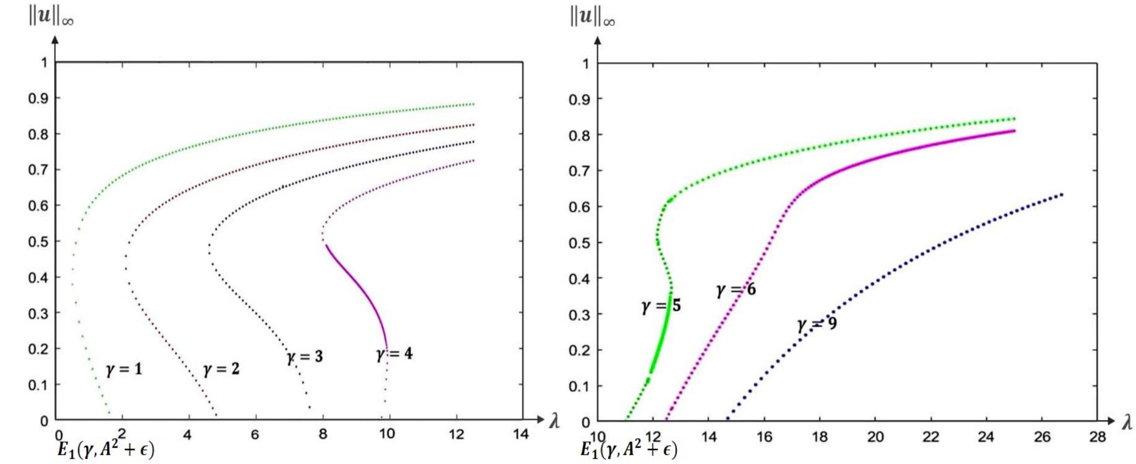

Figure 62. Evolution of Bifurcation Diagrams of (1.24) with Respect to γ When $A = 0.5$ and $\epsilon = 0.1$.

CHAPTER VIII

CONCLUSIONS AND FUTURE DIRECTIONS

8.1 Conclusions

In this dissertation, we analyzed positive solutions to steady state reaction diffusion equations, where a parameter influences the differential equation as well as the boundary conditions. We are motivated to perform this study to answer questions related to the effects of habitat size on the steady states in ecological models. Here, in these ecological models, a parameter related to the habitat size occurs both in the differential equation as well as on the boundary conditions. We are also interested in understanding the effects of the effective matrix hostility on the steady states, and this leads to including a second parameter (measuring this effective matrix hostility) on our boundary conditions. Finally, we are also interested in understanding the effects of density dependent emigration of the population across the habitat boundary, and this leads to dealing with nonlinear boundary conditions. The ecological models we focused on this thesis are those where the growth rate of the population was either scaled logistic or scaled weak Allee. We also studied the effect of grazing. In terms of the density dependent emigration across the habitat boundary, we considered several types, namely, density independent emigration (DIE), positive density dependent emigration (+DDE), negative density dependent emigration (-DDE), U-shaped density dependent emigration (UDDE), and hump-shaped density dependent emigration (hDDE).

We established analytical results on the existence, multiplicity, nonexistence, and uniqueness of steady states, and predicted the corresponding bifurcation diagrams in terms of the patch size parameter versus the number of solutions. We also studied the effects on these bifurcation diagrams as the effective matrix hostility parameter changed. The sub-super solution methods played a central role in establishing our analytical results. In the case of dimension one, we obtained exact bifurcation diagrams of the positive steady states via a modified quadrature method and Mathematica computations. We also obtained exact bifurcation diagrams for certain models in dimension two using the finite element method.

8.2 Future Directions

8.2.1 Uniqueness

We plan to study the model:

$$\begin{cases} -\Delta u = \lambda f(u);\; x \in \Omega, \\ \frac{\partial u}{\partial \eta} + \mu(\lambda)u = 0;\; x \in \partial\Omega. \end{cases} \tag{8.1}$$

Namely, we aim to prove the uniqueness of positive solutions of (8.1) for λ large when $\frac{s}{f(s)}$ is not increasing, which allows a possibility for multiple solutions for a certain finite range of λ (S-shaped bifurcation curve - see Figure 14). Further, we plan to establish such uniqueness results for ecological models with density dependent emigration on the boundary (which leads to nonlinear boundary conditions).

8.2.1.1 *More Numerical Computations of Bifurcation Diagrams when $N = 2$*

Here, we will aim to study the model:

$$\begin{cases} -\Delta u = \lambda f(u);\ x \in \Omega, \\ \alpha(u)\frac{\partial u}{\partial \eta} + \gamma\sqrt{\lambda}[1-\alpha(u)]u = 0;\ x \in \partial\Omega, \end{cases}$$

where $\Omega = (0,1) \times (0,1)$. In Focus 5, we studied this model when $f(s) = s(1-s)$. We studied the cases when $\alpha(s) = \frac{1}{2}$ (density independent emigration) and $\alpha(s) = \frac{1}{1+(A-s)^2+\epsilon}$ (U-shaped density dependent emigration). We will aim to extend this numerical study for other types of emigration $(1-\alpha(s))$ on the boundary. Further, we will also extend our study to scaled weak Allee growth models.

8.2.2 *Ecological Models with a Hump-Shaped Density Dependent Emigration*

Here, we will aim to study the model:

$$\begin{cases} -\Delta u = \lambda f(u);\ x \in \Omega, \\ \frac{\partial u}{\partial \eta} + \gamma\sqrt{\lambda}\frac{u}{(u-A)^2+\epsilon} = 0;\ x \in \partial\Omega, \end{cases}$$

which exhibits a humped-shaped density dependent emigration (see Figure 63) on the boundary, where ϵ is a positive parameter and $A \in (0,1)$. We plan to consider the following reaction terms:

a) $f(s) = s(1-s)$

b) $f(s) = \frac{1}{a}s(s+a)(1-s)$

c) $f(s) = s - \frac{s^2}{K} - \frac{Ms^2}{1+s^2}$.

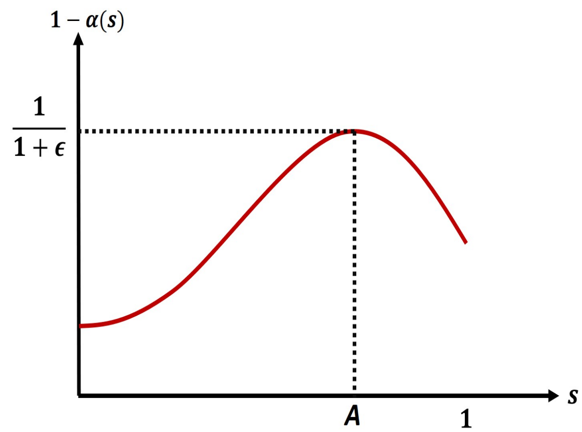

Figure 63. Hump-shaped Density Dependent Emigration on the Boundary.

8.2.3 Existence, Nonexistence, Multiplicity, and Uniqueness of Positive Solutions to Reaction Diffusion Systems which Describe the Interaction between Two Species

We will aim to extend the results established in [FSSS19] to reaction diffusion systems of the form:

$$\begin{cases} -\Delta u = \lambda f(v);\ x \in \Omega, \\ -\Delta v = \lambda g(u);\ x \in \Omega, \\ \frac{\partial u}{\partial \eta} + \mu(\lambda) u = 0;\ x \in \partial\Omega, \\ \frac{\partial v}{\partial \eta} + \mu(\lambda) v = 0;\ x \in \partial\Omega, \end{cases}$$

where u and v are population densities of two species living in the same habitat.

REFERENCES

[Ama76] H. Amann, *Fixed point equations and nonlinear eigenvalue problems in ordered Banach spaces*, SIAM Rev. **18** (1976), no. 4, 620–709.

[Ama98] P. Amarasekare, *Allee effects in metapopulation dynamics*, The American Naturalist **152** (1998), no. 2, 298–302.

[BS02] S. C. Brenner and L. R. Scott, *The mathematical theory of finite element methods*, second ed., Texts in Applied Mathematics, vol. 15, Springer-Verlag, New York, 2002.

[CBG08] F. Courchamp, L. Berec, and J. Gascoigne, *Allee effects in ecology and conservation*, Oxford University Press, 2008.

[CC06] R. S. Cantrell and C. Cosner, *On the effects of nonlinear boundary conditions in diffusive logistic equations on bounded domains*, J. Differential Equations **231** (2006), no. 2, 768–804.

[CC07] ———, *Density dependent behavior at habitat boundaries and the Allee effect*, Bull. Math. Biol. **69** (2007), no. 7, 2339–2360.

[CCY18] R. S. Cantrell, C. Cosner, and X. Yu, *Dynamics of populations with individual variation in dispersal on bounded domains*, J. Biol. Dyn. **12** (2018), no. 1, 288–317.

[CCY20] ———, *Populations with individual variation in dispersal in heterogeneous environments: Dynamics and competition with simply diffusing populations*, Sci. China Math. **63** (2020), no. 3, 441–464.

[CFG$^+$19] J.T. Cronin, N. Fonseka, J. Goddard II, J. Leonard, and R. Shivaji, *Modeling the effects of density dependent emigration, weak allee effects, and matrix hostility on patch-level population persistence*, To appear in Mathematical Biosciences and Engineering **17** (2019), no. 2, 1718–1742.

[CGS93] A. Castro, J.B. Garner, and R. Shivaji, *Existence results for classes of sublinear semipositone problems*, Results Math. **23** (1993), no. 3-4, 214–220.

[CGS19] J.T. Cronin, J. Goddard II, and R. Shivaji, *Effects of patch-matrix composition and individual movement response on population persistence at the patch level*, Bull. Math. Biol. **81** (2019), no. 10, 3933–3975.

[Cia78] P. G. Ciarlet, *The finite element method for elliptic problems*, North-Holland Publishing Co., Amsterdam-New York-Oxford, 1978, Studies in Mathematics and its Applications, Vol. 4.

[CS87] P. Clément and G. Sweers, *Existence and multiplicity results for a semilinear elliptic eigenvalue problem*, Ann. Scuola Norm. Sup. Pisa Cl. Sci. (4) **14** (1987), no. 1, 97–121.

[FGM$^+$] N. Fonseka, J. Goddard II, Q. Morris, R. Shivaji, and B. Son, *On the effects of the exterior matrix hostility and a u-shaped density dependent dispersal on a diffusive logistic growth model*, To appear in Discrete Contin. Dyn. Syst. Ser. S.

[FMS20] N. Fonseka, J. Machado, and R. Shivaji, *A study of logistic growth models influenced by the exterior matrix hostility and grazing in an interior patch*, To appear in Electron J. Qual. Theory Differ. Equ. (2020), no. 17, 1–11.

[FMSS] N. Fonseka, A. Muthunayake, R. Shivaji, and B. Son, *Singular reaction diffusion equations where a parameter influences the reaction term and the boundary condition*, Submitted.

[FOP06] N. I. Fowler, R.D. Overath, and C. M. Pease, *Detection of density dependence requires density manipulations and calculation of lambda*, Ecology **87** (2006), 655–664.

[FSSS19] N. Fonseka, R. Shivaji, B. Son, and K. Spetzer, *Classes of reaction diffusion equations where a parameter influences the equation as well as the boundary condition*, J. Math. Anal. Appl. **476** (2019), no. 2, 480–494.

[GMPS19] J. Goddard II, Q. Morris, C. Payne, and R. Shivaji, *A diffusive logistic equation with U-shaped density dependent dispersal on the boundary*, Topol. Methods Nonlinear Anal. **53** (2019), no. 1, 335–349.

[GMRS18] J. Goddard II, Q. Morris, S. B. Robinson, and R. Shivaji, *An exact bifurcation diagram for a reaction-diffusion equation arising in population dynamics*, Bound. Value Probl. (2018), Paper No. 170, 17.

[Gro98] M.J. Groom, *Allee effects limit population viability of an annual plant*, J. Math. Biol. **151** (1998), no. 6, 487–496.

[GS17] J. Goddard II and R. Shivaji, *Stability analysis for positive solutions for classes of semilinear elliptic boundary-value problems with nonlinear boundary conditions*, Proc. Roy. Soc. Edinburgh Sect. A **147** (2017), no. 5, 1019–1040.

[HGSC20] R. Harman, J. Goddard II, R. Shivaji, and J. T. Cronin, *Frequency of occurrence and population-dynamic consequences of different forms of density-dependent emigration*, To appear in American Naturalist **95** (2020), no. 12.

[Ink82] F. Inkmann, *Existence and multiplicity theorems for semilinear elliptic equations with nonlinear boundary conditions*, Indiana Univ. Math. J. **31** (1982), no. 2, 213–221.

[JBR07] I. D. Jonsen, R. S. Bourchier, and J. Roland, *Influence of dispersal, stochasticity, and an allee effect on the persistence of weed biocontrol introductions*, Ecological Modelling **203** (2007), no. 3, 521–526.

[Kel77] H. B. Keller, *Numerical solution of bifurcation and nonlinear eigenvalue problems*, Applications of bifurcation theory (Proc. Advanced Sem., Univ. Wisconsin, Madison, Wis., 1976), 1977, pp. 359–384. Publ. Math. Res. Center, No. 38.

[Lae71] T. Laetsch, *The number of solutions of a nonlinear two point boundary value problem*, Indiana Univ. Math. J. **20** (1970/1971), 1–13.

[LAW79] D. Ludwig, D. G. Aronson, and H. F. Weinberger, *Spatial patterning of the spruce budworm*, J. Math. Biol. **8** (1979), no. 3, 217–258.

[LMVL09] L. E. Loe, A. Mysterud, V. Veiberg, and R. Langvatn, *Negative density-dependent emigration of males in an increasing red deer population*, Proceedings of the Royal Society B **276** (2009), 2581– 2587.

[LSS11] E. Lee, S. Sasi, and R. Shivaji, *S-shaped bifurcation curves in ecosystems*, J. Math. Anal. Appl. **381** (2011), no. 2, 732–741.

[Mei00] Z. Mei, *Numerical bifurcation analysis for reaction-diffusion equations*, Springer Series in Computational Mathematics, vol. 28, Springer-Verlag, Berlin, 2000.

[Pao92] C.V. Pao, *Nonlinear parabolic and elliptic equations*, Plenum Press, New York, 1992.

[RR19] M. A. Rivas and S. B. Robinson, *Eigencurves for linear elliptic equations*, ESAIM Control Optim. Calc. Var. **25** (2019), Paper No. 45, 25.

[SB11] C. M. Strevens and M.B. Bonsall, *Density-dependent population dynamics and dispersal in heterogeneous metapopulations*, Journal of Animal Ecology **80** (2011), 282–293.

[Sey10] R. Seydel, *Practical bifurcation and stability analysis*, third ed., Interdisciplinary Applied Mathematics, vol. 5, Springer, New York, 2010.

[Shi87] R. Shivaji, *A remark on the existence of three solutions via sub-super solutions*, Nonlinear analysis and applications (Arlington, Tex., 1986), Lecture Notes in Pure and Appl. Math., vol. 109, Dekker, New York, 1987, pp. 561–566.

[SS06] J. Shi and R. Shivaji, *Persistence in reaction diffusion models with weak Allee effect*, J. Math. Biol. **52** (2006), no. 6, 807–829.